PD 75-0117
CONTRACT NAS 8-31370

INVESTIGATION OF LIGHTWEIGHT DESIGNS AND MATERIALS FOR LO_2 AND LH_2 PROPELLANT TANKS FOR SPACE VEHICLES

INTERIM REPORT SUMMARIZING PHASE I

GENERAL DYNAMICS
Convair Division

PD 75-0117

INVESTIGATION OF LIGHTWEIGHT DESIGNS AND MATERIALS FOR LO_2 AND LH_2 PROPELLANT TANKS FOR SPACE VEHICLES

INTERIM REPORT SUMMARIZING PHASE I

December 1975

Prepared for
National Aeronautics and Space Administration
GEORGE C. MARSHALL SPACE FLIGHT CENTER
Huntsville, Alabama
Prepared Under
Contract NAS 8-31370

Prepared by
GENERAL DYNAMICS CONVAIR DIVISION
P.O. Box 80847
San Diego, California 92138

CONTENTS

CONTENTS (Concluded)

ILLUSTRATIONS

ILLUSTRATIONS (Continued)

ILLUSTRATIONS (Concluded)

TABLES

TABLES (Concluded)

SUMMARY

This report covers Phase I, Concept Selection, which involved loads analysis, contour evaluation, support system evaluation and thrust structure definition. Fracture mechanics analysis and limited material properties testing was performed on material processed in a manner simulating actual tank fabrication effects. The configuration selections and data developed in this phase serve as the basis for the predesign effort of Phase II.

Loading conditions were evaluated for each contour in such a way that the conditions were identified which caused the greatest tension and compression stresses in each contour. These designing loads were then used to size each candidate configuration.

The contour evaluation was based primarily on total vehicle weight and length as a function of payload weight. In general the desirable bulkhead contour was one which would produce a low profile, high radius-to-height ratio. The basic contours considered were the ellipsoidal, torispherical, Cassinian and controlled $N\theta/N\phi$ (hoop to meridian stress ratio). The combination of Cassinian contoured bulkheads on the LH_2 tank and elliptical bulkheads on the LO_2 tank resulted in the lightest and shortest system evaluated.

Candidate support systems were defined which represented a range of support slope angles, numbers of struts, and general arrangements. The individual systems were analyzed to determine strut loads as well as bulkhead stresses. System weights, including bulkhead effects, were then compared to select the minimum-weight system. As a result, the laced 24-strut system was selected for the LO_2 tank and the 12-strut system selected for the LH_2 system.

The engine mounting was investigated since it affects the weight of the LO_2 tank as well as the overall length of the Tug vehicle. Three systems were investigated for weight purposes: the NASA baseline engine mounting system, an ellipticonic LO_2 aft bulkhead thrust structure, and a system which mounts a thrust cone directly to an elliptic bulkhead. Ground handling loads were considered under the condition where the LO_2 tank had standby pressure and the engine was cantilevered from the LO_2 tank. This required tank membrane stiffening. Even with this stiffening, the lightest, shortest, LO_2 configuration was the one with the thrust cone mounted directly to the elliptic bulkhead.

A fracture mechanics analysis was performed which showed that the LO_2 and LH_2 tanks are in the thin ductile category and, therefore, proof tests cannot be used to support the fracture mechanics analysis of residual strength and cyclic life.

Curves were developed for the LO_2 and LH_2 tanks showing flaw depth versus quantity of missions to leak, for use during Phase II.

The material testing performed was to evaluate the K_c, K_{th}, and K_{IE} for 2219T87 in the conditions representative of the actual processed tank membrane material.

This report is divided into eight sections, as shown below. The first seven represent the tasks performed, and the eight presents conclusions and recommendation.

I Requirements Assessment and Preliminary Design Concepts

II Reference Configuration

III Preliminary Analysis and Design

VI Material Sample Testing

V Fracture Mechanics Analysis

VI Tug Structural Effects

VII Tank Concept Selection

(Each section includes the data, drawings, curves, analysis, and interpretations generated in Phase I.)

VIII Recommendations and Conclusions

1

REQUIREMENTS, ASSESSMENT, AND PRELIMINARY DESIGN CONCEPTS

The objectives of this task were: (a) to establish preliminary design requirements, (b) to determine typical mission pressure and load spectrum, and (c) to assess previous studies for applicable data base information.

1.1 DESIGN REQUIREMENTS DOCUMENT

A basic study requirements document, PD75-0044, was developed to provide a single source for all major criteria to be used in the lightweight tank design study. This document includes a physical description of the baseline Tug tankage system and interfaces, as well as environmental design conditions. Primarily, the requirements were extracted from the following documents:

a.	MSFC 68M00039-1	— Baseline Space Tug — System Requirements and Guidelines
b.	MSFC 68M00039-2	— Baseline Space Tug — Configuration Definition
c.	NASA TMX 64713	— Natural Environment Design Requirements
d.	JSC 07700 Vol. XIV, Rev. C	— Space Shuttle System Payload Accommodations
e.	MSFC-HDBK-505	— Structural Strength Design and Verification Program Requirements
f.	NASA TM-X64627	— Space and Planetary Environment Criteria Guidelines for Use in Space Vehicle Development
g.	SP 8013	— Meteoroid Environment Model - 1969
h.	CASD-NAS75-017	— Space Tug/Shuttle Interface Compatibility Study - Final Report
i.	CASD-NAS73-033	— Space Tug Systems Study (Cryogenic) — Final Report

Material design allowable stresses were also selected for use in the trade studies and predesign effort.

To simplify testing and to avoid checkout and operational complications, room temperature properties will be used for preliminary tank design (see Table 1-1).

Table 1-1. Lightweight tank material properties (R.T.).

Material	Form	Use	F_{Tu} KN/cm^2 (KSI)	F_{Ty} KN/cm^2 (KSI)	F_{Cy} KN/cm^2 (KSI)	F_{Su} KN/cm^2 (KSI)
2219-T87	Sheet	Basic Membrane	43.6(63)	35.8(52)	35.8(52)	25.5(37)
2219-T852	Ring Forging	Door Rings	39.3(57)	31.7(46)	31.7(46)	23.4(34)
2219-T851	Plate	Doors, Ftgs	42.7(62)	31.7(46)	32.4(47)	24.8(36)

To minimize the lightweight tank weld land weight, the 2219 aluminum welds will be designed using ultimate strength considerations. The "A" allowable F_{Tu} (as welded) for 2219 welds is 33.2KSI, based on tests performed by Convair on 2219-T87/T-82, 2219-T851/-T62, 2219-T852/-T62, and 2219-T62/-T62 TIG welds, in thicknesses from .318 cm (.125 in.) to .636 cm (.250 in.). To account for weld imperfections, an ultimate weld allowable of 31.5 KSI will be used for all 2219 aluminum welds in the lightweight tank design. This weld allowable (which is 50% of the 2219-T87 parent metal F_{Tu}) was used for the 2219 aluminum welds in the Saturn S-1C.

Based on a series of tests performed by Convair, the 0.2 percent offset yield strength for 2219 welds is 16 KSI (typical). For these tests, strain gages were used to obtain stress/strain curves from which the yield stress of the welds could be measured. A typical 2219 aluminum weld stress/strain curve is shown in Figure 1-1. As indicated, using the proposed ultimate design criteria for the welds, stresses will exceed the 0.2 percent offset yield stress when the tank is proof tested. This will result in a permanent set in the weld after proof test of approximately two percent. Since the maximum operating stress is less than the proof stress, the weld will be cycled along a new linear stress/strain curve, as shown. Due to the high ductility (>10% elongation) and strain hardening characteristic of the weld, this approach represents a realistic method for minimizing tank weight without sacrificing structural integrity.

Acceleration/pressure time histories shown in Figure 1-2 were developed for this study, using tank pressure rise rates taken from: Convair's recent Space Tug/Shuttle Interface Compatibility Study (ST/SICS) (NAS8-31012); orbiter cargo bay internal pressure histories, per PD 75-0044 (Figure 4.1-1); and Orbiter acceleration histories for Tug reference mission No. 1 (modified to reflect maxima per PD 75-0044, Table 4.1-4).

For the RTLS abort confition, the acceleration and propellant volume histories shown in Figure 1-3 were developed, using acceleration data per Rockwell International report SSP-SF-73-167-S and flow rates from the abort dump analyses conducted during the ST/SICS.

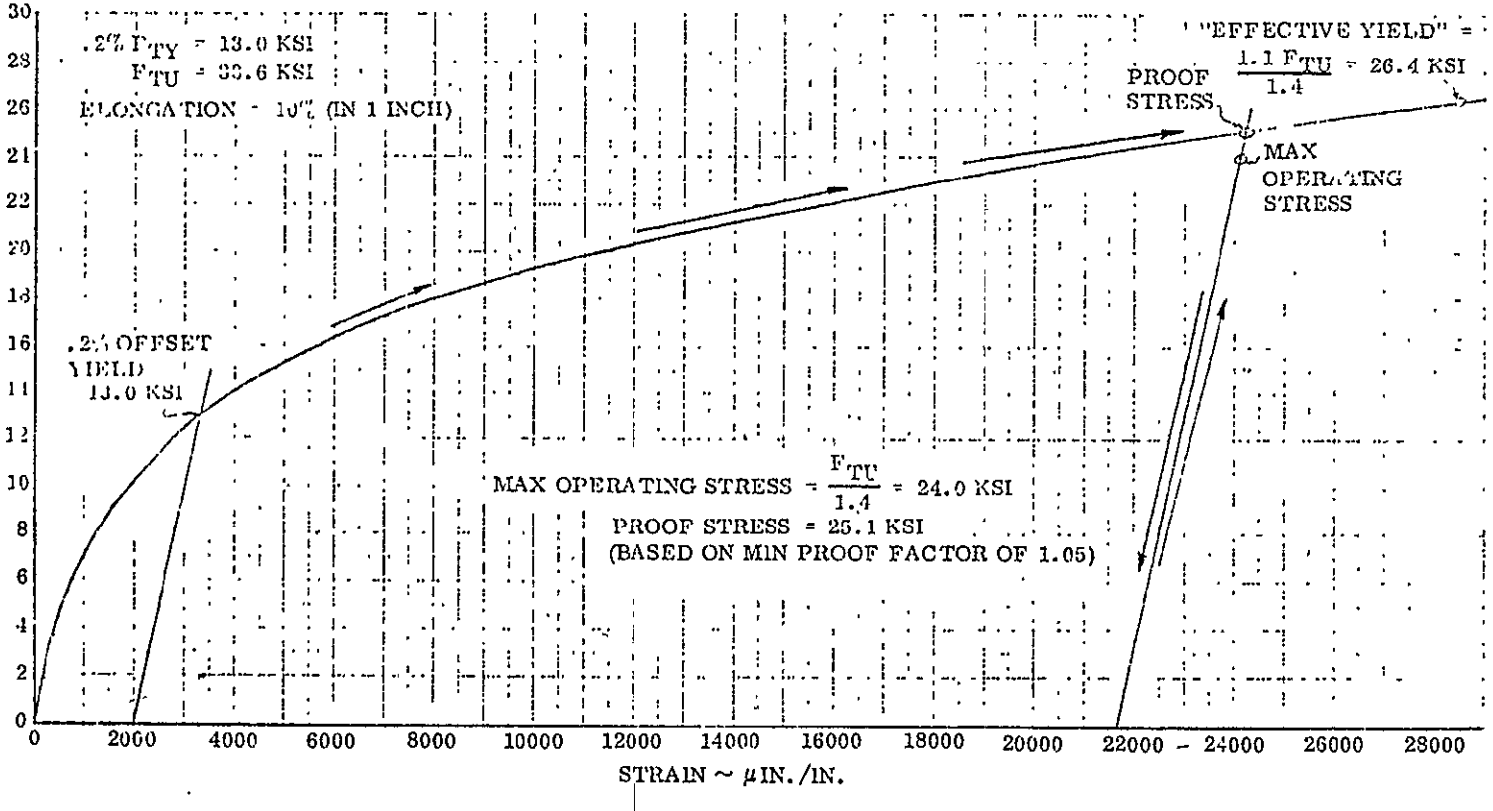

Figure 1-1. Typical stress/strain curve — 2219 weld (TIG - as welded).

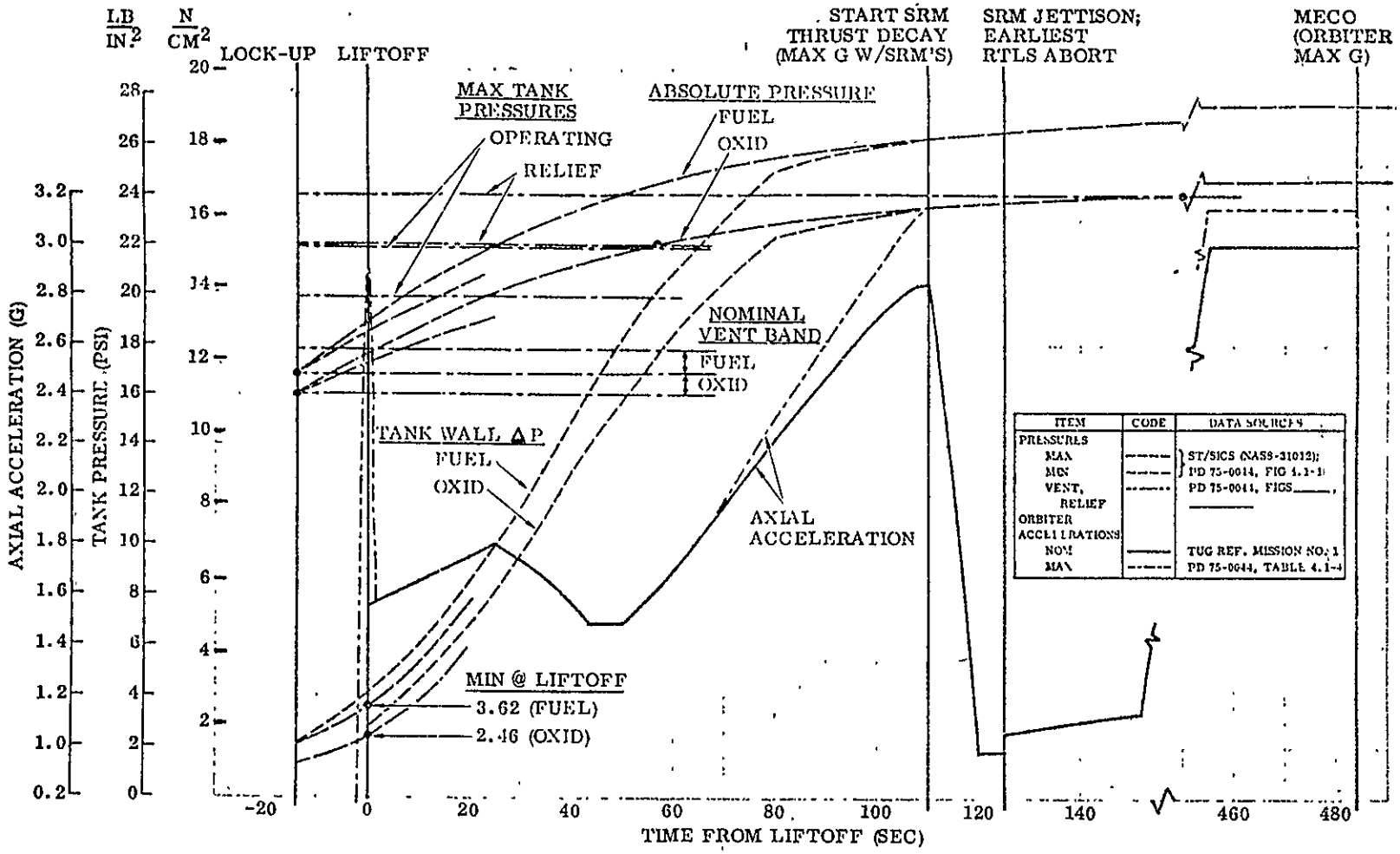

Figure 1-2. Flight pressure history.

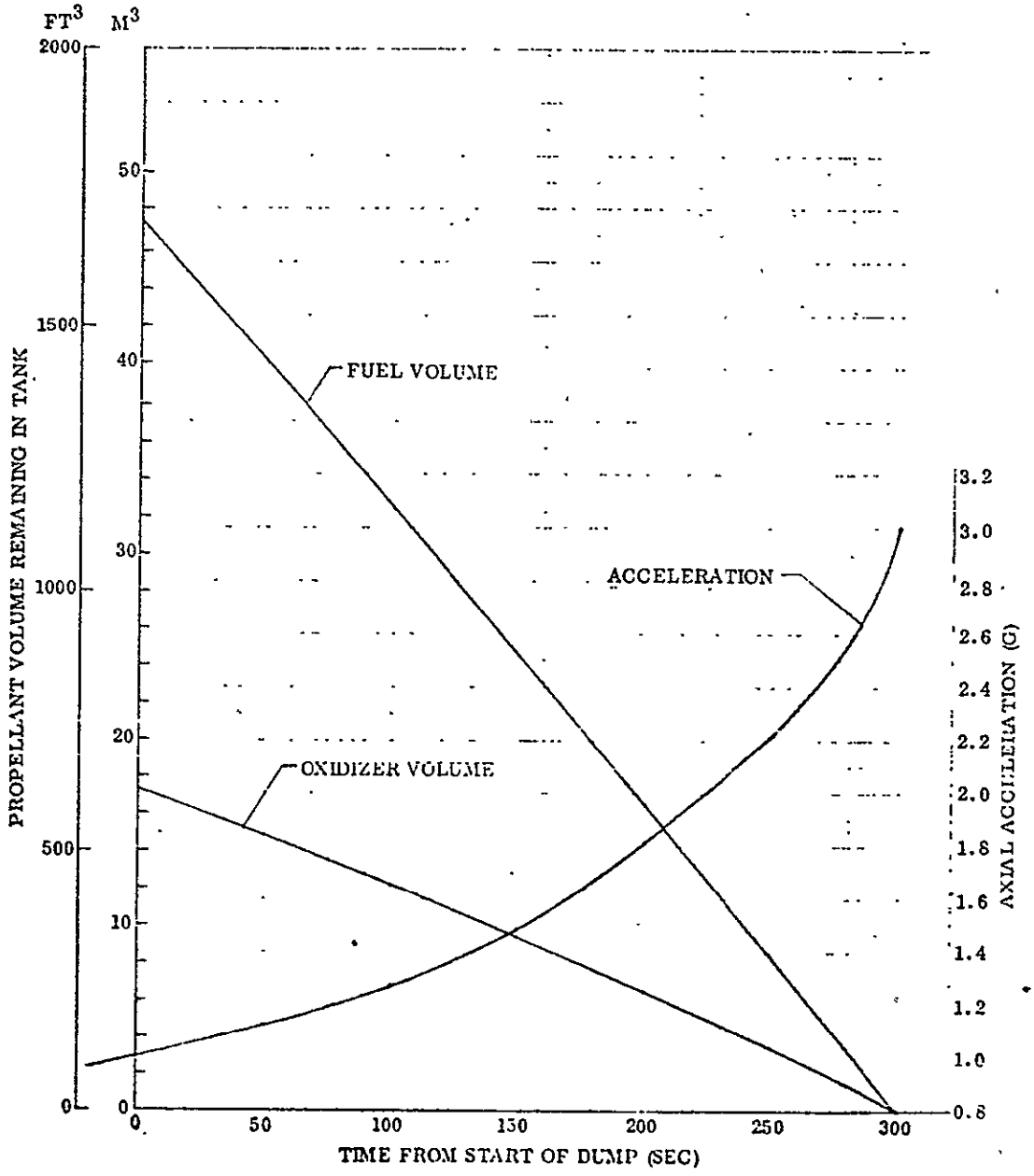

Figure 1-3. Propellant dump history.

For Tug operation, the stage weight and propellant quantities given in Table 1-2 were developed from the dual deployment/single retrieval mission data given in MSFC 68M00039-2.

Table 1-2. Baseline Tug stage and main propellant weights.

Burn(1)	Stage Weight (2) Start		Stage Weight (2) End		Fuel Weight in Tank (2) Start		Fuel Weight in Tank (2) End		Oxid Weight in Tank (2) Start		Oxid Weight in Tank (2) End	
	Kg	LB_M	Kg	LB_M	Kg	LB_M	Kg	LB_M	Kg	LB_M	Kg	LB_M
1	26657	58769	19627	43271	3384	7461	2380	5247	19628	42373	13603	29989
2	19617	43248	15276	33678	2379	5246	1759	3879	13603	29989	9882	21786
3	15198	33506	10219	22529	1748	3854	1037	2286	9831	21674	5563	12265
4	8567	18888	5754	12686	836	1844	435	958	4688	10336	2277	5020
5	5727	12627	4423	9751	428	943	241	532	2267	4998	1149	2533
6	4411	9725	3302	7280	238	525	80	176	1146	2526	195	430

(1) For dual deployment, single retrieval Geosynchronous mission, main engine full thrust burns.

(2) Derived from MSFC 68M00039-2.

1.2 MISSION PRESSURE AND LOAD SPECTRUM

LH_2 and LO_2 tank design pressures were developed, based on a preliminary thermodynamics analysis of the baseline Tug propulsion system using ambient helium prepressurization and autogenous main stage pressurization. A computer-controlled pressurization and vent system is used to maintain pressure within the regulated pressure range. Propellants are tanked at the minimum regulated pressure. Tables 1-1 and 1-2 show the LH_2 and LO_2 tank pressure development, respectively.

The LH_2 tanking pressure, shown in Table 1-3, is 116 KN/m^2. This is also the propellant saturation pressure. The engine start requirements are 14.5 KN/m^2 above saturation pressure, which sets the lower level of the regulator band at 130 KN/m^2. A tolerance of 6.9 KN/m^2 is placed on the regulator, establishing the maximum regulator pressure (137 KN/m^2). For design purposes, this value is considered the maximum operating pressure. The proof pressure is 1.05 times the operating pressure ($1.05 \times 137 = 144$ KN/m^2). The relief valve lower level is established at the upper limit of the regulator and given a reasonable band of 13.8 KN/m^2, establishing the maximum relief pressure at 153 KN/m^2. The ultimate tank design pressure is 1.4 times the operating pressure ($1.4 \times 137 = 192$ KN/m^2).

Table 1-3. LH_2 tank pressure development.

Ultimate Design Pressure	192 KN/m^2
Maximum Relief Valve Pressure	151.2 KN/m^2
Relief Valve Tolerance Band	(13.8 KN/m^2)
Proof Pressure	144 KN/m^2
Maximum Regulator Pressure (Maximum Operating Pressure)	137.4 KN/m^2
Regulator Tolerance	(6.9 KN/m^2)
Minimum Regulator Pressure	130.5 KN/m^2
Delta Pressure for MES	(14.5 KN/m^2)
Tanking Pressure (Minimum Regulated Pressure)	116 KN/m^2

The LO_2 tanking pressure (saturation pressure) is 110 KN/m^2 (Table 1-4). The engine start requirement is 34.5 KN/m^2 above the saturation pressure. Therefore, the lower limit for the regulator band is 114.5 KN/^{2}. A tolerance of 6.9 KN/m^2 is placed on the regulator, which establishes the maximum regulator pressure at 151.4 KN/m^2. This is the maximum operating pressure for design purposes. The proof pressure is 1.05 times the operating pressure (1.05 × 151.4 = 159 KN/m^2). The relief valve lower level is the upper limit of the regulator (151.4 KN/m^2). A relief band of 13.8 KN/m^2 establishes the maximum relief pressure at 165.2 KN/m^2. The ultimate tank design pressure is 1.4 times operating pressure (1.4 × 151.4) 212 KN/m^2.

Table 1-4. LO_2 tank pressure development.

Ultimate Design Pressure	212 KN/m^2
Maximum Relief Valve Pressure	165.2 KN/m^2
Relief Valve Tolerance Band	(13.8 KN/m^2)
Proof Pressure	159 KN/m^2
Maximum Regulator Pressure (Maximum Operating Pressure)	151.4 KN/m^2
Regulator Tolerance	(6.9 KN/m^2)
Minimum Regulator Pressure	144.5 KN/m^2
Delta Pressure for MES	(34.5 KN/m^2)
Tanking Pressure (Minimum Regulated Pressure)	110 KN/m^2

The maximum vent pressure is considered the maximum operating (limit) pressure in this study because the Tug vents are redundant both mechanically and electrically, and there are two additional vent valves in the Orbiter, providing quad redundancy. Therefore, multiple failures (four while in the Orbiter and two outside the Orbiter) must occur to produce tank overpressure. If a mechanical relief is incorporated in the vent system, a bandwidth of approximately 13.8 KN/m^2 above the maximum operating pressure must be allowed to accommodate typical valve crack/reseat tolerances. This band represents an approximate ten percent increase in fuel tank pressure.

It is assumed for this study that if a relief valve should be required (none is currently recommended) the relief valve stress level will be acceptable, based on reduced margins; i.e., relief pressures will not be considered in defining maximum operating pressures for purpose of tank design but must exhibit a positive ultimate margin.

The specified tanking pressures result in the propellant characteristics shown in Table 1-5. Densities are based on Figure 4.2-1 of the Design Requirements (PD 75-0044).

Table 1-5. Propellant characteristics.

Item	Units	Fuel	Oxidizer
Tank Pressure (Absolute)	N/CM^2 ($lb/in.^2$)	11.6 (16.8)	11.0 (16.0)
Saturation Pressure (Absolute)	N/CM^2 ($lb/in.^2$)	11.6 (16.8)	11.0 (16.0)
Propellant Density	Kg/M^3(lb/ft^3)	70.24 (4.385)	1136.5 (70.95)
Total Propellant Weight	Kg (lb_M)	3338. (7360)	19595 (43199)
Total Propellant Volume	M^3 (ft^3)	47.5337 (1678.45)	17.2432 (608.87)
Propellant Tank Volume	M^3 (ft^3)	49.5034 (1748.00)	18.1248 (640.00)
Ullage Volume	M^3 (ft^3)	1.9697 (69.55)	0.8816 (31.13)
Ullage Percentage	—	3.98	4.86

Design, proof, and ultimate pressures are calculated by multiplying the maximum regulated pressures and the safety factors from Table 4.3-1 of the Design Requirements Document.

The Tug LO_2 and LH_2 tank differential pressure histories for a typical six-burn deployment/retrieval mission were constructed as shown in Figures 1-4 and 1-5. These profiles represent the worst case pressure/time histories for the range of planned tug missions and for purpose of the tank fracture mechanics analysis, for the entire 50-mission operational life.

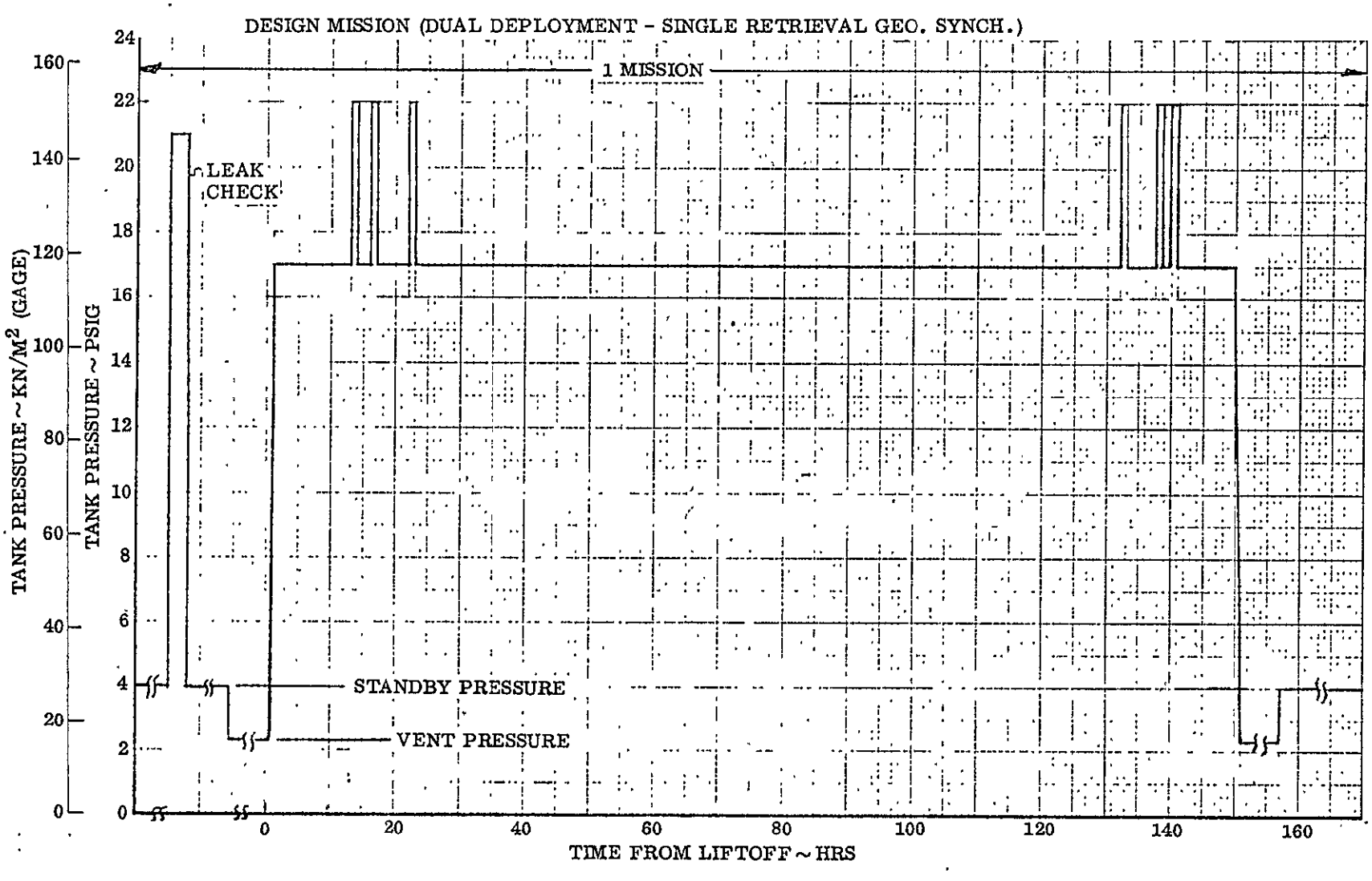

Figure 1-4. LO_2 tank design pressure profile.

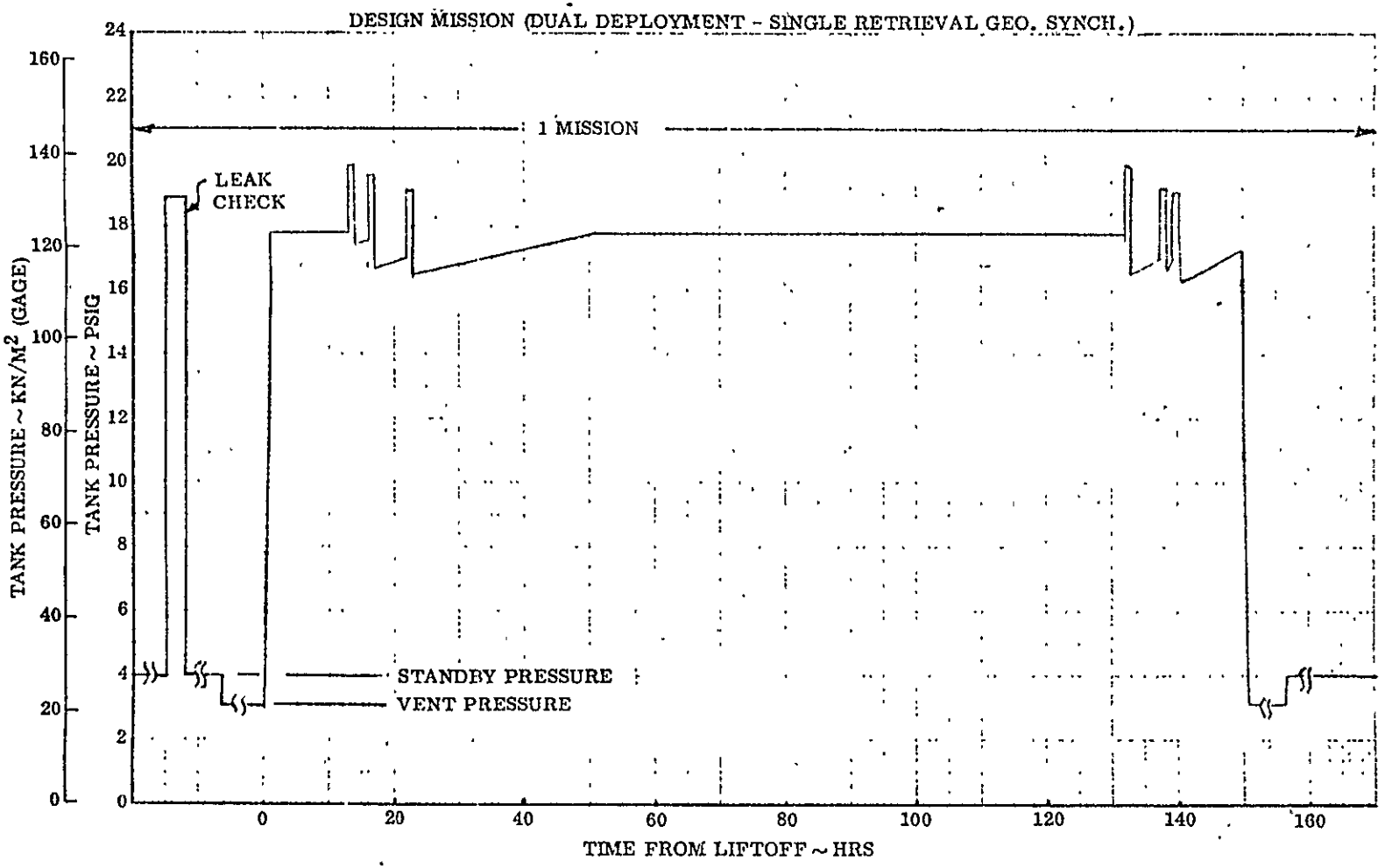

Figure 1-5. LH_2 tank design pressure profile.

Current Tug operational checkout philosophy requires an operating pressure leak check on each Tug propellant tank at some point in the ground checkout prior to each flight. These pressure cycles are included in each mission total pressure history (Figures 1-4 and 1-5). The ground standby pressure is 27 ±7 KN/m^2 (4 ±1 psid) for both tanks, as given in NASA report NAS8-3101.

1.3 ASSESSMENT OF PREVIOUS STUDIES

The data generated in Convair's Space Tug Systems Study (STSS) was reviewed in depth to determine what data was applicable to the present study and what, additional effort would be required to expand that data for this study. Five primary areas were reviewed: (1) Detail design, (2) Bulkhead Contour, (3) Support Systems, (4) Producibility, and (5) Material Evaluation.

In the detail design area, primarily access door joint designs, weld transition designs, and thrust structure designs were identified for further study. The flush door design with the cono seal gasket was considered a good representative access door concept and therefore would be used on the baseline configuration. The weld transition design was also selected for the baseline. The thrust structure selected in the STSS was an ellipticonic configuration, which seemed very promising. The configuration was selected as an alternate to the truss engine mount used on the NASA baseline. In the present study, these systems were to be compared after the LO_2 tank contour was selected.

Consideration of the bulkhead contour was limited in the STSS effort, so additional parametric data had to be generated before a contour selection could be made. It was decided that this data should be developed for ellipsoidal, controlled force ratio, Cassinian, and torispherical bulkhead contours.

LO_2 tank support system analysis in the STSS effort showed that the selected support system had a low stiffness (<5 Hertz). The criteria defined in our requirements document is 10 Hertz; therefore, a new support system had to be developed. The producibility analysis reviewed the forming capabilities: spin forming, bulge forming, and stretch forming. The trades made in the STSS were in sufficient depth and are still valid. Spin forming of entire bulkheads of the size and shape necessary for the LH_2 and LO_2 tanks can be produced, but only in the T62 condition; therefore, bulge forming and stretch forming methods are considered in the sizing of gore and cap lengths and widths.

Thirteen candidate material alloys were evaluated for the LH_2 tank and LO_2 tank during the STSS effort, and 2219-T87 aluminum alloy was selected. As part of this study this complete evaluation was reviewed for:

a. New candidates

b. Improved properties

c. Weight trade-off changes (due to the above)

The conclusion was that 2219 is still the leading candidate, based on its excellant fracture toughness, good weldability, and repair weldability, plus high stress-corrosion cracking resistance. Therefore, 2219 is the material selected for this study.

2

REFERENCE CONFIGURATION

The Reference Configuration drawing is shown in Figure 2-1. This drawing is fundamentally a copy of the NASA baseline tug drawing, with emphasis on the tankage systems.

The Reference Configuration defines the various tank/shell interface points and the overall baseline lengths of the tankage systems as well as the engine location relative to the LO_2 tank. The geometry data was used in the tradeoff of Tug systems effects relative to tank contour and support system variations. The alternate engine mounting system (ellipticonic) was also defined here, for use in the trade studies. This drawing became a part of the Requirements document to define the envelopes and physical interfaces of the Tug and tanks.

3

PRELIMINARY ANALYSIS AND DESIGN

The objectives of this task were to (a) investigate the effects of bulkhead contours, (b) investigate the interrelationship of contour, propellant inertia, and ullage pressure, (c) evaluate support strut arrangement and geometry, (d) determine discontinuity effects, (e) define candidate tank and support concepts, and (f) determine membrane thickness requirements.

3.1 BULKHEAD CONTOURS

Desk computer programs were developed which would calculate volumes, areas and lengths as well as plot hoop and meridional membrane loads and contours for ellipsoidal, Cassinian, torispherical and controlled N_θ/N_ϕ bulkhead contours. Figures 3-1a thru 3-2b are examples of these program outputs.

Figure 3-1a is a composite plot of n = 1.9 Cassinian bulkhead data. The basic contour is plotted with the vertical scale being proportional to the maximum bulkhead radius, a. N_θ/P_a are plotted versus the same horizontal (r) scale but using (+) at each point to differentiate the curves. The geometry data, N, A (unity), and Z maximum are printed for reference and the Volume and Area are calculated and printed as factors of A cubed and A squared, respectively.

Figure 3-1b is the n = 1.9 Cassinian bulkhead containing LO_2 under 3.0 g longitudinal force. This program requires an actual radius (not unity) to be entered along with - propellant density, T/W, N, cylindrical length, and ullage pressure. N_θ and N_ϕ are then plotted versus r.

Figures 3-2a and 3-2b present similar data as Figures 3-1a and 3-1b, respectively, except the bulkhead is an a/b = $\sqrt{2}$ ellipsoidal shape.

These programs developed geometry data in terms of a unit radius. For preliminary contour selection the data was formulated into Volumetric sensitivity parametric curves. These curves are presented in Figures 3-3, 3-4, 3-5 and 3-6 for the Cassinian, torispherical, ellipsoidal and controlled N_θ/N_ϕ contours, respectively. The bulkhead volume divided by a cubed is plotted with respect to the bulkhead aspect ratio (a/b). A cutoff point is noted on each curve. This cutoff point is the highest aspect ratio for that contour class that can be constructed without hoop compression due to gas pressure only.

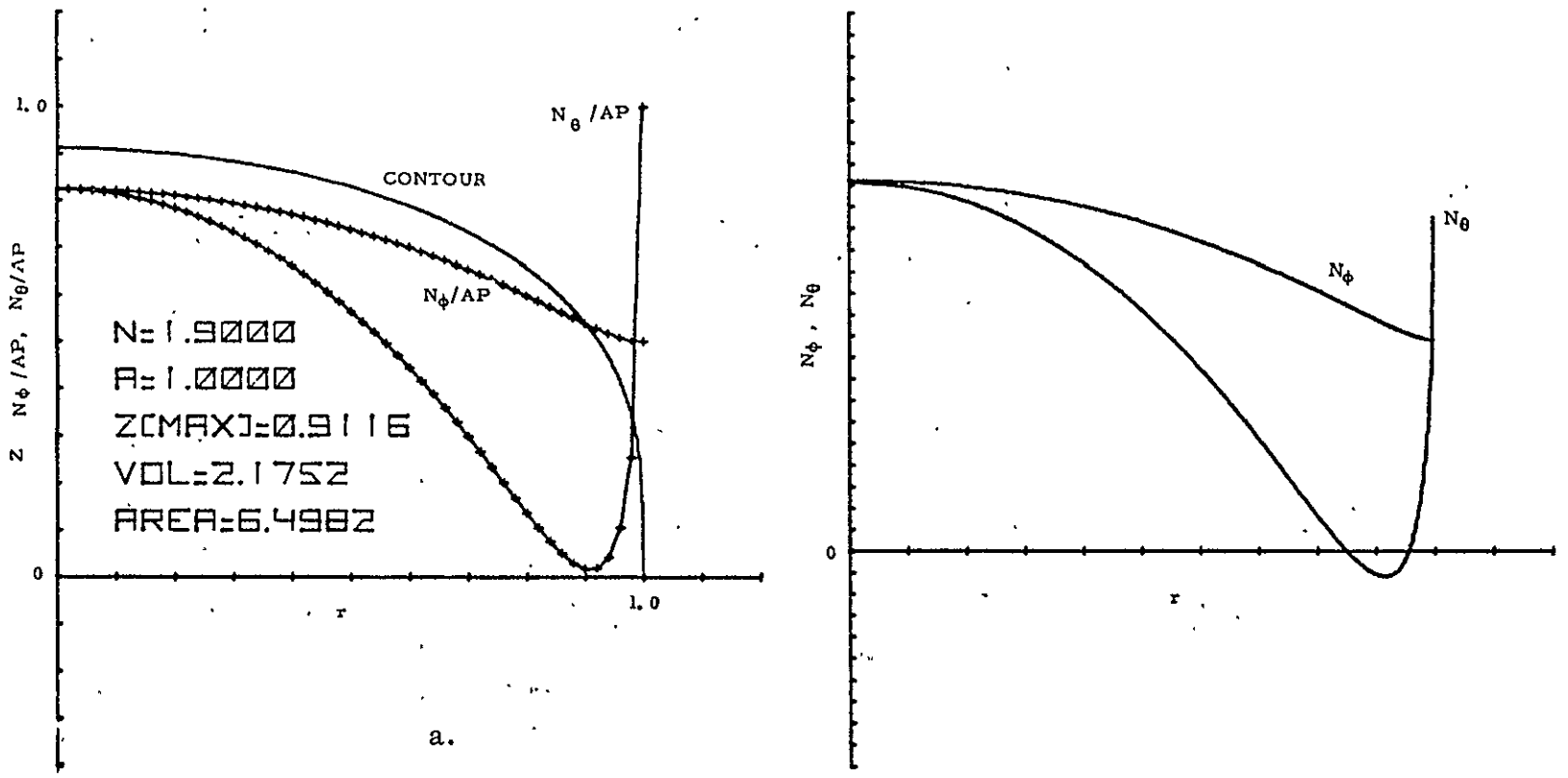

Figure 3-1. Cassinian bulkhead.

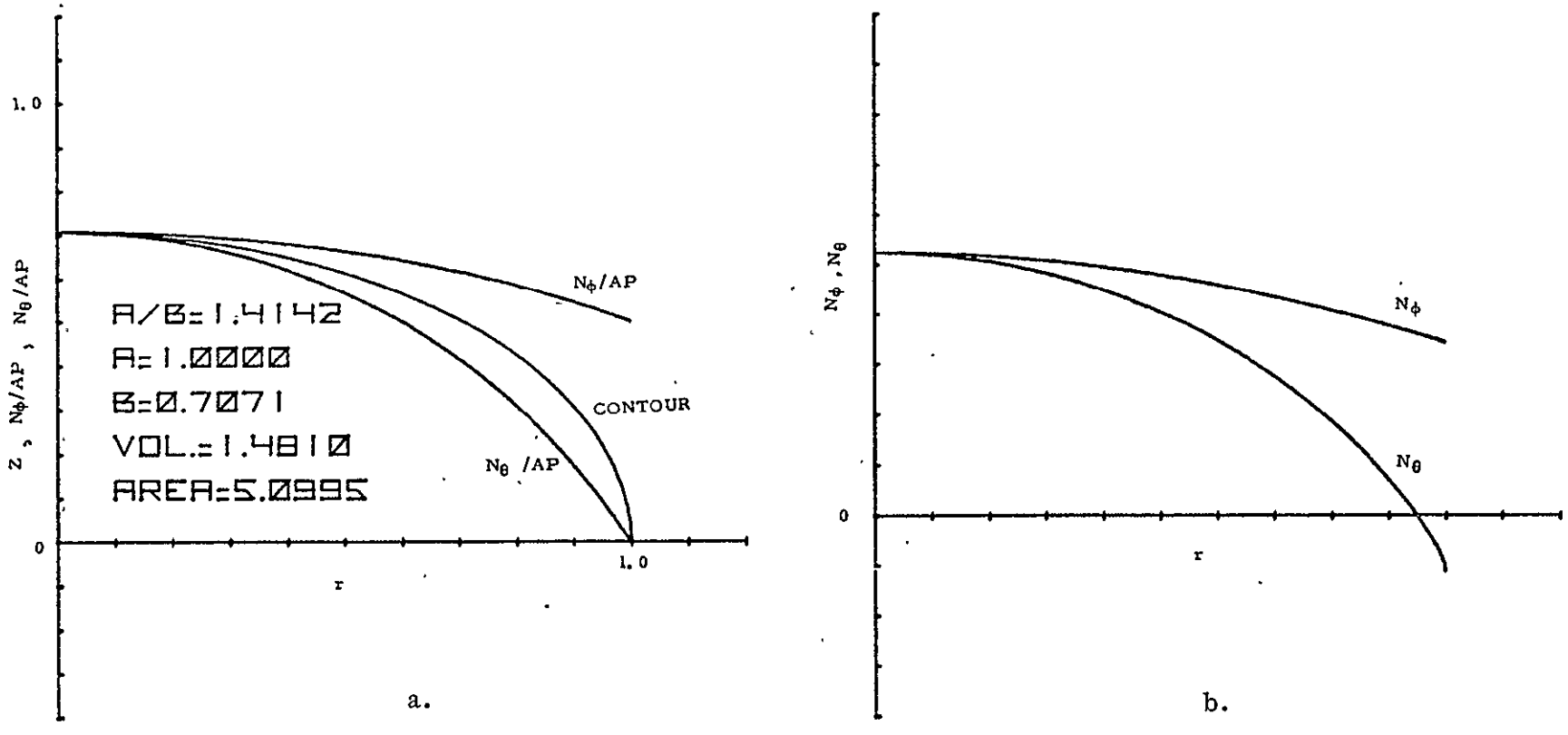

Figure 3-2. Ellipsoidal bulkhead.

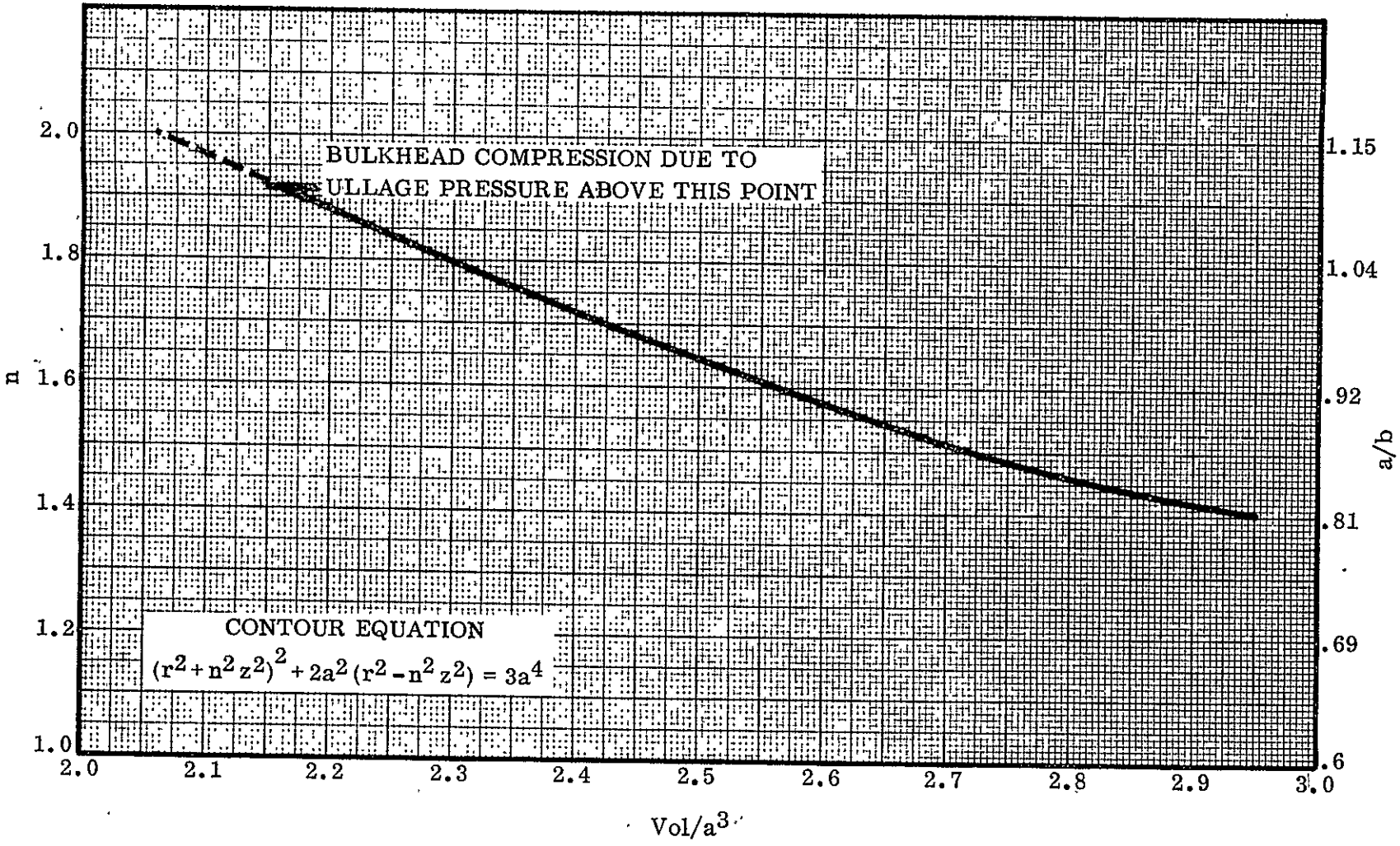

Figure 3-3. Cassinian bulkhead volumetric sensitivity.

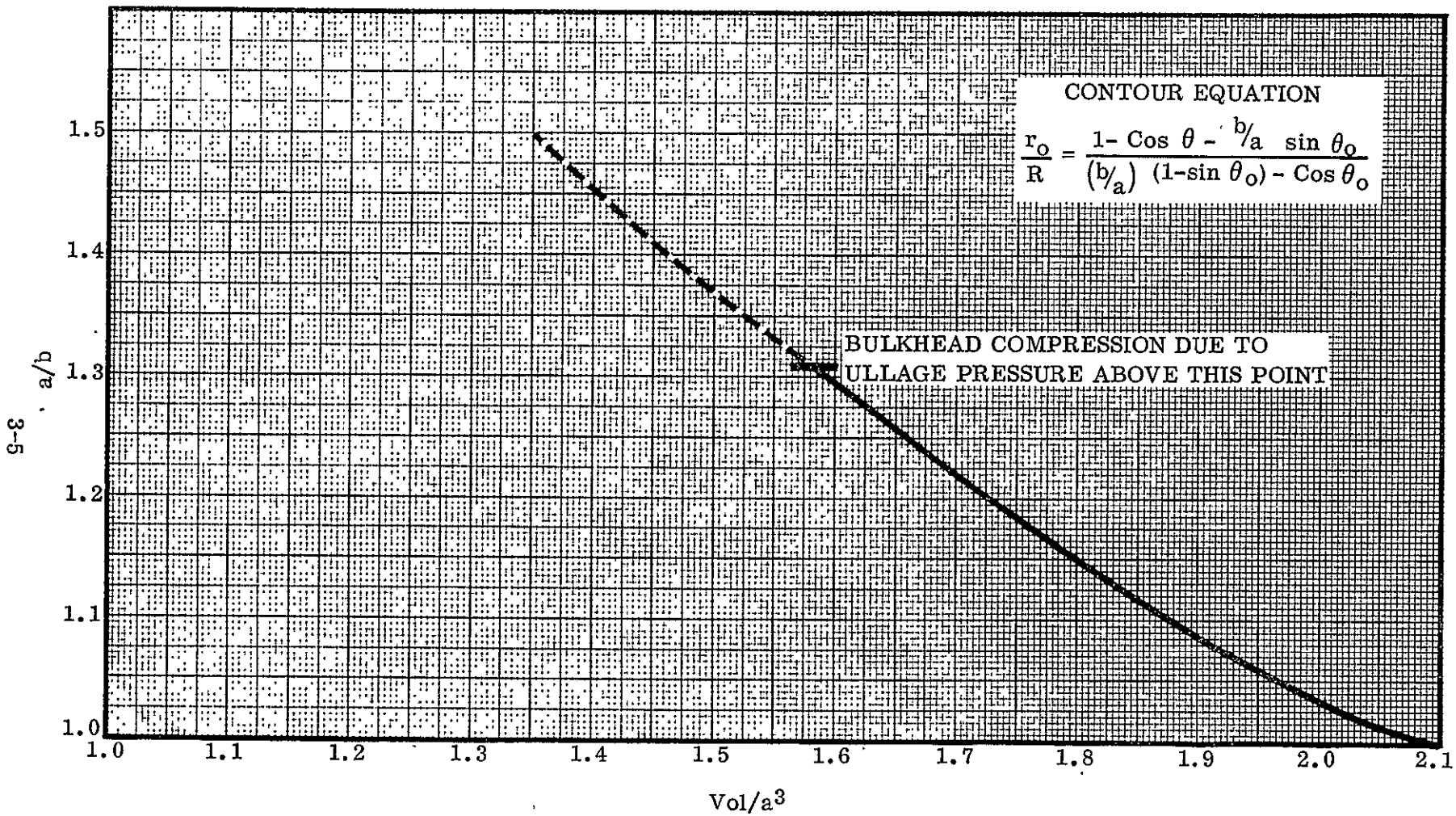

Figure 3-4. Torispherical bulkhead volumetric sensitivity.

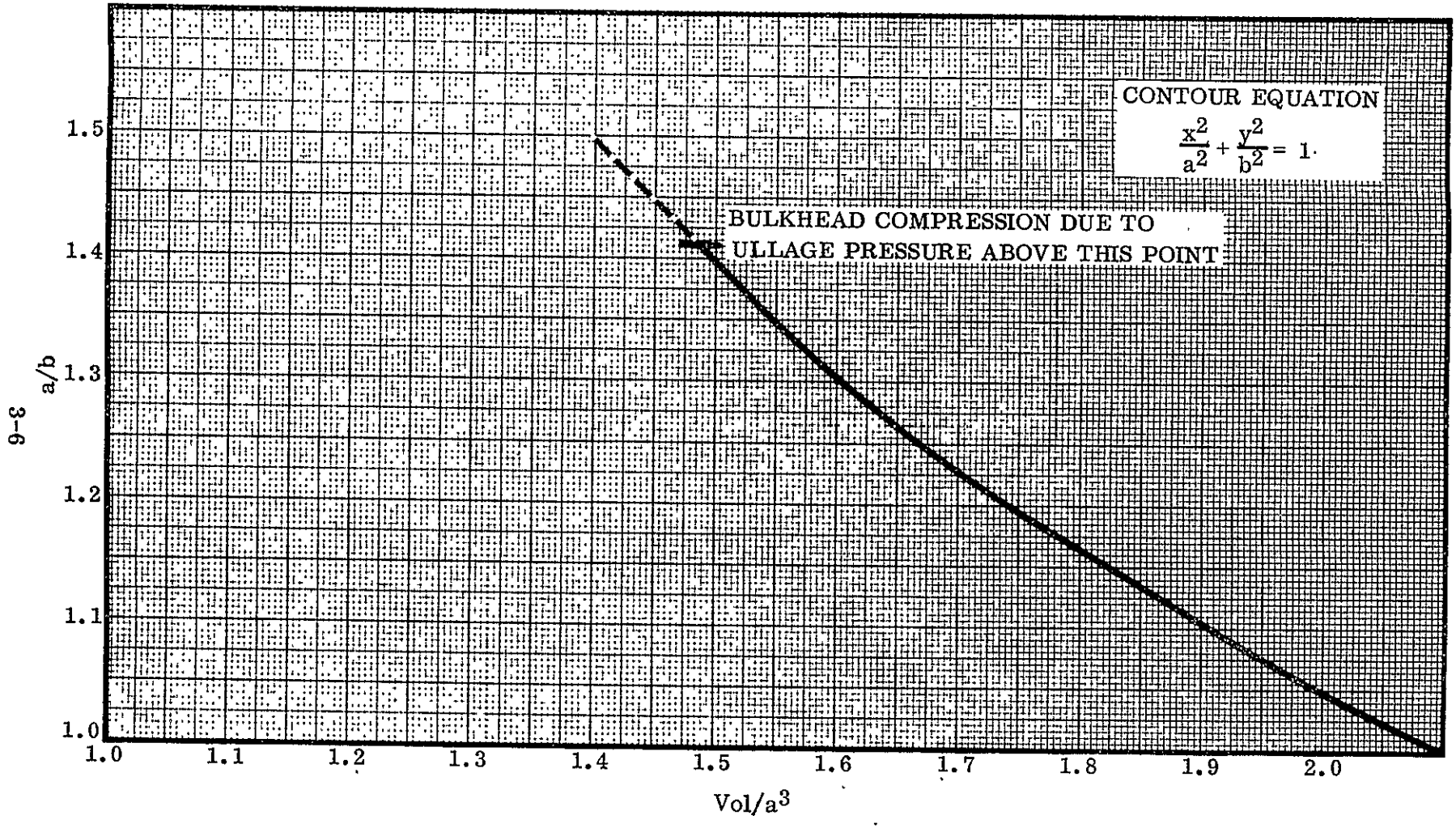

Figure 3-5. Ellipsoidal bulkhead volumetric sensitivity.

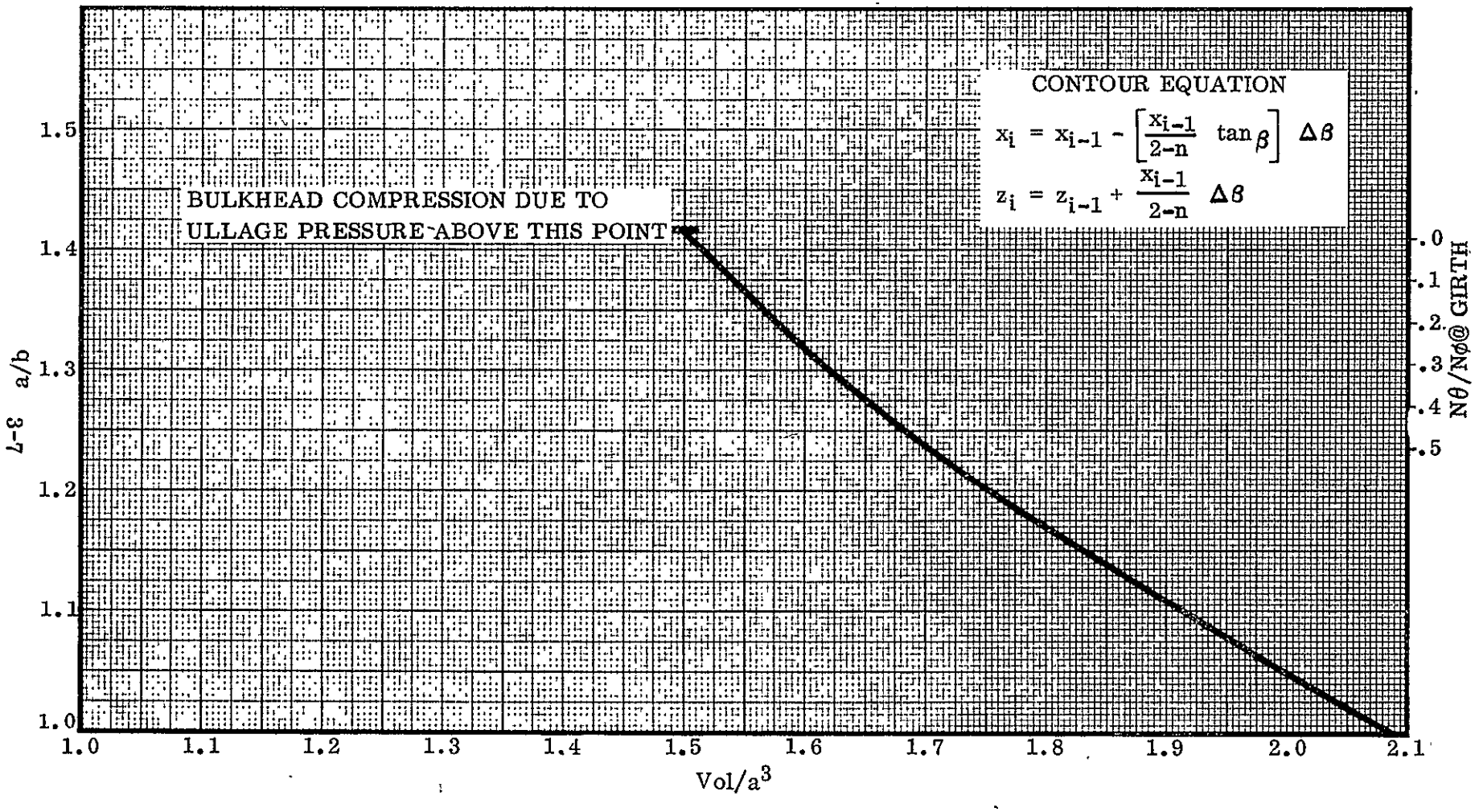

Figure 3-6. Controlled N_θ/N_ϕ volumetric sensitivity.

The data from these curves was then used to develop tank length effects. Figure 3-7 presents a comparison of total tank length (LO_2 plus LH_2 tanks) using the various contour classes based on fixed tank volumes. As can be seen the short tank systems can be obtained by selecting the highest acceptable aspect ratio for a given contour class. The cutoff points for each contour class are defined in Table 3-1. Elliptical ($a/b = \sqrt{2}$) and Controlled N_θ/N_ϕ bulkheads result in almost equal length vehicles whereas torispherical and Cassinian bulkheads would result in vehicles approximately three tenths of a meter longer than the baseline tug using the same propellant volumes. Therefore, the torispherical and Cassinian bulkheads was not considered in further studies for the total tankage systems. The primary virtue of the Cassinian bulkhead is its non-discontinuity feature in the transition to a cylindrical section. This becomes a handicap in the LO_2 tank which normally would not have a cylindrical section but in the LH_2 the size of Cassinian bulkheads results in the shortest LH_2 tank. Therefore, the Cassinian bulkhead contour was continued as a candidate for the LH_2 tank.

Table 3-1. Design concepts preliminary bulkhead contour review.

(No Compression)	Cassinian N = 1.92	Torispherical A/B = 1.31	(Baseline) Elliptical A/B = $\sqrt{2}$	Controlled $N\theta/N\phi$ $N\theta/N\phi$ .0 → 1
LH_2 Tank:				
L	4.35 (171.3)	4.56 (179.4)	4.43 (174.5)	4.41 (173.6)
D	4.29 (169.0)	4.29 (169.0)	4.29 (169.0)	4.29 (169.0)
Area	65.9 (102,200)	65.7 (101,835)	65.8 (102,020)	65.5 (101,507)
LO_2 Tank:				
L	2.91 (114.7)	2.74 (107.9)	2.58 (101.8)	2.58 (101.6)
D	3.22 (127.1)	3.59 (141.4)	3.65 (144.0)	3.64 (143.3)
Area	33.6 (52,170)	33.9 (52,523)	34.1 (52,880)	33.8 (52,453)
Total:				
L	7.26 (286.0)	7.30 (287.3)	7.02 (276.3)	6.99 (275.2)
Area	99.6 (154,370)	99.6 (154,358)	99.9 (154,900)	99.3 (153,960)

Units:

L - m (in)
D - m (in)
Area - m^2 (in^2)

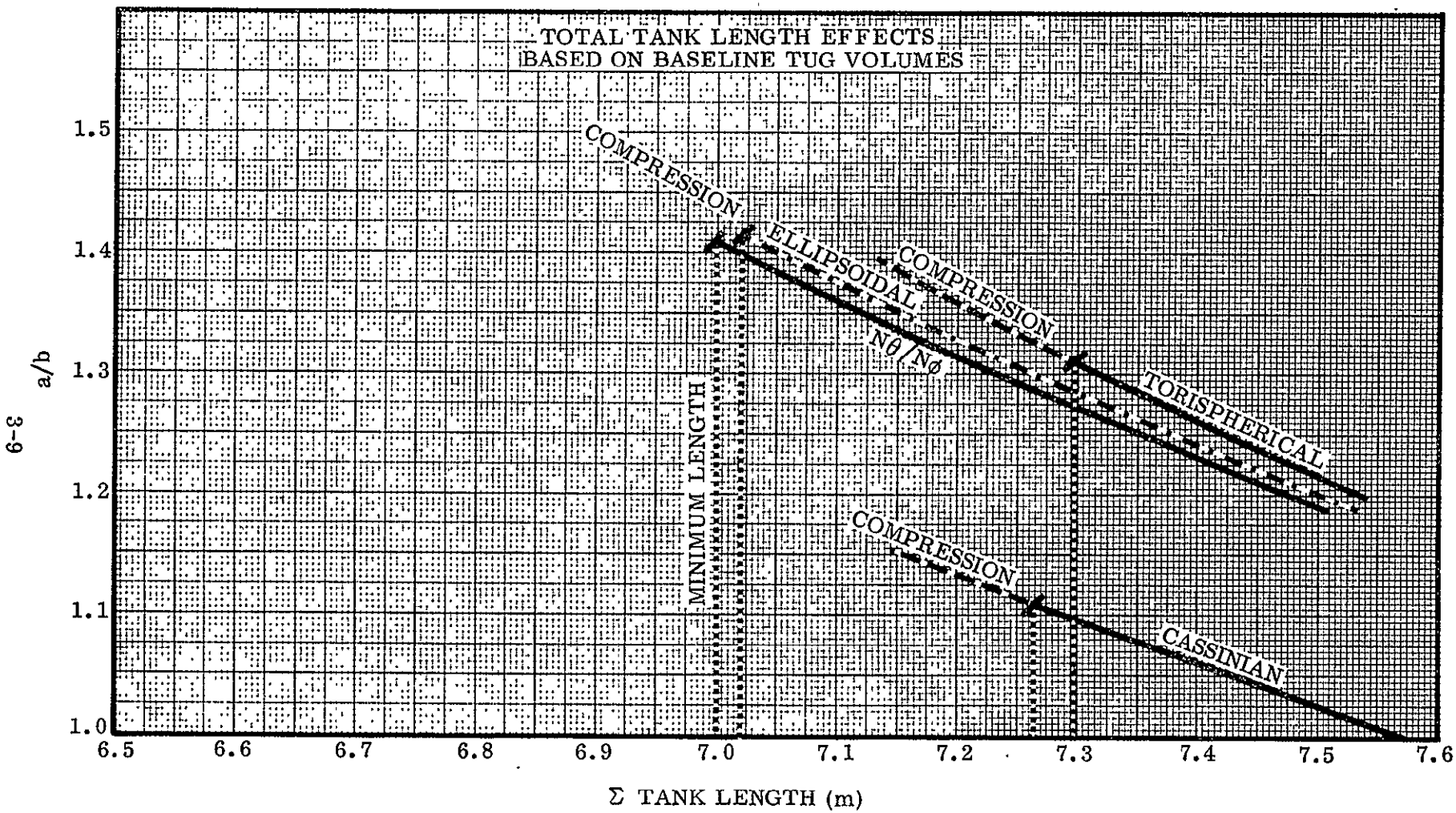

Figure 3-7. Total tank length effects based on baseline Tug volumes.

3.2 INTERRELATIONSHIP OF CONTOUR, PROPELLANT INERTIA, AND ULLAGE PRESSURE

A propellant tank parametric weight data desk computer program was developed to analyze the various tank contour configurations and develop tank size and weight data to evaluate total Tug effects. A simplified flow chart for this program is shown in Figure 3-8.

The basic program will analyze a tank with controlled N_θ/N_ϕ, ellipsoidal or Cassinian bulkheads based on the following characteristics, which can be varied as the operators desire:

a. Bulkhead caps diameter
b. Material allowable
c. Material density
d. Minimum gage
e. Propellant density
f. Tank maximum radius
g. Height of propellant in tank
h. Ullage pressure
i. Acceleration
j. Support system location
k. Cylindrical length

As indicated in Figure 3-8, several options are available for the selection of bulkhead geometry, program codes (which govern the type and quantity of output data), and tank bulkhead locations (forward or aft).

The program accommodates the choice of bulkhead contour "family" (ellipse, Cassinian, or controlled N_θ/N_ϕ ratio) through a unique subroutine (for each family) loaded separately from the basic program.

The output of the subroutine is a value for a parameter "n" which defines the relationship between hoop and meridional stress resultants (N_θ, and N_ϕ, respectively) at any point on the bulkhead surface and in so doing, defines the contour. The parameter is derived, based on elementary membrane theory, as follows:

P = total outward differential pressure acting on membrane

R_1 = principal radius of curvature of membrane in meridional (longitudinal) direction

R_2 = principal radius of curvature of membrane in hoop (circumferential) direction

$N_\phi = PR_2/2$ (stress resultant in meridional direction)

$N_\theta = PR_2\,(1 - R_2/2R_1)$ (stress resultant in hoop direction)

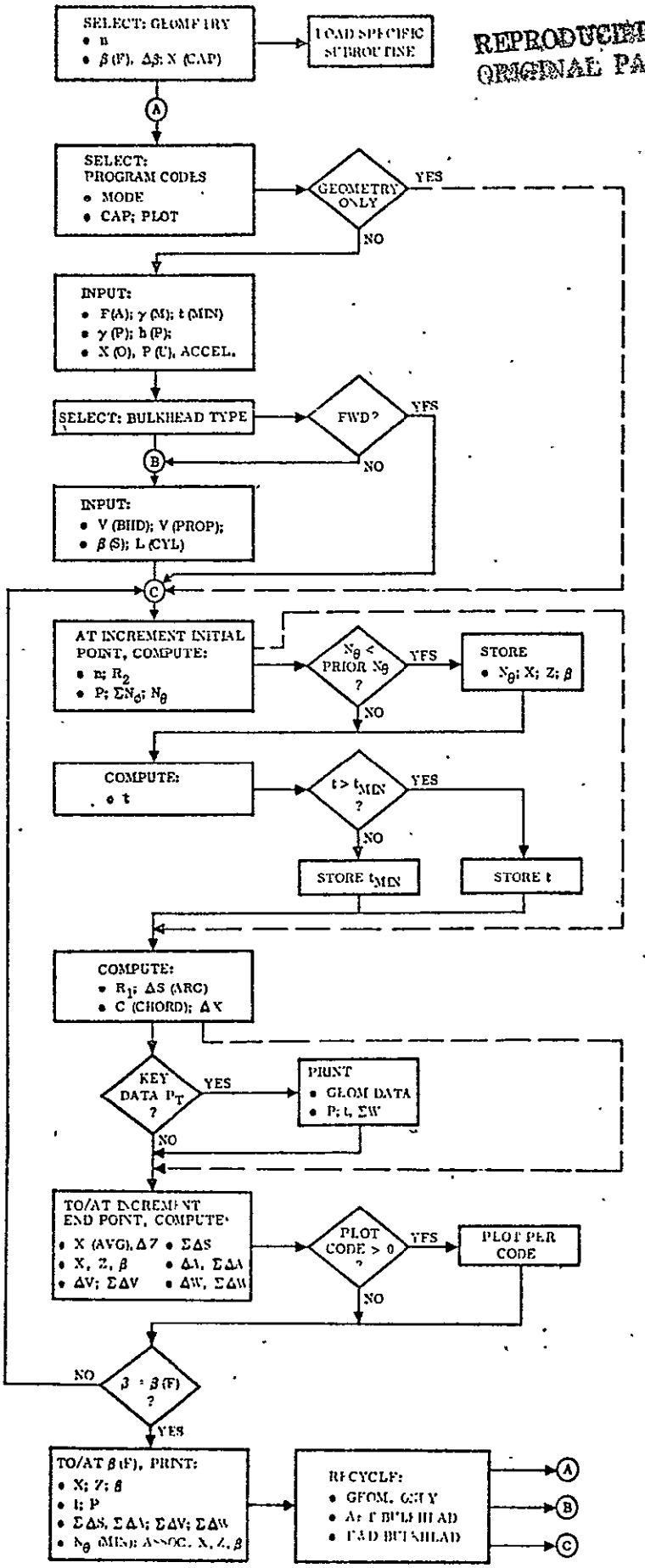

Figure 3-8. Program flow chart.

$$n = N_\theta/N_\phi = 2\left(1 - \frac{R_2}{2R_1}\right) = 2 - R_2/R_1 \text{ (contour parameter)}$$

The reason for the use of this parameter to define the contour is that it permits specification of a controlled relationship between stress resultants in order to avoid hoop compression in the membrane. Furthermore, by simple manipulation of the equation for n, low bulkhead height can be achieved.

This approach was originally developed early in this study to investigate the controlled N_θ/N_ϕ contour family which in turn is an outgrowth of earlier Convair studies of constant force ratio contours ($N_\theta/N_\phi = C$). Among these $C = 0$ was the contour of primary theoretical interest since it exhibited zero hoop stress throughout. However, all constant force ratio contours required a transition to a spherical cap at some point approaching the bulkhead apex in order to satisfy the necessary condition that $N_\theta = N_\phi$ at the apex.

This requirement for a step function (discontinuous) change in N_θ/N_ϕ ratio implied substantial discontinuity weight penalties in the shallower bulkheads and led to the concept of contours based on a continuously varying n which might exhibit low height, provide sphericity (i.e., $n = 1$) at the apex, and avoid hoop compression due to both ullage pressure along ($n > 0$) and due to fluid axial inertia (by tailoring the equation for n).

Subsequently it was also found that relatively simple (continuous) expressions for the parameter n could be developed for both the ellipse and Cassinian contours. Therefore, a single computer program, based on incremental construction of the contour from girth toward apex, using the parameter n, could be developed. By suitable choice of increment size ($d\beta$) very close agreement of all geometrical characteristics (height, arc length, surface area and volume) can be obtained with those computed from closed-form ellipse and Cassinian contour equations.

In addition to the basic contours from girth to apex, an option to incorporate a spherical cap from X (CAP) to the apex has also been incorporated and is selected by means of the cap code as indicated.

Sample program output data is shown in Figures 3-9, 3-10, and 3-11 for bulkhead tangent angles, membrane loads and volumes.

Tank Design Conditions which are required as input data for the various contour programs were developed. Of primary importance is the determination of potentially critical load conditions with the appropriate combinations to tank ullage pressure, axial acceleration and propellant quantity (volume, liquid level) associated with each.

Potential tank design loading conditions were analyzed with respect to each candidate configuration to determine which load condition would produce the maximum weight

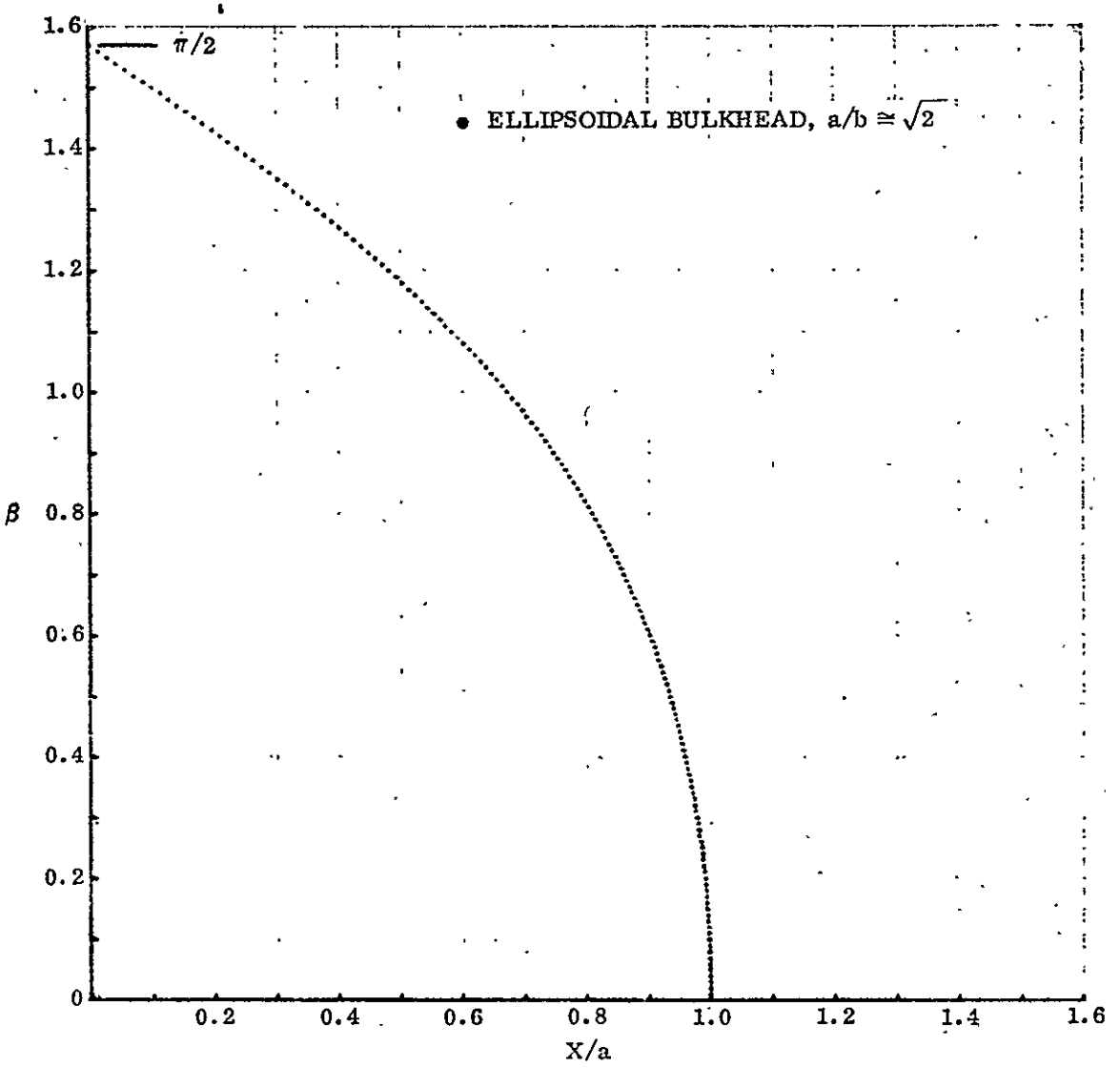

Figure 3-9. Ellipse, a/b = $\sqrt{2}$, tangent angle (β) versus radius.

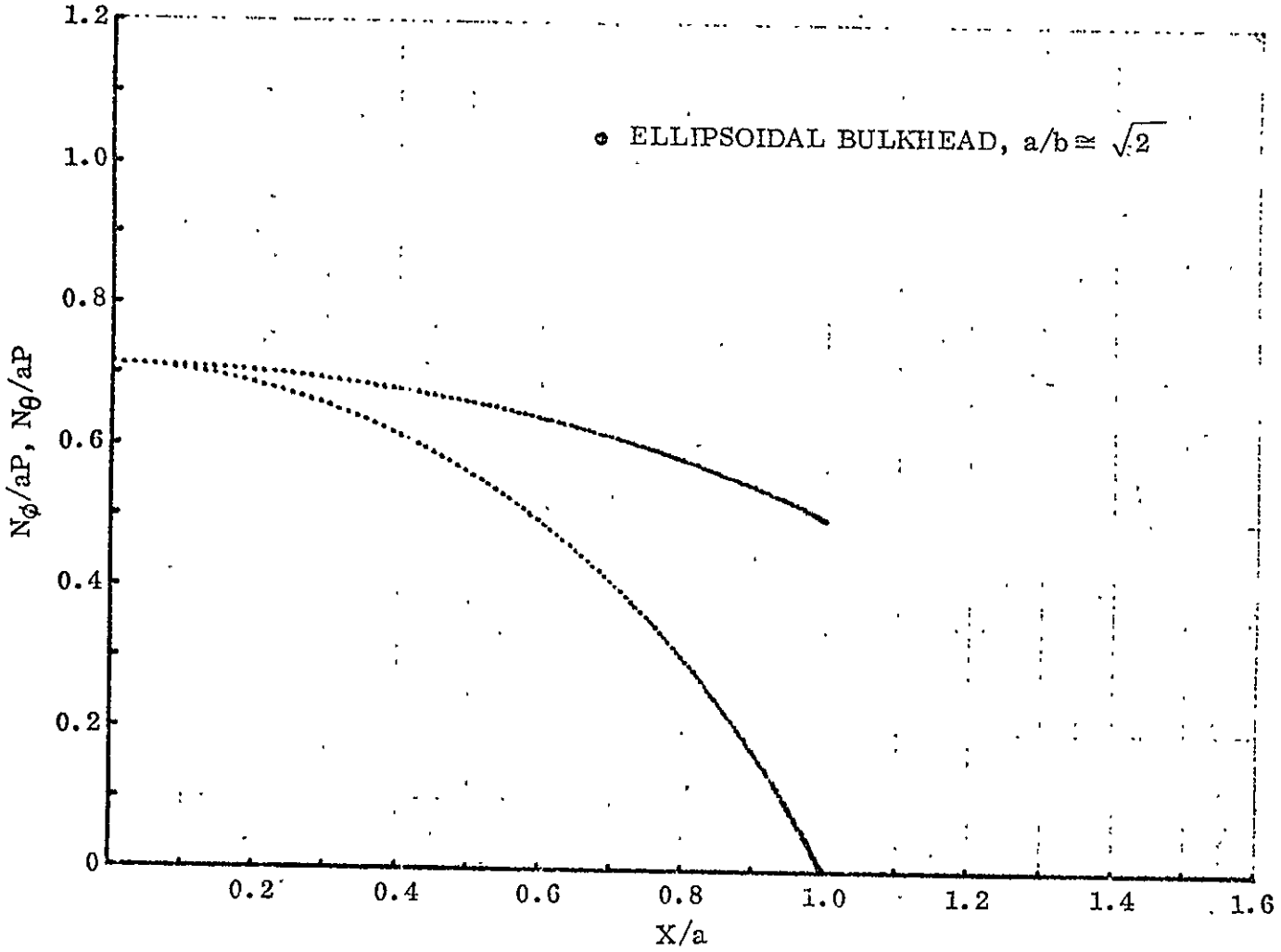

Figure 3-10. Ellipse, $a/b = \sqrt{2}$, membrane line loads versus radius.

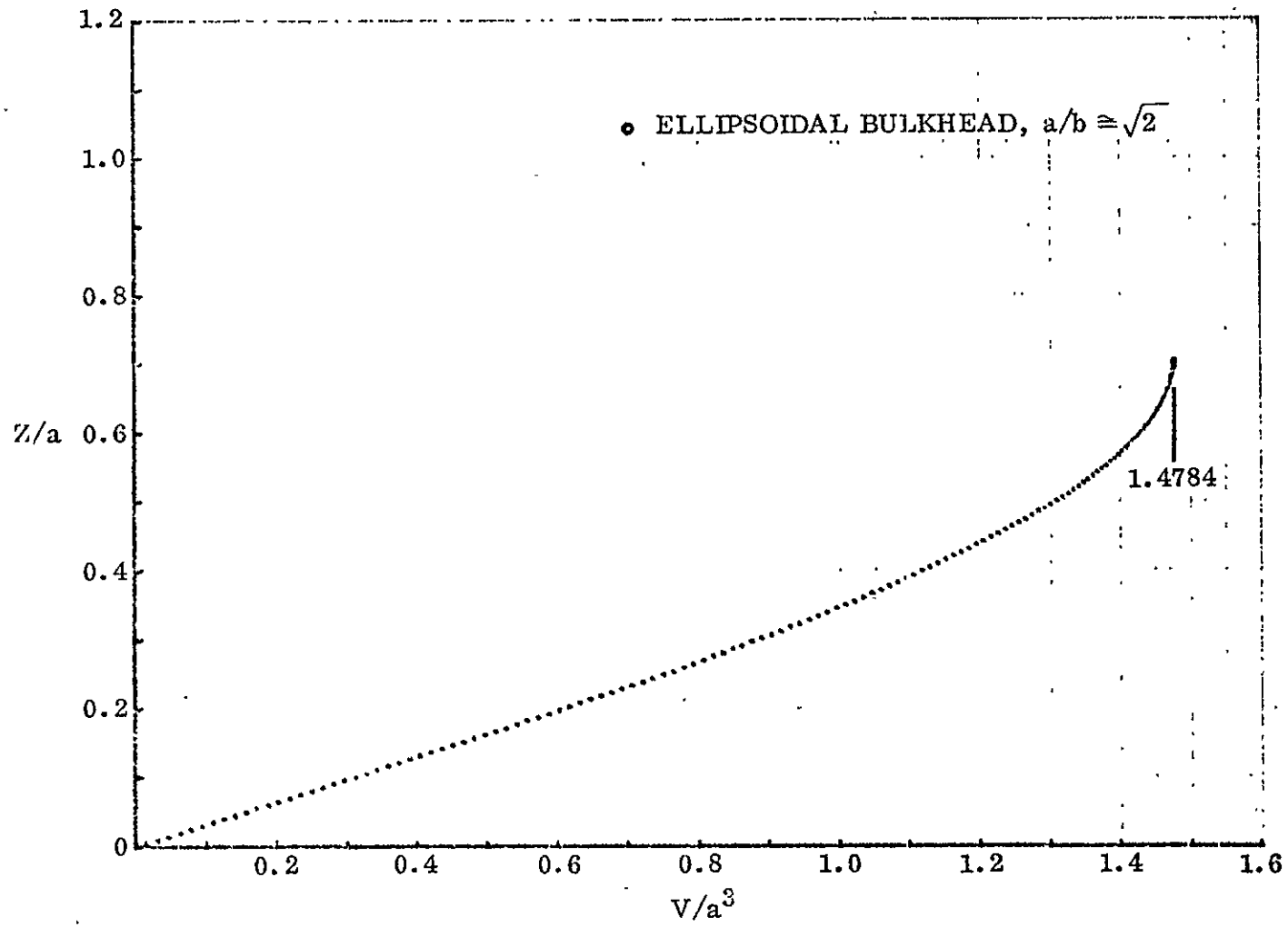

Figure 3-11. Ellipse, a/b = $\sqrt{2}$ height versus volume.

tank for each configuration. In this way the loading condition drivers for each candidate configuration was identified for use in further configuration definition studies. Tank design loading conditions derived from Design Requirements (PD75-0044) are tabulated in Table 3-2, Propellant tank pressures and accelerations.

Table 3-2. Propellant tank pressures and accelerations.

Condition	Differential Pressures, N/cm^2 (psi)				Acceleration	
	Oxidizer Tank		Fuel Tank			
	Max	Min	Max	Min	Max	Min
Tanking	0.896 (1.30)	0.896 (1.30)	1.45 (2.10)	1.45 (2.10)	1.00	1.00
Liftoff	2.01 (2.92)	1.70 (2.46)	2.85 (4.14)	2.50 (3.62)	2.90	0.30
Max G (Orbiter)	11.72 (17.00)	11.03 (16.00)	12.27 (17.80)	11.58 (16.80)	3.15	2.85
Abort	15.17 (22.00)	14.48 (21.00)	13.72 (19.90)	13.03 (18.90)	3.00	1.00
Tug OPS						
Start Burn 1	15.17 (22.00)	14.48 (21.00)	13.72 (19.90)	13.03 (18.90)	0.26	0.26
End Burn 1	15.17 (22.00)	14.48 (21.00)	13.72 (19.90)	13.03 (18.90)	0.35	0.35
2	15.17 (22.00)	14.48 (21.00)	13.51 (19.60)	12.82 (18.60)	0.45	0.45
3	15.17 (22.00)	14.48 (21.00)	13.17 (19.10)	12.48 (18.10)	0.67	0.67
4	15.17 (22.00)	14.48 (21.00)	13.72 (19.90)	13.03 (18.90)	1.20	1.20
5	15.17 (22.00)	14.48 (21.00)	13.20 (19.15)	12.51 (18.15)	1.57	1.57
6	15.17 (22.00)	14.48 (21.00)	13.17 (19.10)	12.48 (18.10)	2.11	2.11

Since all "controlled N_θ/N_ϕ" candidates are similar to a $\sqrt{2}$ ellipse in terms of volume, surface area, height, etc., the $\sqrt{2}$ ellipse was used as the reference contour for defining the driving condition. For tank weights the actual contour is used.

The Cassinian contour candidates are considerably deeper than all other candidates therefore, the $N_c = 1.92$ was used as the fuel tank reference contour.

The method used for determining the driving load condition is outlined below:

1. Select load (pressure and accelerations) combinations from Table 3-2.
2. Consider only full tank Tug operations case.
3. Select contour definition data (min. gage = 0.064 cm).
4. Run tank weight program for each combination (load condition and contour).

The results of this study are tabulated in Table 3-3 and are covered in the following discussion:

a. Oxidizer tank forward reference bulkhead is minimum gage throughout. However, for flatter N_θ/N_ϕ shapes the thickness near the apex may exceed t_{min}. Therefore, the Tug OPS (full) case is used for oxidizer tank forward bulkhead weight.

Table 3-3. Reference tank membrane weight for design load conditions.

Bulkhead Contour	Characteristics	Load Condition	Oxidizer Tank			Fuel Tank			
			Forward	Aft	Total	Forward	Cyl	Aft	Total
Ellipse	$\sqrt{2}$	Max G (Orbiter)	30.59 (67.45)	31.27 (68.95)	61.86 (136.40)	42.27 (93.18)	47.22 (104.10)	42.09 (92.80)	131.38 (289.67)
		Tug OPS (full)	30.59 (67.45)	30.59 (67.45)	61.18 (134.90)	42.08 (92.78)	50.75 (111.89)	42.09 (92.80)	134.92 (297.47)
Cassinian	1.92	Max G (Orbiter)	—	—	—	55.96 (123.37)	15.70 (34.61)	56.71 (125.03)	128.37 (283.01)
		Tug OPS (full)	—	—	—	56.99 (125.65)	17.00 (37.48)	57.07 (125.81)	131.06 (288.94)
Ellipse	$\sqrt{2}$	Tug OPS Burn 1	30.59 (67.45)	30.59 (67.45)	61.18 (134.90)	42.08 (92.78)	50.73 (111.83)	42.09 (92.79)	134.90 (297.40)
		2	—	—	—		49.92 (110.05)	42.08 (92.77)	134.08 (295.60)
		3	—	—	—		48.57 (107.07)	42.08 (92.77)	132.73 (292.62)
		4	30.59 (67.45)	30.59 (67.45)	61.18 (134.90)	42.08 (92.78)	50.60 (111.55)	42.09 (92.79)	134.77 (297.12)
Cassinian	1.92	Tug OPS Burn 1	—	—	—	56.99 (125.65)	16.98 (37.44)	57.05 (125.77)	131.02 (288.86)
		2	—	—	—		16.71 (36.84)	56.69 (124.99)	130.39 (287.48)
		3	—	—	—	56.99	16.27 (35.88)	56.14 (123.77)	129.40 (285.30)

b. Oxidizer tank aft bulkhead is minimum gage for all Tug OPS cases (full and Burns 1 through 4) whereas it is somewhat heavier for the Max G case due to increased thickness near the apex. Therefore, the Max G case is used for oxidizer tank aft bulkhead weight in all contours and Tug OPS (full) case is used as a check for flattest N_θ/N_ϕ contour.

c. Elliptical fuel tank forward bulkhead is essentially minimum gage throughout for the two conditions - Max G and Tug OPS. However, the thickness near the apex may exceed t min. in flatter N_θ/N_ϕ shapes. Therefore, the Tug OPS (full) is used as a check case for ellipse and N_θ/N_ϕ forward bulkhead weight.

d. Elliptical fuel tank aft bulkhead is very slightly heavier than minimum gage forward bulkhead but it is also minimum gage throughout (based on t data on calculator output tapes) for both Max G and Tug-OPS cases. However, the pressure at girth, which dictates cylindrical sidewall sizing, is greater for the Tug OPS case. Further, since LH_2 is very light, head pressure differences between various contours is negligible (since all tanks fall within a relatively small total length band) and Max G case will result in minimum gage aft bulkhead for all contours, whereas (as above) N_θ/N_ϕ shapes may exceed t_{min} near apex. Therefore, the Tug OPS (full) case is used for ellipse and N_θ/N_ϕ aft bulkhead weight and for defining pressure to be used in sizing cylindrical sections.

e. Cassinian fuel tank forward bulkhead is approximately one kilogram heavier for Tug OPS (full) case than for the Max G case (due to greater thickness at both girth and apex). Therefore, the Tug OPS (full) case is used for Cassinian fuel tank forward bulkhead.

f. Cassinian fuel tank aft bulkhead is also heavier for the Tug OPS case than for the Max G case due to greater girth and apex thicknesses. Also, the Tug OPS full case results in a heavier bulkhead than any of the Tug OPS end burn cases. Furthermore, the Tug OPS (full) case exhibits higher pressure at the girth, which results in a heavier cylindrical section. Therefore, the Tug OPS (full) case is used for Cassinian fuel tank aft bulkhead weight and for defining pressure to be used in sizing cylindrical section.

g. A summary of critical conditions for membrane weight is shown in Table 3-4.

3.3 SUPPORT STRUT ARRANGEMENT AND GEOMETRY

The support system affects the design of the tank at the strut-to-tank interfaces, where bracket weldments and increased thickness are required. To determine the minimum weight system, these weldments weights, strut weights, and resulting boiloff must be considered.

The loads in the struts, strut lenghts, tank clearances, and shell support frame locations are all functions of the strut plane tangency angle and the angle between the struts in a pair. The basic geometry used in the support analysis for a single pair of struts is defined in Figure 3-12.

Table 3-4. Summary of critical conditions for membrane weights.

Contour	Tank	Bulkhead	Critical Case	$P_{(ULL)}$ N/m^2 (psi)	Acceleration
Ellipse and N_θ/N_ϕ	Fuel	Forward	Tug OPS (full)	13.72 (19.90)	0.26
		Aft		13.72 (19.90)	0.26
	Oxidizer	Forward	Tug OPS (full)	15.70 (22.00)	0.26
		Aft	Max G (Orbiter)	11.72 (17.00)	3.15
		Aft	Tug OPS (full)	15.17 (22.00)	0.26
Cassinian	Fuel	Forward	Tug OPS (full)	13.72 (19.90)	0.26
		Aft	Tug OPS (full)	13.72 (19.90)	0.26

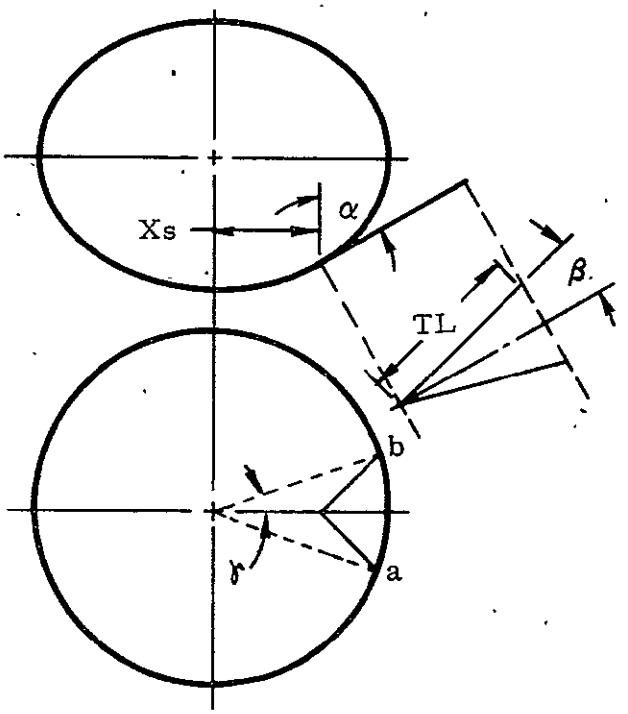

α - strut pair slope tangent to the tank

β - half angle between struts

γ - angle formed by lines passing through the shell ring strut intercepts and the center of the tank

Xs - radius to strut/tank intercept point

TL - true length of strut from tank tangent point to shell support ring intercept

Figure 3-12. Basic support strut geometry.

The strut tangency angle affects the location of the shell support frame, which is also the separation frame in the case of the LO_2 tank. Therefore, a parametric curve was developed for the location of this separation frame as a function of the strut tangent angle, β, see Figure 3-13. This information was necessary to determine the Tug shell weight variation with respect to strut geometry.

There is a substantial difference between the actual support strut length and the theoretical true length from the tank tangency point to the pierce point on the middle surface of the body sidewall, because of the need to provide clearance between the strut end fittings and the adjacent surfaces of the tanks, body sidewall, and body support frame webs.

The portion of the true length which must be allocated to the body shell attach fitting is essentially constant (i.e., independent of the slope of the strut relative to the body). The same is not true at the tank attachment fitting. Due both to the tangential approach of the strut and the double curvature of the tank surface, the distance along the strut axis from the tangent point (TP) to a point at which sufficient clearance is available for strut attachment varies as a function of both α and β. The length of the attachment fitting on the tank dictates both the size of the weld pad and the minimum permissible width of the belly-band upon which the fittings are mounted.

Support system weight varies not only due to load (which is a function of α and β) but also due to the relative lengths of support struts and tank fittings.

Families of curves were developed which defined the usable length of the theoretical strut true length; i.e., from the shell pierce point to the tank tangency point (as a function of strut slope). These curves are presented in Figure 3-14. These data are based on the distance along the strut centerline from the tangency point to a point where sufficient clearance exists to allow for strut end fitting radius, fitting clearance (gap), bracket base, weld pad thickness, and nominal membrane thickness.

To size the cross section of the struts, the loading conditions were analyzed to determine the conditions which produce maximum tension and compression loads as well as the loads direction which produces the greatest load resultants. The strut loading conditions were defined by the following equations:

Load due to axial forces:

$$F_A = \frac{W}{N} \left[\frac{1}{\cos \alpha \cos \beta} \, n_x \right]$$

Load due to overturning moments:

$$F_{Mi} = \frac{2Wd}{NXs} \left[\frac{1}{\cos \alpha \cos \beta} \right] \sin \theta \, (n_{lat})$$

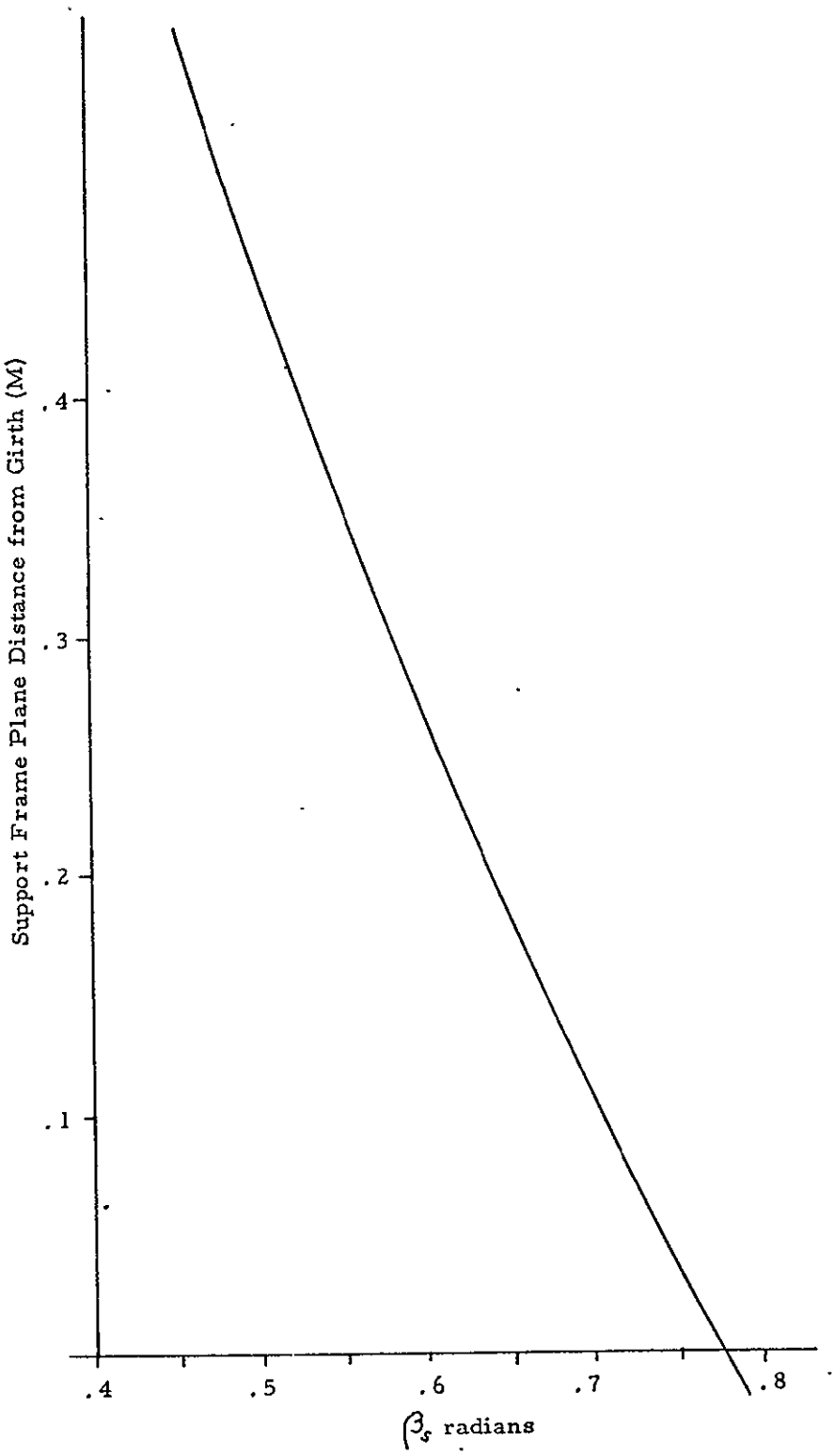

Figure 3-13. Oxidizer shell frame location.

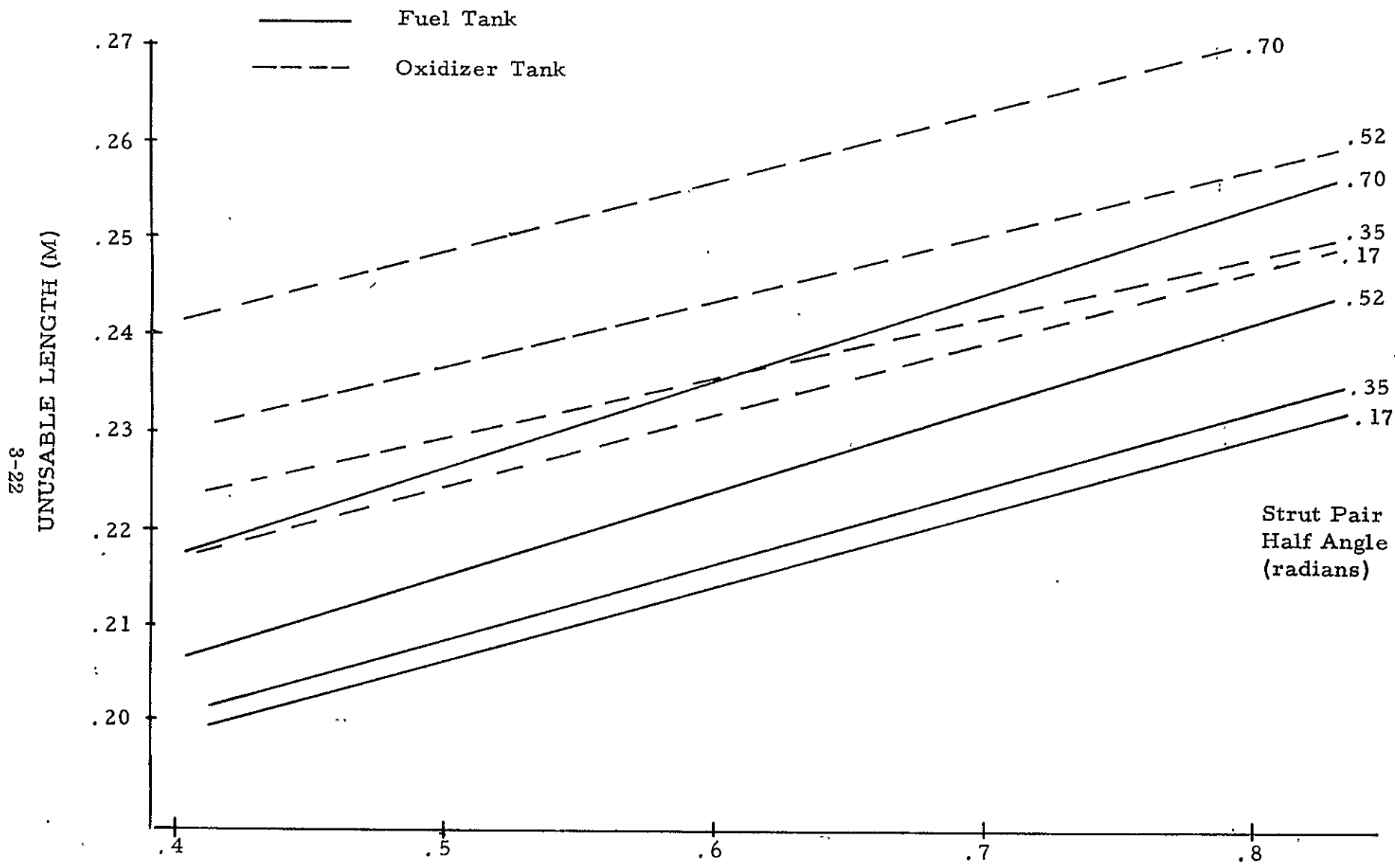

Figure 3-14. Unusable portion of strut true length.

Load due to side forces -

$$F_{Li} = \frac{W\,(n_{lat})}{2} \quad \frac{Ki}{\Sigma Ki} \left[\frac{\cos \phi}{\sin \alpha \cos \beta} \pm \frac{\sin \alpha}{\sin \beta} \right]$$

where

$$Ki = \frac{AE}{L} \left[\frac{2}{\left(\frac{\cos \phi}{\sin \alpha \cos \beta} \right)^2 + \left(\frac{\sin \phi}{\sin \beta} \right)^2} \right]$$

W = propellant weight

N = number of struts

n_x = axial load factor

n_{lat} = lateral load factor

d = distance from strut plane to longitudinal c.g. location

Xs = radius to strut tangency point

A = strut cross-sectional area

E = strut material modulus

L = strut length

θ = load angular direction in plane of struts

The baseline oxidizer strut configuration was used to determine the load sensitivity. Tank support strut maximum loads will only occur during load cases with a full tank and significant axial and/or lateral accelerations. The following cases were considered for tank strut load maximization:

a. Liftoff - $n_x = 0.3$

$n_{lat} = 1.36$

b. Liftoff - $n_x = 2.9$

$n_{lat} = 1.36$

c. Maximum G - $n_x = 3.15$

$n_{lat} = 0.78$

(Ref PD75-0044, Requirements Document)

A typical strut loads envelope is shown in Figure 3-15. This case is for a sixteen strut system with the lateral load application midway between pairs of struts. The resultant load is a function of the clocking of the n_{lat} vector (θ) relative to the array of support pair node points. The maximum case was determined by testing the cases first where the load was in line with the centerline of a pair of struts and then halfway between two adjacent strut pairs. Load cases 1 and 2 (minimum and maximum axial loads at liftoff, respectively), produced the minimum and maximum strut load envelopes, while clocking the load direction between strut pairs produced the greatest reactions.

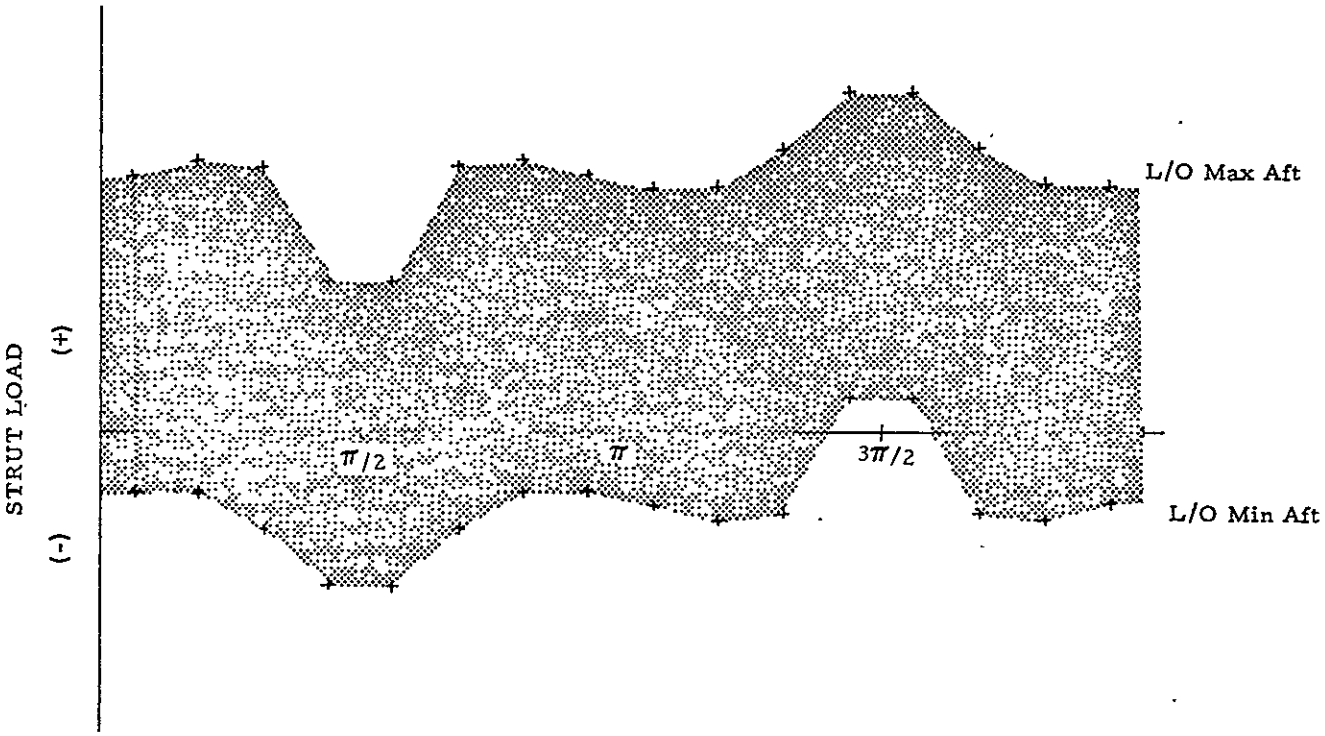

Figure 3-15. Strut load envelope.

To evaluate the LO_2 tank strut geometry effects on strut loads, a series of candidate arrangements were selected, as shown in Figure 3-16. Three basic strut patterns were considered: (1) a laced pattern where the strut centerlines intersected at the tank and the shell; (2) a half-space system where the strut from one pair were a half-space away from the next strut pair at the shell (one space being the distance between struts in a pair measured at the shell diameter); and (3) a full-space system where there are equal spaces between all struts at the shell diameter. Three strut plane slopes were considered: 0.7168 radians (baseline), 0.6109 radians, and 0.4363 radians. These slopes are the strut-to-tank tangency angles. Three strut quantities were considered: 20, 24, and 32.

Two strut materials were investigated, boron/epoxy (B/E) and glass/epoxy (G/E). Tables of strut lengths, stiffnesses and detail strut loads were developed as shown in Table 3-5.

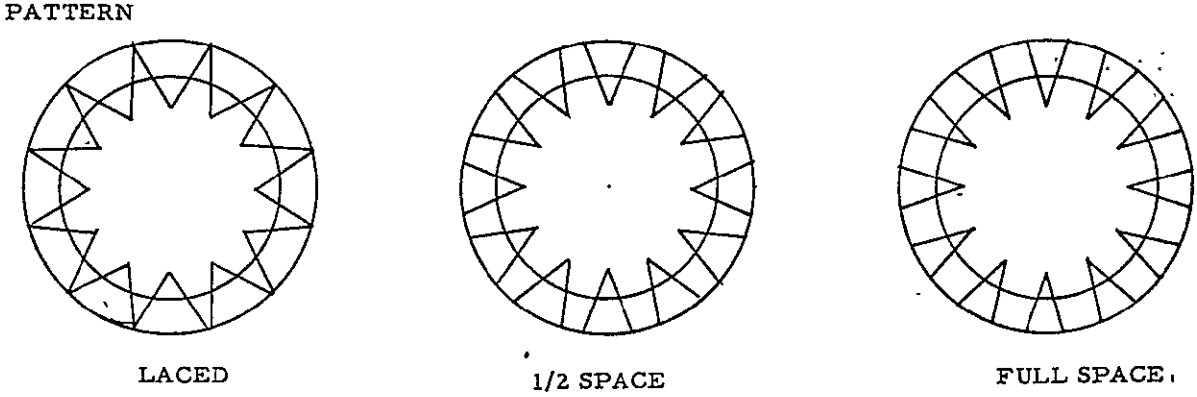

Figure 3-16. Strut geometries used in trades.

An initial screening of the fifty-four candidates was performed, resulting in the following observations.

a. Laced arrangement resulted in the stiffest system due to geometry.

b. Boron epoxy systems are strength-designed.

c. Glass epoxy systems are stiffness-critical in all cases except laced geometry.

d. Laced arrangement has the lowest compression loads for N = 32 and 24.

e. The groups with the baseline strut slope have the lowest load within the same strut quantity family.

f. The strut lengths in the groups with the slope equal to 0.611 and 0.762 are all essentially identical.

Based on these observations, three configurations were selected for further study: twenty-four struts for each configuration, with slopes of 0.762, 0.611, and 0.436 radian in a laced pattern.

The fuel tank support system was analyzed in a similar manner using the general approach outlined for the oxidizer tank. Since stiffness is not critical for this tank, only glass/epoxy was considered. The strut quantities considered were 12, 16, and 20, with the same slopes as those used for the LO_2 tank analysis. Tables 3-6 and 3-7 present fuel tank strut system sizing and weight data.

Occurrence of hoop compression depends on support location (dictated by β_S). The probability of encountering hoop compression increases as β_S decreases, since a greater mass of propellant is supported beneath the support plane and since the N_θ margin is lower (nearer zero) approaching the girth (for all ellipse and N_θ/N_ϕ contours).

The oxidizer tank is the major hoop compression concern, due to LO_2 density. The baseline Tug oxidizer tank support system slope is approximately 0.78 radian and

Table 3-5. Oxidizer support system strut sizing.

Strut Quantity	Slope (rad)	Configuration	Strut Length (M) Fitting to Fitting	K/(AE/L)	$F_{T_{Max}}$ (N)	$F_{C_{Max}}$ (N)
32	0.762	Laced	0.80	8.2696	42396	12361
	0.762	1/2 space	0.78	5.91550	52613	24091
	0.762	Full space	0.78	4.50441	63218	35203
	0.611	Laced	0.79	6.95259	44553	17944
	0.611	1/2 space	0.78	4.96367	53085	27872
	0.611	Full space	0.78	3.79855	64508	39753
	0.436	Laced	0.91	4.76034	49295	25016
	0.436	1/2 space	0.92	3.30999	57444	34843
	0.436	Full space	0.92	2.51382	71274	49006
24	0.762	Laced	0.81	7.46439	58334	15204
	0.762	1/2 space	0.79	5.66117	59722	20453
	0.762	Full space	0.78	4.40311	69868	31836
	0.611	Laced	0.80	6.28049	61016	22588
	0.611	1/2 space	0.79	4.75851	60291	25537
	0.611	Full space	0.78	3.71526	71332	37712
	0.436	Laced	0.89	4.43841	67711	33864
	0.436	1/2 space	0.91	3.22686	67310	36333
	0.436	Full space	0.92	2.48170	77933	47800
20	0.762	Laced	0.83	6.71904	75860	19964
	0.762	1/2 space	0.80	5.41658	67150	18465
	0.762	Full space	0.79	4.36342	68124	21654
	0.611	Laced	0.81	5.63133	80032	29812
	0.611	1/2 space	0.79	4.55447	70429	27259
	0.611	Full space	0.79	3.64086	73854	32752
	0.436	Laced	0.88	4.06357	87679	43619
	0.436	1/2 space	0.91	3.13747	76803	38517
	0.436	Full space	0.91	2.49805	84151	47431

its major diameter is 3.65 meters. Since the oxidizer tank diameter is considerably less than the Tug shell diameter, it is unlikely that small values of β_s will result in total tank weight optimization, as strut lengths and weights become prohibitive. A minimum slope of approximately 0.35 radian is realistic and compatible with the load optimization trades conducted in the Convair STSS effort.

Table 3-6. Fuel tank support system strut sizing.

Strut Quantity	Slope (radians)	Length (meters)	$F_{T\ Max}$ (Newtons)	$F_{C\ Max}$ (Newtons)
12	.436	.10	22552	5880
	.581	.18	18994	4564
	.698	.26	18086	3674
16	.436	.10	17295	4995
	.581	.18	14283	3461
	.698	.26	13656	2851
20	.436	.10	14061	4221
	.581	.18	11392	2736
	.698	.26	11067	2424

Individual strut weight*

Slope, rad	Strut Weight, Kg with Rod End
0.581	0.233
0.691	0.235

*Using minimum gage considerations, the individual strut weights for all configurations within a given slope are equal.

Table 3-7. Total LH_2 strut system weights (Kg).

n	β	Strut	Tank Effects	Boiloff	Σ
12	.581	2.80	6.12	.59	9.51
	.698	2.82	6.12	.432	9.37
16	.581	3.73	6.41	.78	10.92
	.698	3.76	6.41	.58	10.75
20	.581	4.66	7.24	.98	12.88
	.698	4.70	7.24	.72	12.66

Before a study of bulkhead membrane versus strut locations could be performed the critical loading conditions had to be determined. The method used for determining the critical load conditions for hoop compression in the oxidizer tank is outlined as follows:

a. Select the flattest contour in each group since these contours have least hoop compression margins

   ellipse, $a/b = \sqrt{2}$

   controlled N_θ/N_ϕ, $n_o = 0$, $M = 2.5$

b. Select minimum strut slope = 0.35 radian

c. Determine propellant volumes and heights for full, 3/4 full, 1/2 full, and 1/4 full. Results are shown in Table 3-8.

d. Develop N_θ data in localized compressive areas for each contour.

Table 3-8. Bulkhead liquid level and propellant volumes.
a = 2.146 m

	N_θ/N_ϕ ($N_o = 0$, m = 2.5)		Ellipse $a/b = \sqrt{2}$		Cassinian n = 1.92	
	Volume (m^3)	Z (m)	Volume (m^3)	Z (m)	Volume (m^3)	Z (m)
Full	13.94	1.38	14.62	1.51	21.35	1.94
7/8 Full	12.20	1.26	12.79		18.68	1.74
3/4 Full	10.45	1.14	10.96	1.25	16.01	1.57
5/8 Full	8.71	1.02	9.14		13.35	1.38
1/2 Full	6.97	0.89	7.31	0.98	10.68	1.19
3/8 Full	5.23	0.74	5.48		8.01	0.99
1/4 Full	3.48	0.58	3.65	0.66	5.34	0.78
1/8 Full	1.74	0.39	1.83	0.46	2.67	0.53

Loading condition effects are shown in Figure 3-17 for an elliptical $a/b = \sqrt{2}$ bulkhead contour. The effects on the controlled N_θ/N_ϕ contour are very similar. For both contours, tanking and liftoff are the critical conditions. The tanking condition boundary is an envelope of the individual N_θ distributions associated with various fill levels. A considerable region of the bulkhead experiences hoop compression for β = 0.35 radian. Increased ullage pressure alleviates the liftoff hoop compression somewhat.

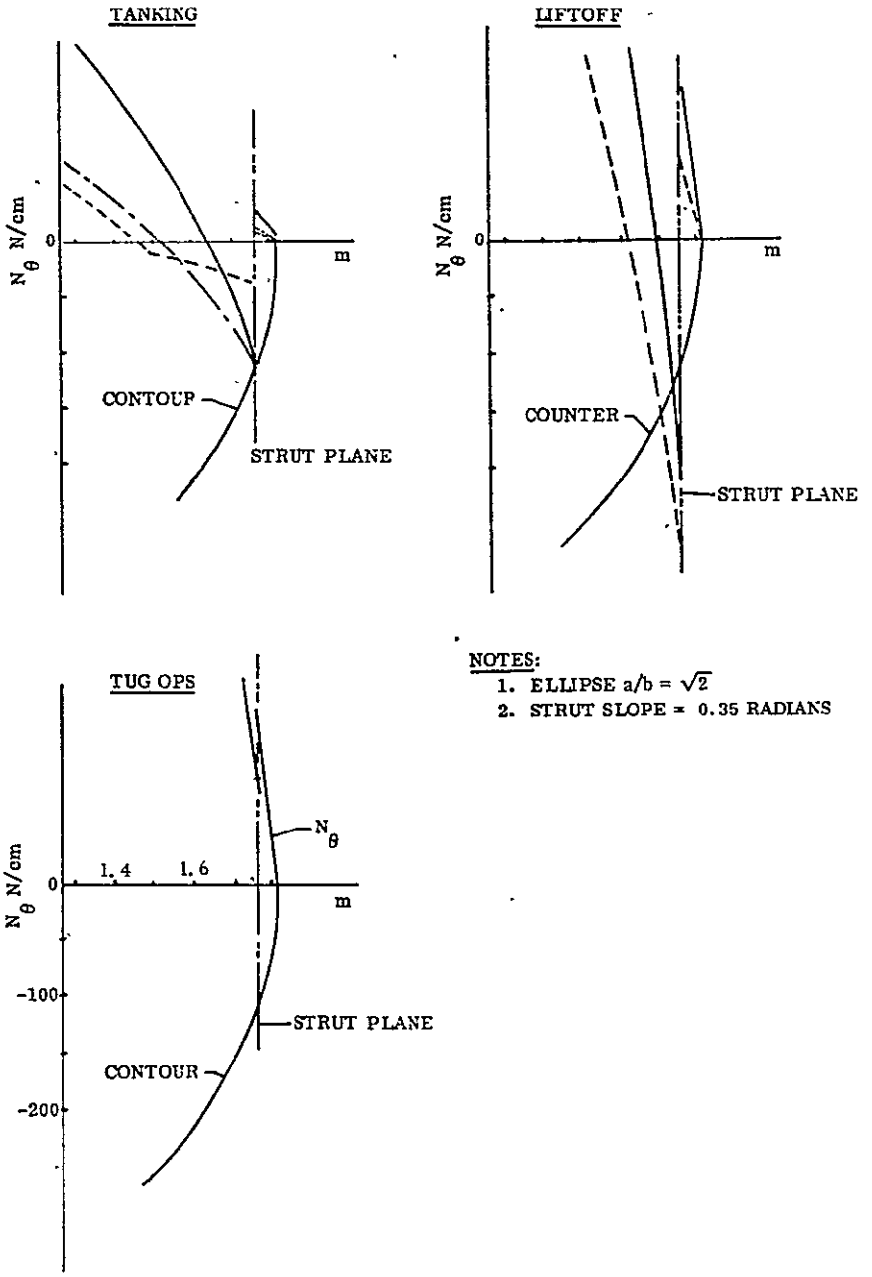

Figure 3-17. Critical hoop compression load condition analysis.

The effects of support slope (β_S) on hoop force variation was investigated for several potentially critical loading conditions as follows:

Support Slope (β_S)

0.76 radian (baseline configuration)

0.52 radian (STSS selection)

Load Conditions

Tanking (bulkhead 0.5 full)

Tanking (bulkhead 0.25 full)

Liftoff

The bulkhead analysis program results for the baseline oxidizer tank are shown in Figure 3-18. A close analysis of these curves shows identical curves of N_θ aft of the support plane. The step in the curves is due to the switch from "supporting" propellant mass outboard of the support plane to "holding up" the propellant mass inboard of the support plane, which is transferred to the support system. No step will occur in curves for $\beta_S = 0$. Therefore, a master curve can be prepared using the bulkhead program by assuming that the support plane is at the bulkhead girth. Then the location of the support plane may be selected either to an acceptable compression level, or such that no compression exists. This will define the acceptable tangency point.

The LH_2 tank was investigated using identical procedures.

As in the case of the oxidizer tank support, the flattest contours in each family were considered in an investigation of the fuel tank support system: ellipse $a/b = \sqrt{2}$; N_θ/N_ϕ, $n_o = 0$, $m = 2.5$; and Cassinian, $n = 1.92$. The bulkhead analysis program was run with $\beta_S = 0$ and the aft bulkhead full, 1/2 full, 1/4 full, and 1/8 full.

The program results are shown in Figure 3-19. For both the ellipse and N_θ/N_ϕ contours, liftoff and the full bulkhead tanking case produce the greatest hoop compression, with liftoff being the more severe of the two in both magnitude and extent. In both cases, however, the N_θ plot crosses zero at an X-coordinate corresponding to an unacceptably small β_S, based on the baseline shell frame depth and on a 1.896 cm clearance. Consequently, neither bulkhead will exhibit compression for permissible values of β_S. In the Cassinian contour, the same condition again produces the greatest hoop compression, with the liftoff again being the more severe. However, the hoop compression region is essentially centered on the baseline support slope X-coordinate. In this case, the tank frame clearance is 3.56 cm and, therefore, may represent an acceptable support configuration. The minimum permissible β_S to avoid compression lies well beyond the baseline value (approximately 0.70 radian).

The basic hoop characteristics of various ellipsoidal contours were investigated to determine the hoop compression loading trends. Three bulkhead a/b ratios were used: 1.25, 1.30, and 1.35. The bulkheads were assumed supported at the girth, and the critical loading conditions (tanking and liftoff) were used. The fundamental analytical results are shown in Figure 3-20.

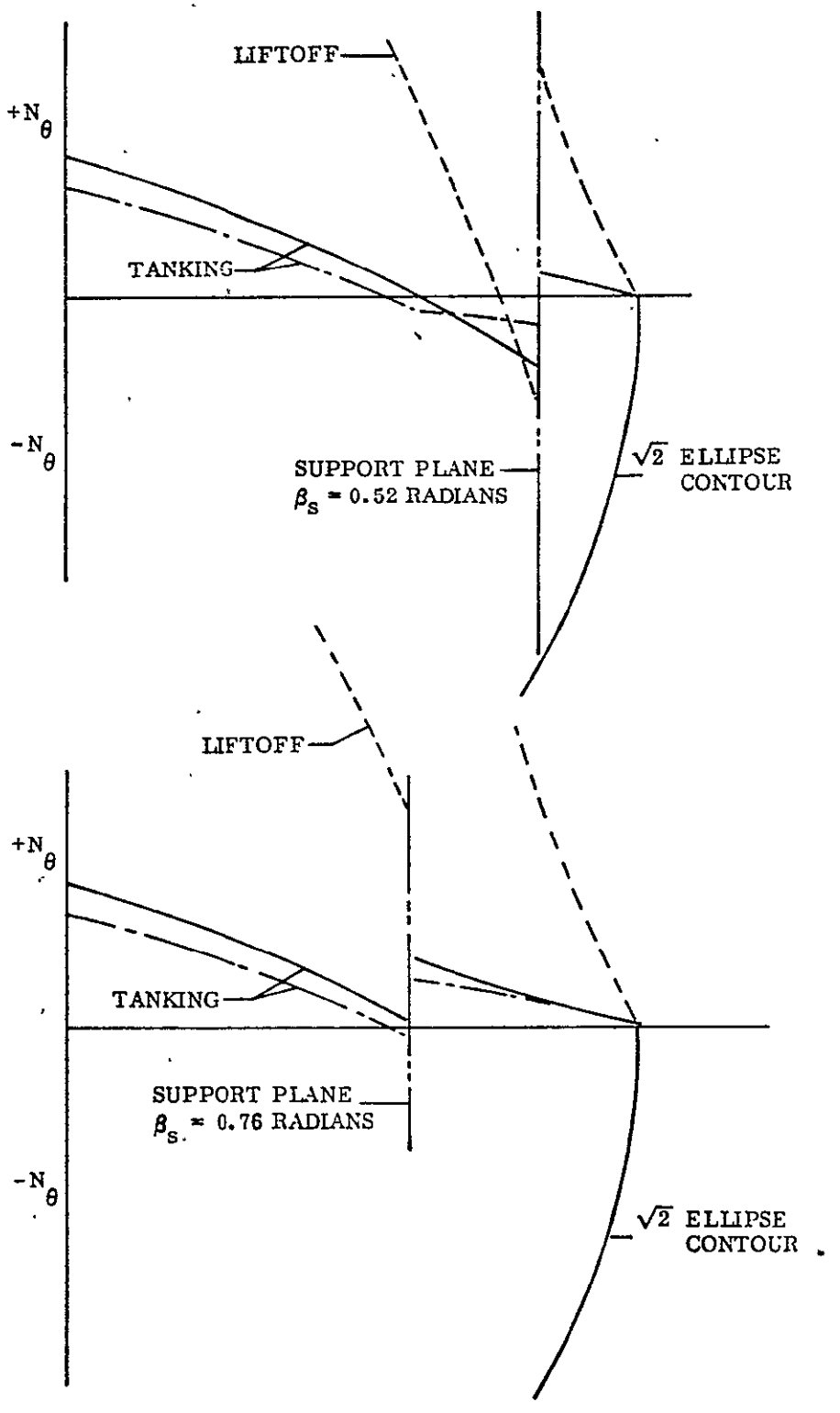

Figure 3-18. Support slope effects study.

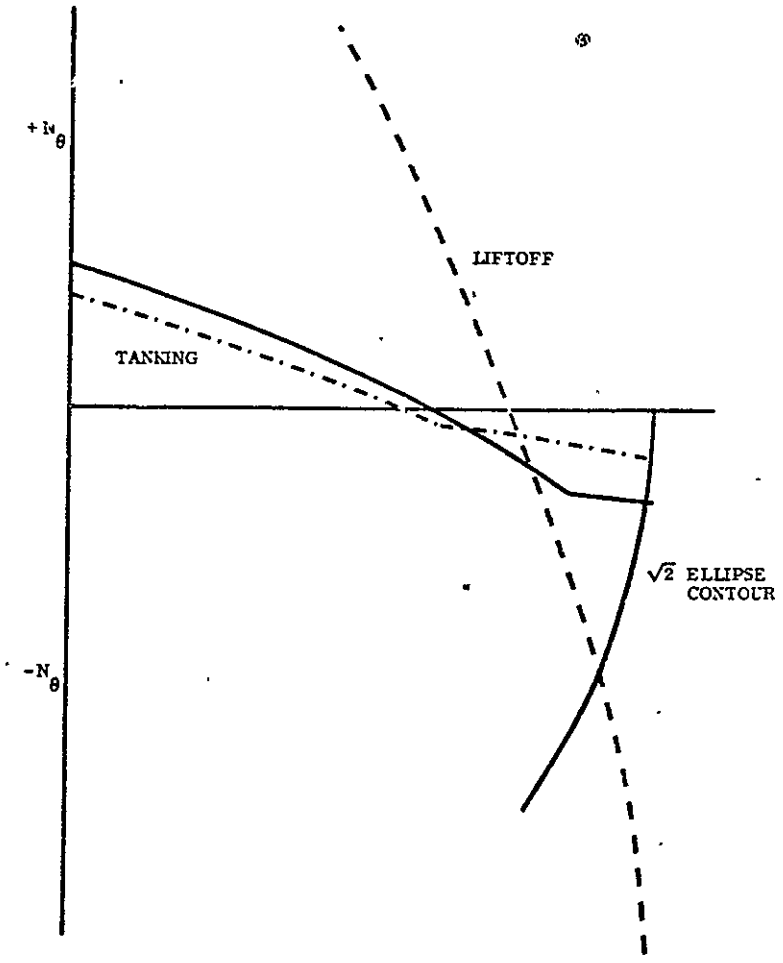

Figure 3-19. Master N_θ curve example.

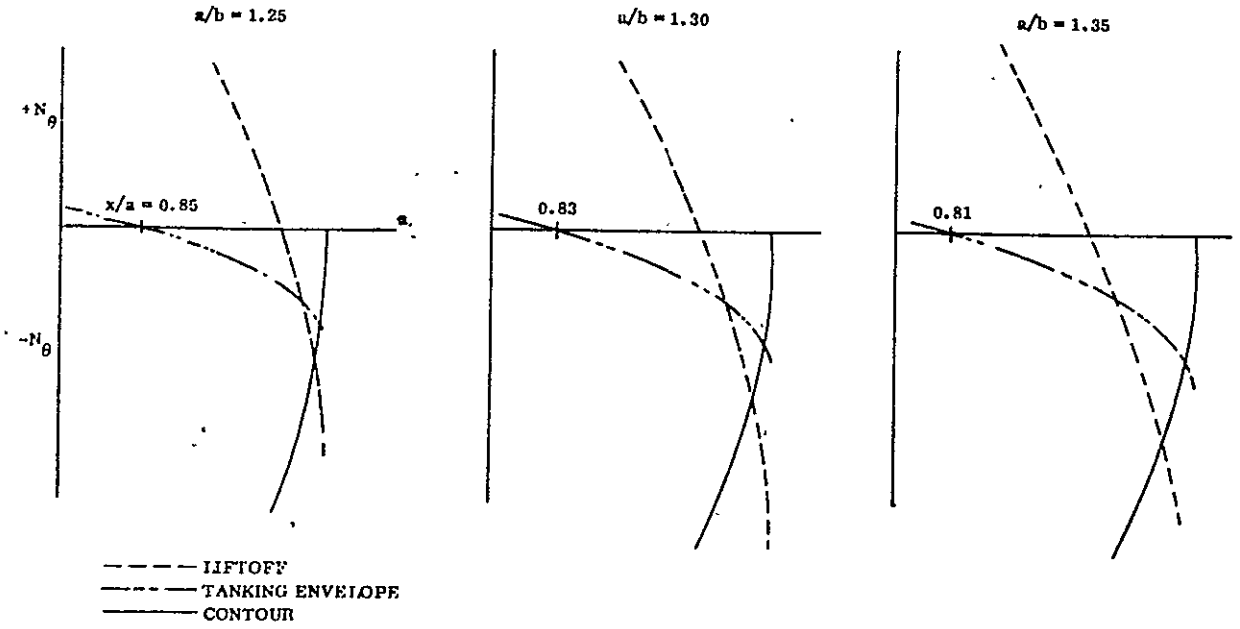

Figure 3-20. Hoop compression study for varying a/b ratios.

Based on these results, it can be seen that the load envelopes change as the contour changes, with a decrease in both magnitude and extent as a/b decreases. For the lift-off condition, the x-axis intercept shifts toward the girth with increased a/b ratios. The data thus developed was expanded to investigate the strut slope as a function of a/b, based on selected hoop compression allowables: $N_\theta = 0$, -43.8, and -87.6 N/cm. Figure 3-21 is a plot of points extracted from the original hoop compression study curves. This composite curve defines the smallest strut slope which can be used on a selected bulkhead (a/b from 1.25 to $\sqrt{2}$) based on acceptable values of hoop compression. The baseline configuration with $\beta_S = 0.76$ radian shows a slight hoop compression for a $\sqrt{2}$ bulkhead. The minimum β_S for a $\sqrt{2}$ bulkhead based on the $N_\theta = 0$ curve is 0.82 radian.

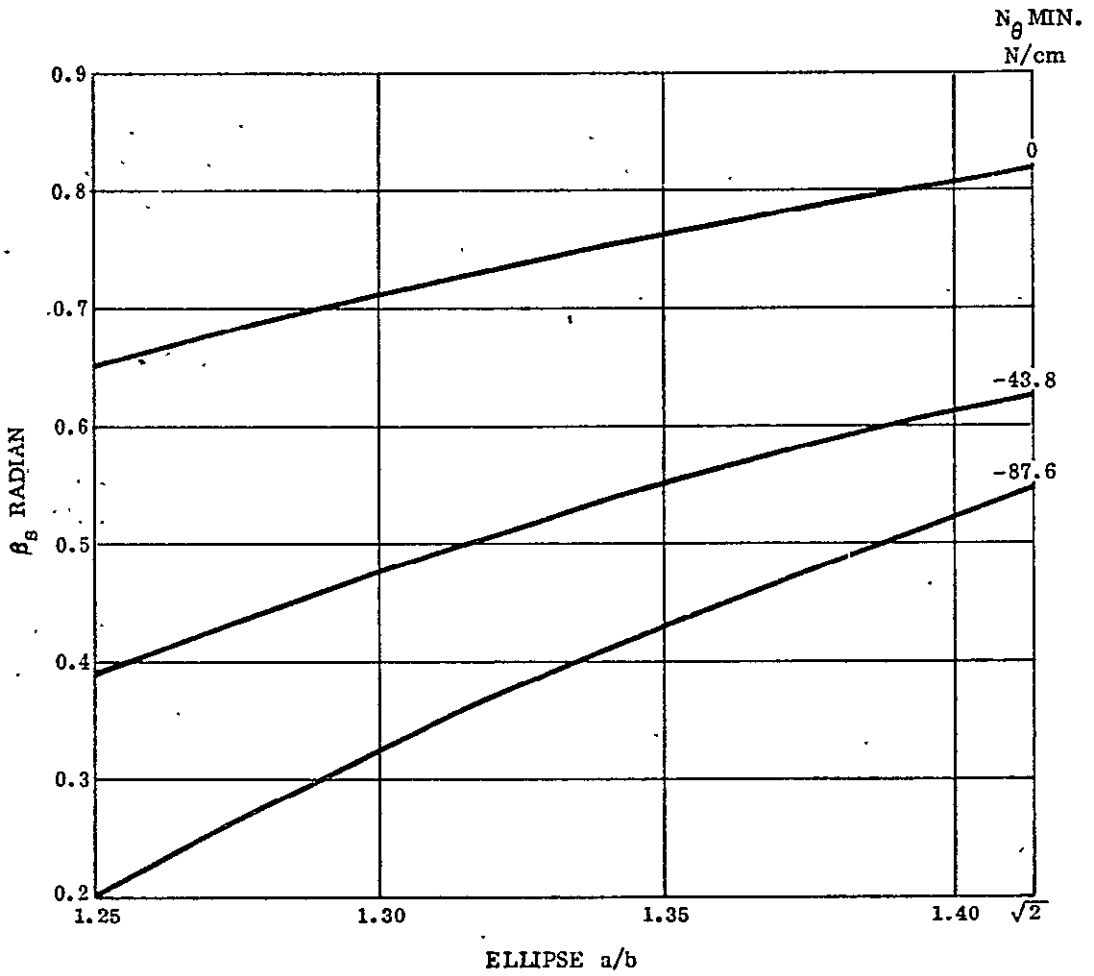

Figure 3-21. Minimum permissible support slope versus ellipse a/b.

A preliminary heat transfer analysis was performed on the support strut candidates using the following guidelines:

a. Two strut materials were used

   (1) glass fiber - epoxy composite

   (2) boron - epoxy composite

b. Thermal conductivity data was obtained from Reference 1 for glass fiber - epoxy, and from Reference 2.

c. Space thermal equilibrium conditions were used for analysis with both LH_2 and LO_2 tanks.

The cryogenic tank support struts for the Space Tug are essentially hollow tubes with structural attachment fittings in each end. The structural shroud end of the struts will generally attain an average temperature of approximately 520 R during space residency conditions. Under these conditions, various studies (References 3, 4, 5) have shown that "radiation tunnelling" down the strut can increase the heat leak down the strut many times above the value for conduction only. The use of radiation shielding in the tube, however, can reduce the radiation heat leak to a vanishingly small value, making the strut heat-leak mode conduction dominated. Multilayer insulation (MLI) and chopped dexiglass have been used successfully for this purpose by Convair and Lockheed (References 3 and 5). For strut performance screening purposes, it is also assumed all candidate designs will be perfectly insulated on the exterior surface. This condition can be effectively approached through the use of MLI on the strut surface. Therefore, a one-dimensional conduction analysis was used to determine parametrically the average steady-state strut heat leak.

Two cases were analyzed for heat leak comparisons: a hydrogen tank strut and an oxygen tank strut. The conductivity of the end fittings of the strut is very large compared with the tube and was thus considered to be at essentially constant temperature and equal to the end environments temperatures.

LH_2 Strut	LO_2 Strut
520R to 37R	520R to 160R
(289K to 20K)	(289K to 89K)

An average value of conductivity at the midpoint of each temperature range was used in the calculations. The conductivity values for the glass fiber/epoxy and boron/epoxy struts are shown in Figures 3-22 and 3-23. The fiber constructions selected as most representative of potential Space Tug strut construction are shown as Curves 2(a) on both figures. The heat leak predictions are plotted in Figures 3-24 through 3-27.

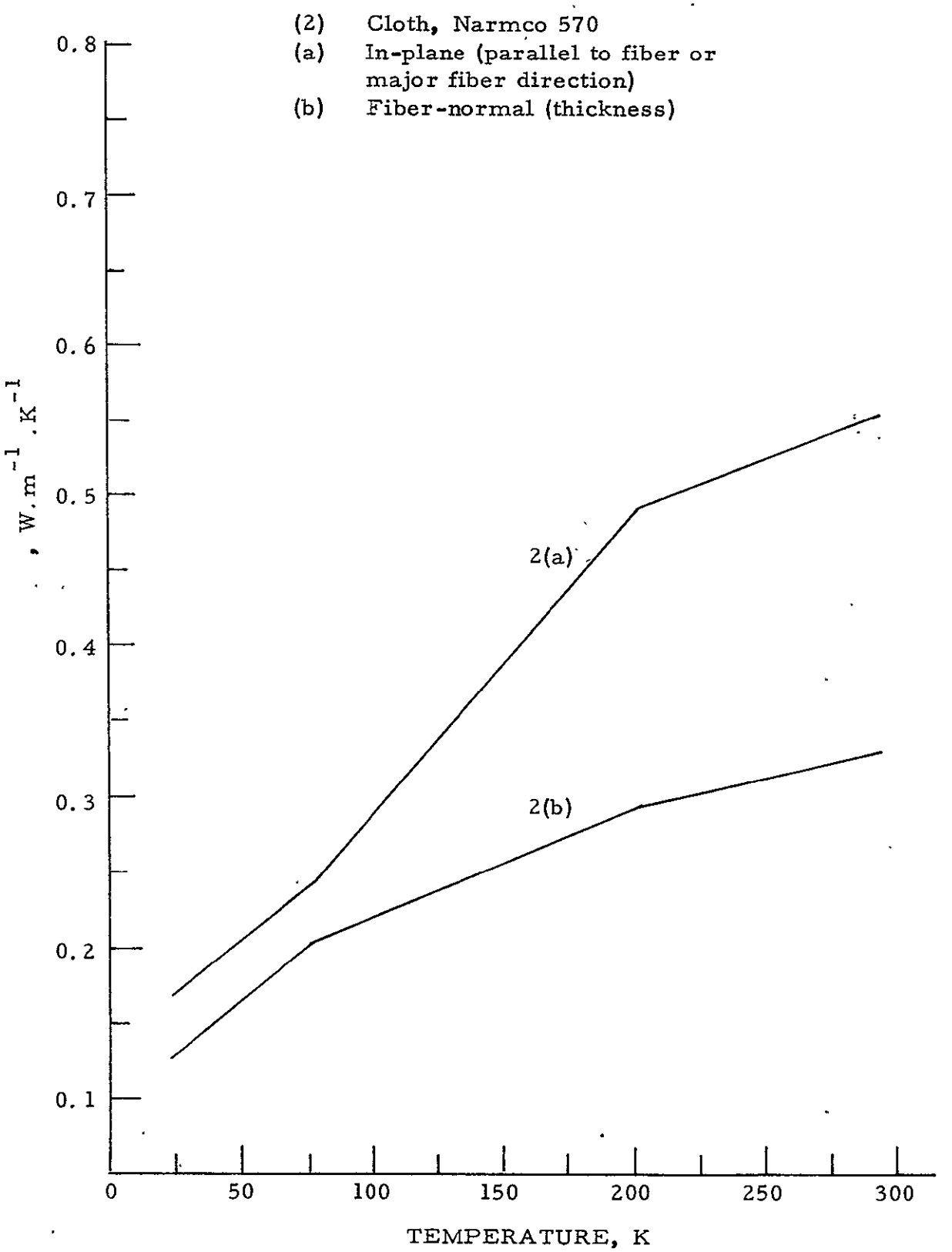

Figure 3-22. Fiber/epoxy thermal conductivity.

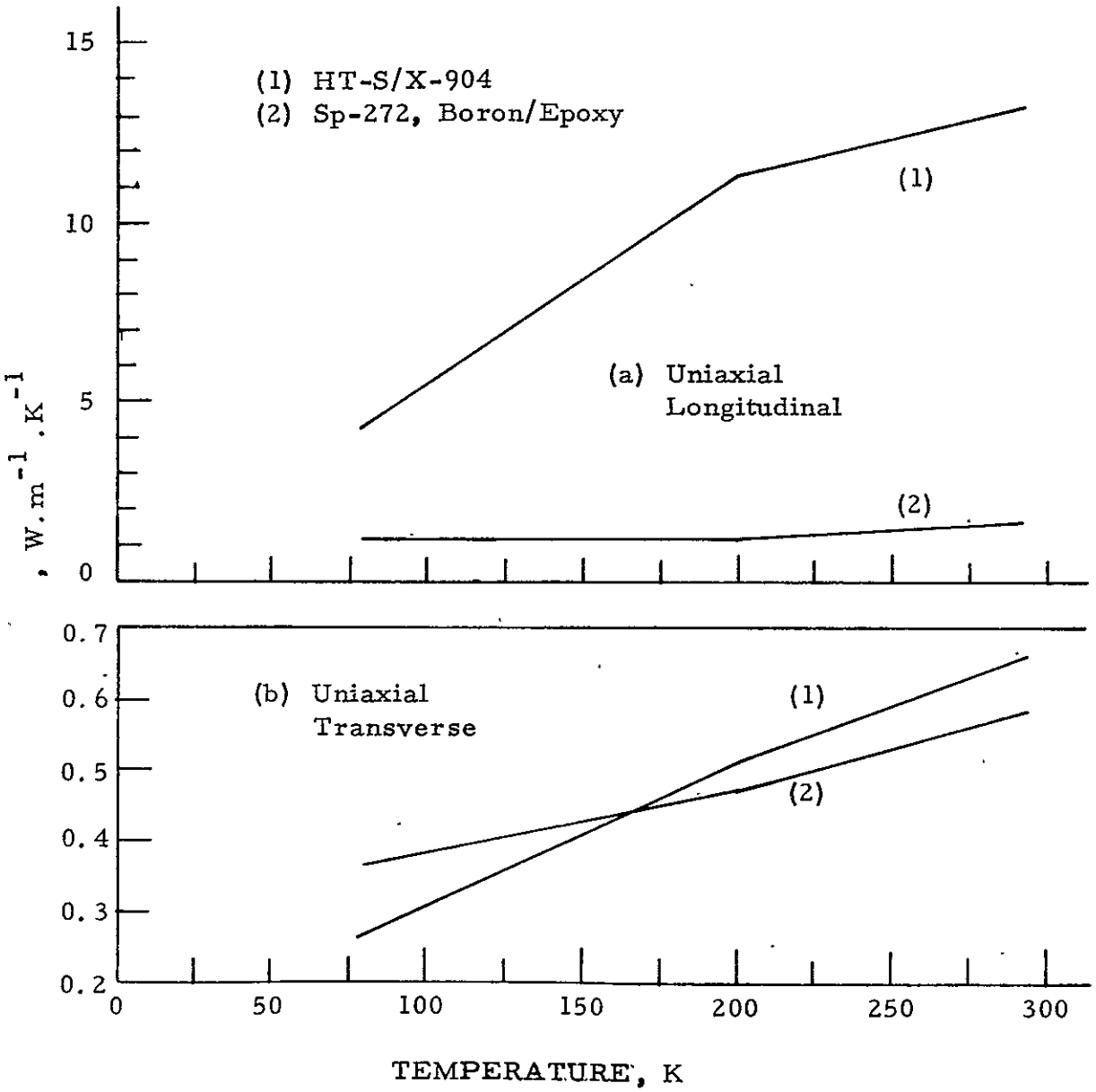

Figure 3-23. Boron/epoxy thermal conductivity.

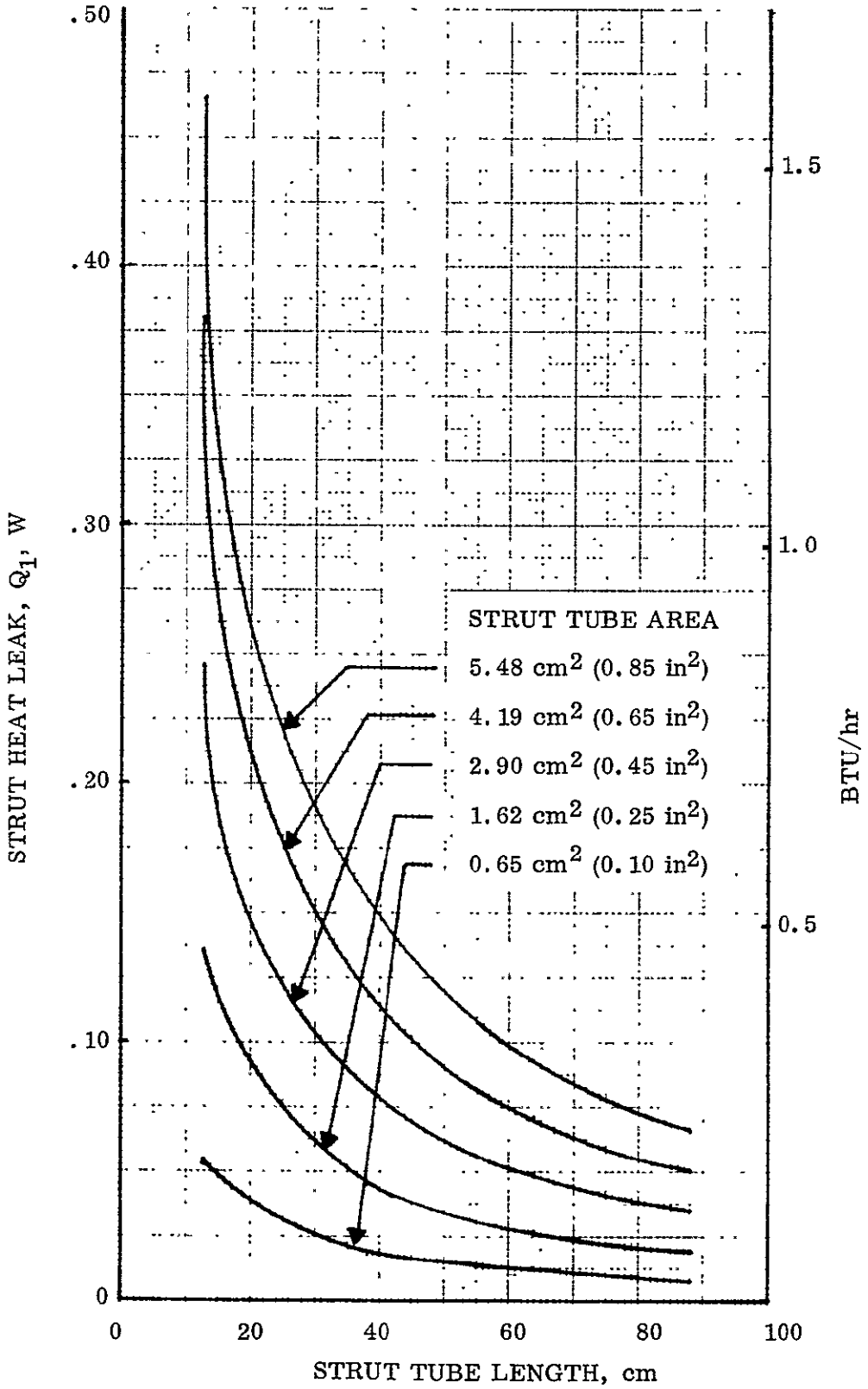

Figure 3-24. Predicted heat leak for glass fiber/epoxy cyrogenic tank support strut (ΔT 289K - 20K).

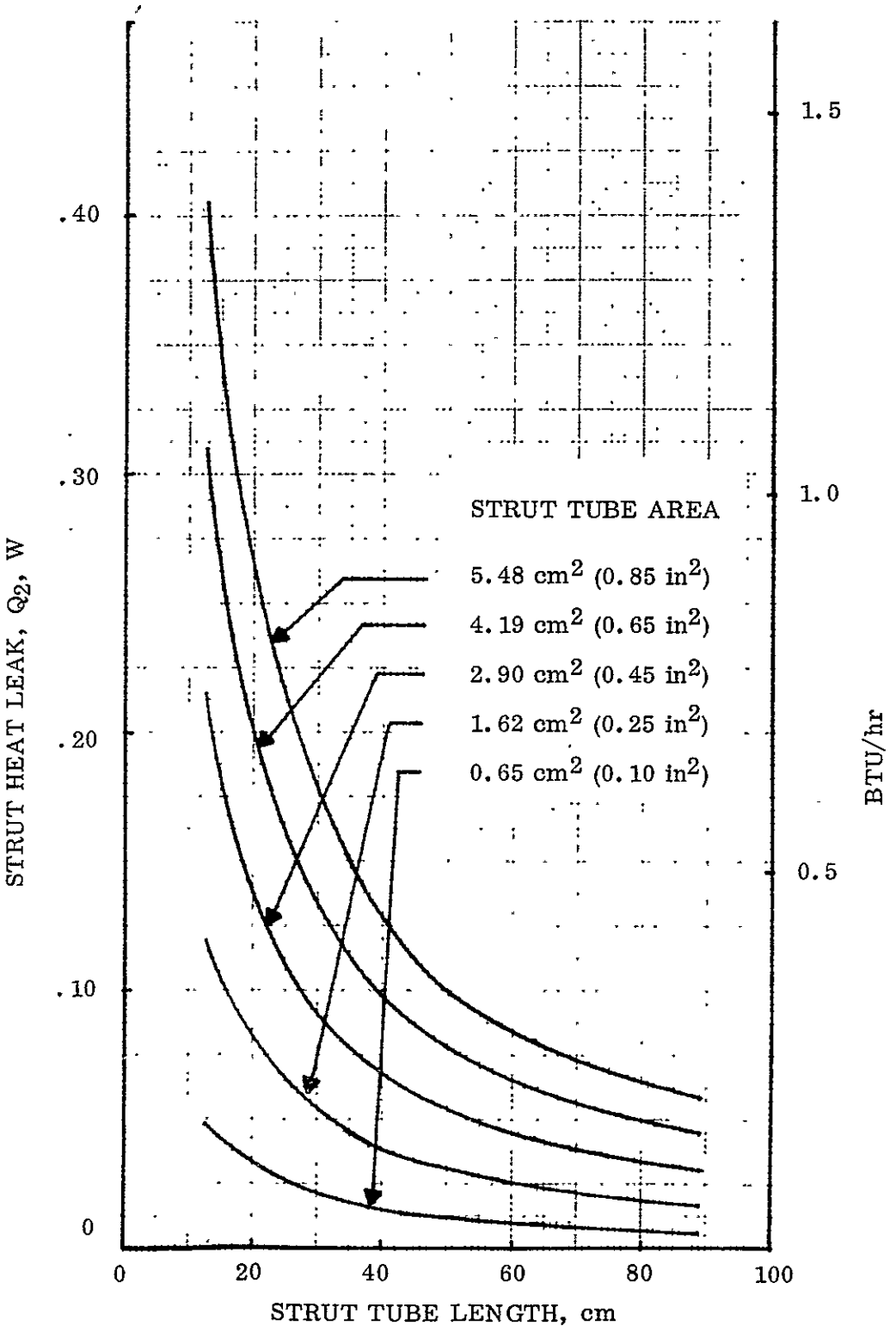

Figure 3-25. Predicted heat leak for glass fiber/epoxy cryogenic tank support strut (ΔT 289K - 89K).

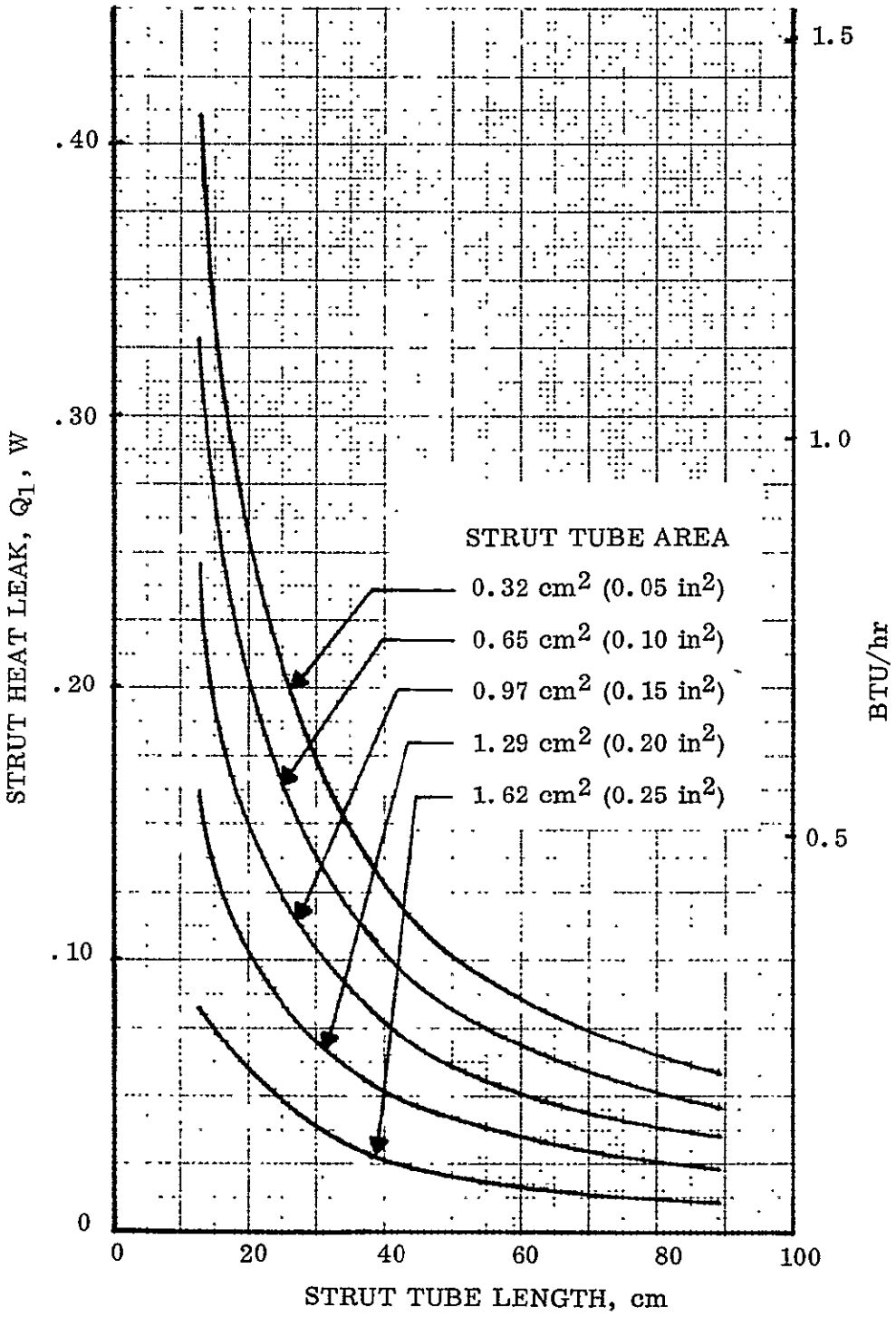

Figure 3-26. Predicted heat leak for boron/epoxy cryogenic tank support strut (ΔT 289K - 20K).

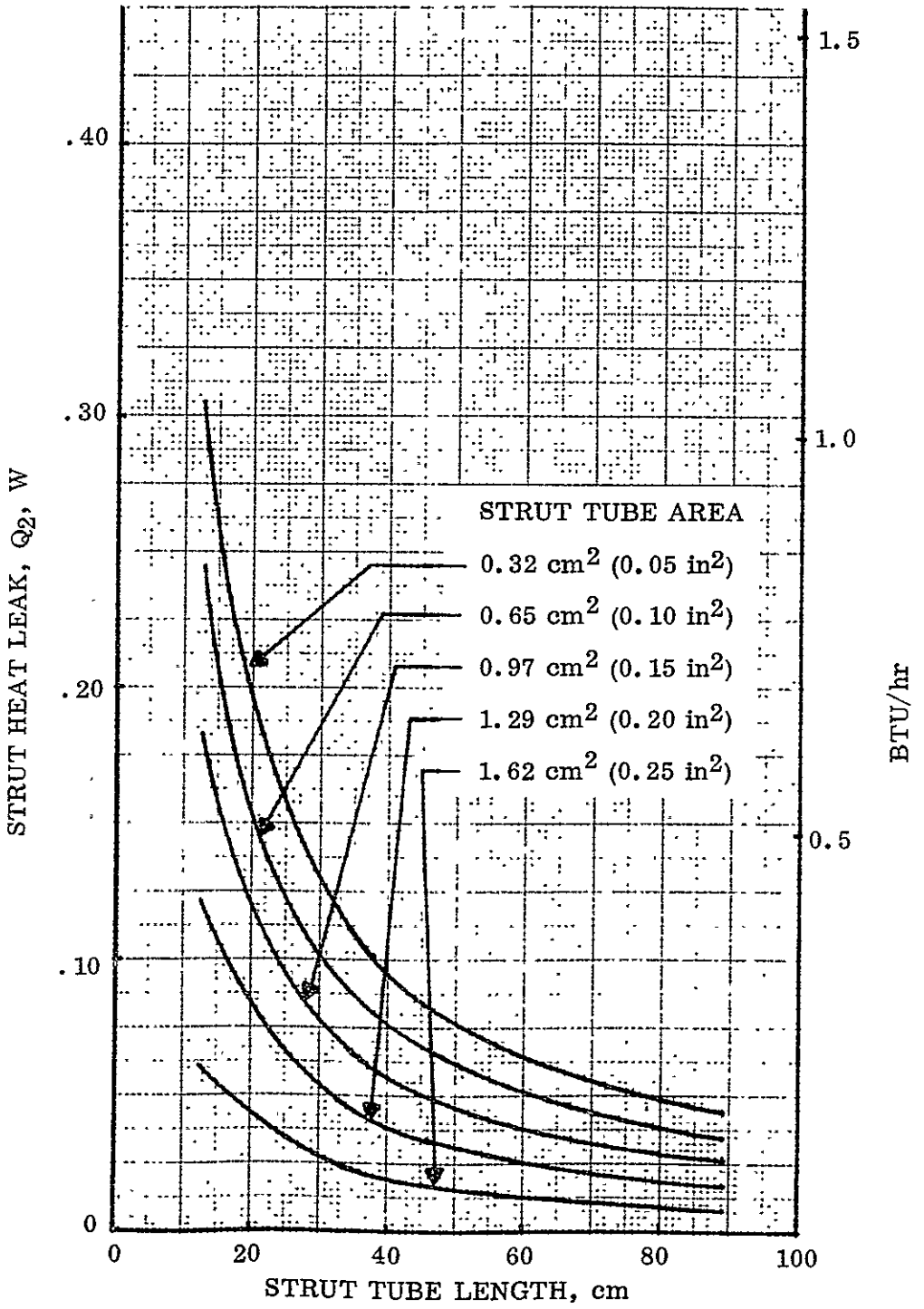

Figure 3-27. Predicted heat leak for boron/epoxy cryogenic tank support strut (ΔT 289K - 89K)

3.4 DISCONTINUITY EFFECTS

Discontinuity stresses at tank joints can have significant impact on the tank joint design. To develop realistic tank designs, it is important to understand and include these effects, both in the configuration trade studies during design and in a detailed tank predesign.

Joint discontinuities can be grouped into two categories: (1) design discontinuities resulting from overall tank geometry and local weld land design, and (2) manufacturing discontinuities which include joint mismatch and weld sinkage. In this study, the categories were evaluated separately.

3.4.1 DESIGN DISCONTINUITIES. The selected design methods used to handle the joint discontinuity effects were evaluated in a semi-parametric manner using Convair's Shell Discontinuity Program (P5007). This program performs an elastic analysis of shells, including the coupled effects of meridional load due to internal pressure.

The analysis was performed on a tank configuration representative of the baseline Tug LH_2 tank shown in Figure 3-28. The $\sqrt{2}$ elliptical-bulkhead-to-cylinder joint was used for the analysis. A design operating pressure of 15.17 N/cm^2 (22.0 psig) was used. The basic bulkhead thickness was set at 0.064 cm (0.025 in.) and the basic cylinder thickness was set at 0.128 cm (0.050 in.).

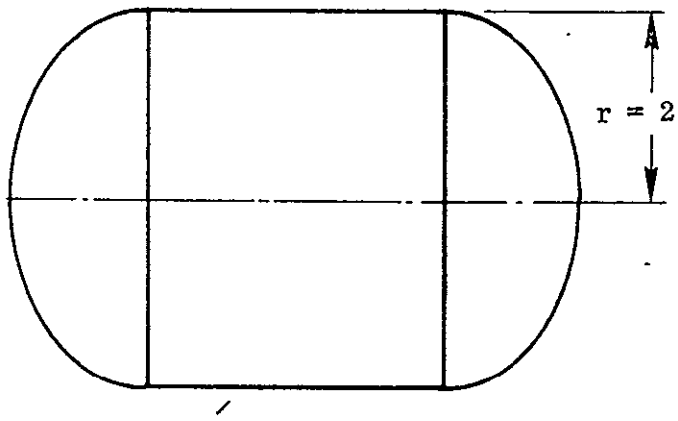

Mat'l
2219-T87 Aluminum

Allowable operating stress 31.0 KN/cm^2 (parent metal) = 15.5 KN/cm^2 (weld)

Figure 3-28. Baseline Tug LH_2 tank geometry.

This analysis evaluated joint design discontinuity effects for four basic types of $\sqrt{2}$ elliptical bulkhead joints under internal pressure. Eccentric as well as aligned joint designs were considered. For the eccentric analysis, the full geometric eccentricity (0.50 t) was conservatively used to calculate discontinuity stresses. The following descriptions and sketches illustrate the four basic bulkhead joints, with eccentric and aligned versions described separately.

Case 1

Constant thickness (t = 0.127 cm) across joint to establish baseline. Included was an analysis of the effects of meridional pressure coupling.

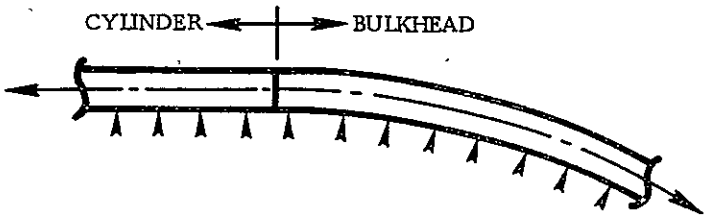

Case 2 (A)

Single step (0.127 to 0.064 cm) on one side to represent chem-milling one one side only.

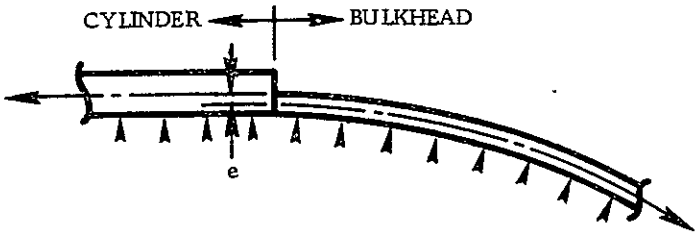

Case 2 (B)

Single step (0.127 to 0.064 cm) with the neutral axis aligned to represent chem-milling from both sides.

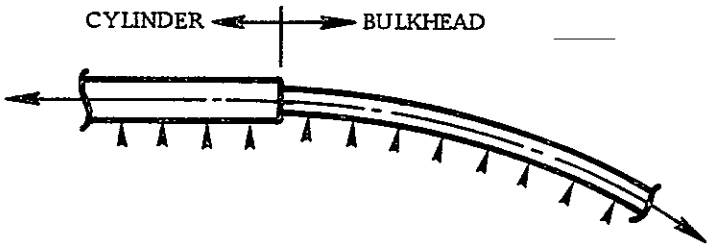

Case 3 (A)

Multiple steps (0.127 to 0.097 cm) on one side to define interrelation effects of adjacent steps.

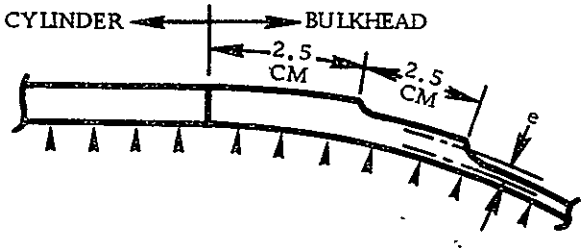

Case 3 (B)

Multiple steps (0.127 to 0.097 to 0.064 cm) with neutral axis aligned to represent chem-milling from both sides.

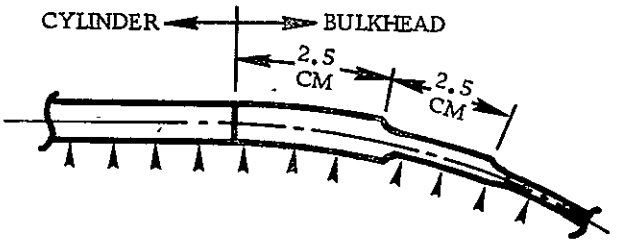

Case 4 (A)

Taper (0.127 to 0.064 cm) on one side to represent taper chem-milling or dressing down on one surface.

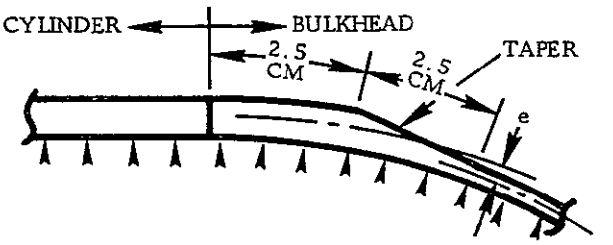

Case 4 (B)

Taper (0.127 to 0.064 cm) on both sides to represent taper chem-milling or dressing down on both surfaces.

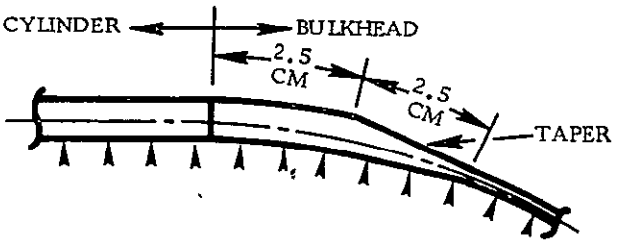

The results of an evaluation of the effects of including meridional pressure coupling in the discontinuity analysis (Case 1) are shown in Figure 3-29. Meridional pressure coupling significantly reduces the meridional discontinuity stresses from those obtained by classical analysis of the cylinder $\sqrt{2}$ elliptical bulkhead discontinuity. Peak hoop stress at the cylinder-to-bulkhead joint is unchanged with or without meridional pressure coupling. However, due to the modified shear distribution, the hoop stress is less damped for the case where meridional pressure coupling is included. The meridional discontinuity stresses add directly to the meridional membrane stresses for both the cylinder and bulkhead. Compressive hoop discontinuity stresses relieve the hoop membrane stresses in the cylinder, and the tensile hoop discontinuity stresses in the bulkhead are not critical, due to the low hoop membrane stresses for a $\sqrt{2}$ elliptical bulkhead

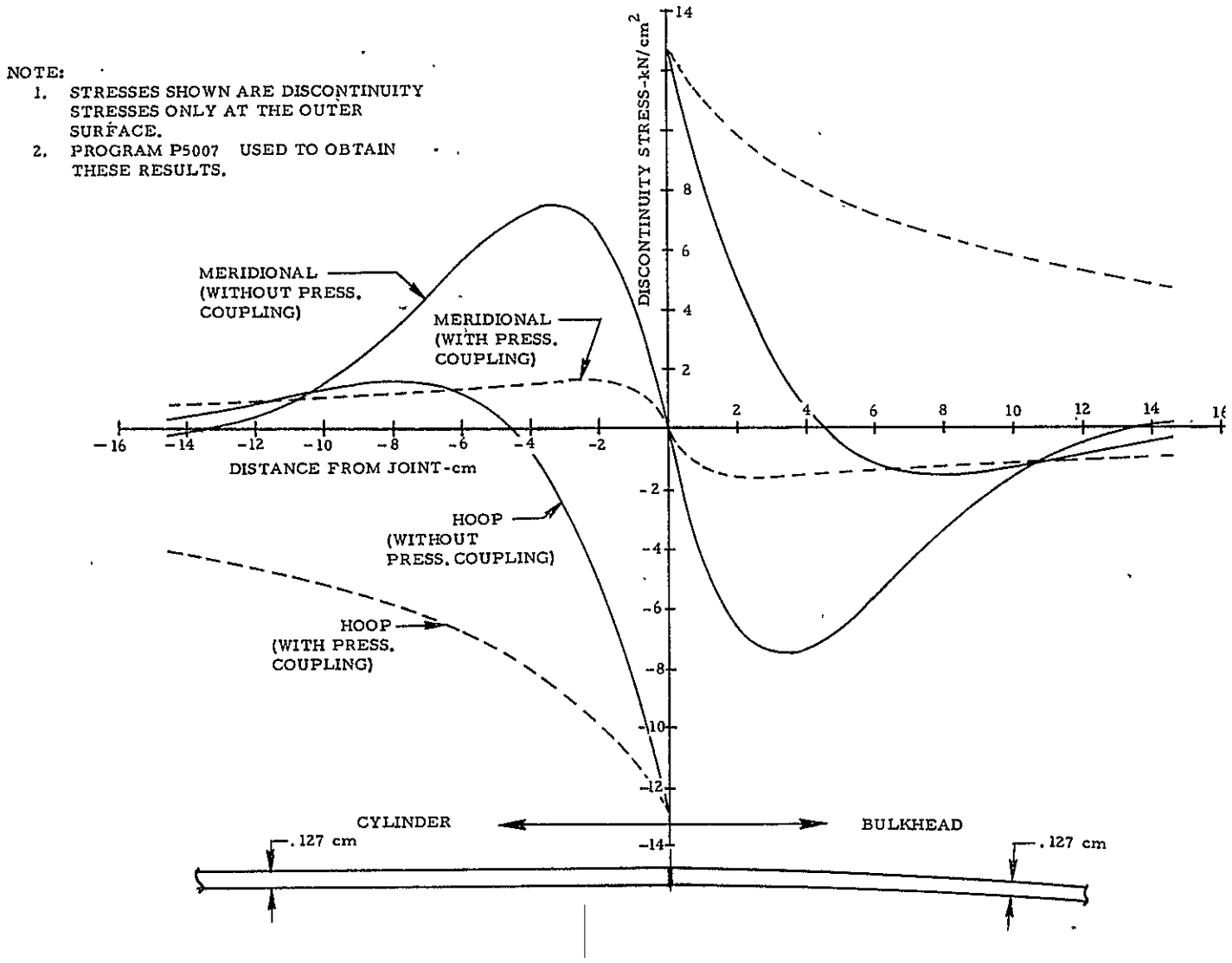

Figure 3-29. Effects of meridional pressure coupling on discontinuity stresses for a simple cylinder/bulkhead intersection.

near its girth. Therefore, it can be concluded from the results shown in Figure 3-29, that the inclusion of the pressure coupling in the analysis will significantly reduce the critical total membrane-plus-discontinuity stresses at the cylinder-to-bulkhead joints for the lightweight tank configuration. Meridional pressure coupling was thus included in all joint discontinuity analysis.

Figure 3-30 presents the results of a discontinuity analysis of the cylinder-to-bulkhead joint, including the effects of a single-step thickness change from 0.127 to 0.064 cm at the joint (Case 2). For this joint configuration without eccentricity, peak discontinuity stresses are slightly higher than for Case 1 (constant thickness). However, with full eccentricity both the peak meridional and hoop discontinuity stresses increase significantly over Case 1. This is especially significant, since the peak stresses occur at the joint, where the allowable stresses due to the weld are minimum. For this configuration with eccentricity, the combined membrane and discontinuity stresses exceeded the allowable stress in the weld (min. M.S. = -0.67).

Figure 3-31 presents the results of a discontinuity analysis of the cylinder-to-bulkhead joint, including the effects of a two-step thickness change from 0.127 to 0.064 cm in the bulkhead adjacent to the cylinder-to-bulkhead joint (Case 3). For this configration, peak dicontinuity stresses occur away from the weldjoint. Without eccentricity assumed, peak discontinuity stresses occur in the 0.064 cm thick membrane at the 0.096-to-0.064 cm weld land step. For this configuration, the peak meridional discontinuity stress is approximately 60% of the peak stress for Case 2 (single step). It is interesting to note that the high discontinuity stresses due to eccentricity are almost completely damped out less than 1,5 cm from the step. For the Case 3 configuration with eccentricity, the combined membrane and discontinuity stresses in the basic membrane at the step slightly exceed the allowable stresses (min. M.S. = 0.17).

Figure 3-32 presents the results of a dicontinuity analysis of the cylinder-to-bulkhead joint, including the effects of a continuously tapered thickness change from 0.127 to 0.064 cm in the bulkhead adjacent to the cylinder-to-bulkhead joint (Case 4). Without eccentricity, the peak discontinuity stresses are only slightly higher than for Case 1 and they occur at approximately the same location (within 2 cm of the joint). With eccentricity, the peak discontinuity stresses occur at the ends of the tapered transition section. These peak stresses are significantly lower than for either Case 2 or Case 3. Peak meridional discontinuity stress is approximately 35% of the Case maximum. For the Case 4 configuration, the maximum combined membrane and discontinuity stresses are below the allowable stresses (min. M.S. = +0.10).

Results of the joint design discontinuity effects are summarized in Tables 3-9 and 3-10 for the weld heat affected zone and the $\sqrt{2}$ elliptical bulkhead. Since the basic cylinder is not critical for meridional stresses and the discontinuity hoop stresses are relieving, the cylinder section of the tank is sized by membrane hoop stresses away from the bulkhead joint.

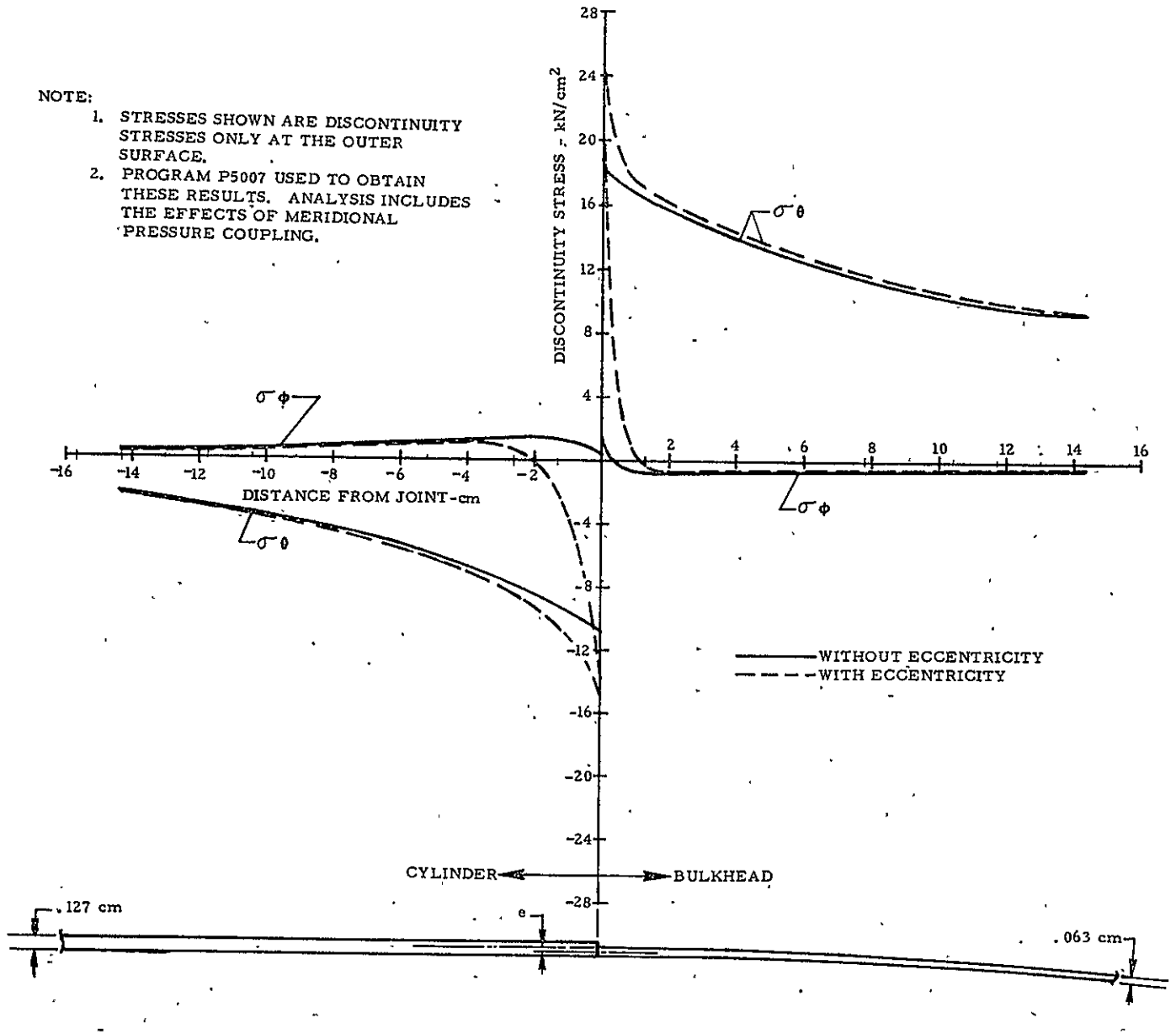

Figure 3-30. Cylinder/bulkhead discontinuity stresses-single step thickness change.

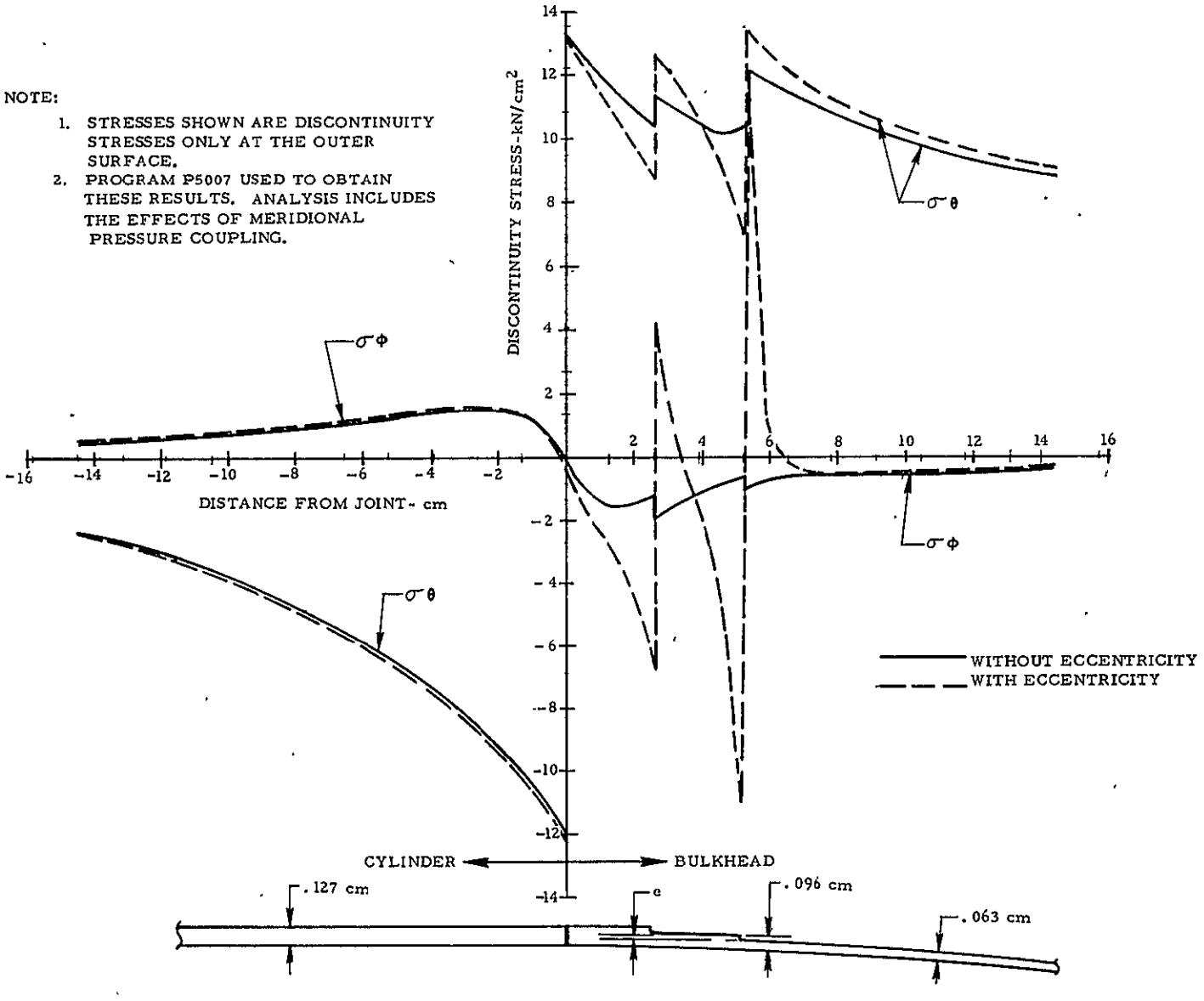

Figure 3-31. Cylinder/bulkhead discontinuity stresses - two step thickness change.

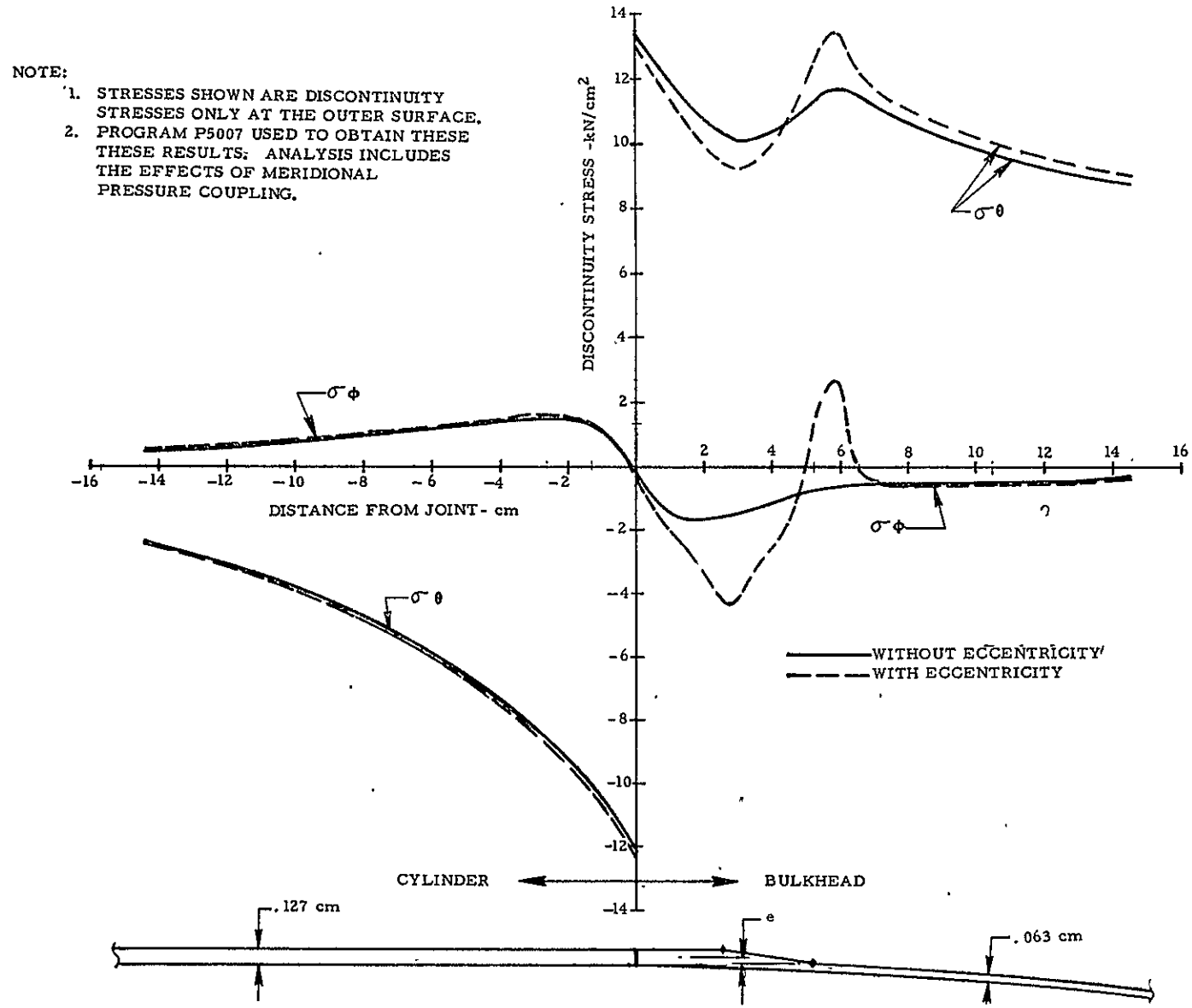

Figure 3-32. Cylinder/bulkhead discontinuity stresses - continuous taper thickness change.

Table 3-9. Summary of joint design discontinuity effects - max weld stresses.

Configuration	Eccentricity	Max Meridional Stress (KN/cm^2)					Max Hoop Stress (KN/cm^2)				
		$\sigma\phi$ memb.	$\sigma\phi$ disc.	$\sigma\phi$ ToT	$\frac{\sigma\phi \text{ ToT}}{\sigma\phi \text{ memb.}}$	M.S. ϕ	$\sigma\theta$ memb	$\sigma\theta$ disc.	$\sigma\theta$ ToT	$\frac{\sigma\theta \text{ ToT}}{\sigma\theta \text{ Memb}}$	M.S. θ
1 (constant thickness)	no	12.8	.6	13.4	1.05	+.15	25.6	-12.2	13.4	.52	+.15
2 (single step)	no	25.6	1.3	26.9	1.05	-.42	0.0*	18.8	18.8		-.18
	yes	25.6	21.4	47.0	1.83	-.67	0.0*	25.2	25.2		-.38
3 (double step)	no	12.8	.5	13.3	1.04	+.17	25.6	-11.4	14.2	.56	+.09
	yes	12.8	1.2	14.0	1.09	+.11	25.6	-12.2	13.4		
4 (taper)	no	12.8	.5	13.3	1.04	+.17	25.6	-11.4	14.2	.56	+.09
	yes	12.8	1.0	13.8	1.08	+.12	25.6	-11.7	13.9	.54	+.11

NOTES:
1. Weld allowable = 15.5 KN/cm^2
2. (Max stress in weld heat affected zone. Weld heat affected zone assumed .318 cm (2.5t) on each side of weld joint.
3. Weld thickness = .127 cm

* Critical in $\sqrt{2}$ elliptical bulkhead.

Table 3-10. Summary of joint design discontinuity effects - max bulkhead stresses.

Configuration	Eccentricity	Max Meridional Stress (KN/cm^2)					Max Hoop Stress (KN/cm^2)				
		$\sigma\Phi$ memb.	$\sigma\Phi$ disc.	$\sigma\Phi$ ToT	$\frac{\sigma\Phi \text{ ToT}}{\sigma\Phi \text{ memb.}}$	M.S. Φ	$\sigma\Theta$ memb	$\sigma\Theta$ disc.	$\sigma\Theta$ ToT	$\frac{\sigma\Theta \text{ ToT}}{\sigma\Theta \text{ Memb}}$	M.S. Θ
1 (constant thickness)	no	12.8	1.7	14.5	1.13	+ 1.14	0	12.6	12.6	—	+ 1.46
2 (single step)	no	25.6	.8	26.4	1.03	+ .17	0	18.1	18.1	—	+ .72
	yes	25.6	7.4	33.0	1.29	- .06	0	20.8	20.8	—	+ .50
3 (double step)	no	25.6	1.3	26.9	1.05	+ .15	0	13.6	13.6	—	+ 1.28
	yes	25.6	11.6	37.2	1.45	- .17	0	13.4	13.4	—	+ 1.31
4 (taper)	no	25.6	.8	26.4	1.03	+ .17	0	13.6	13.6	—	+ 1.28
	yes	25.6	2.8	28.4	1.11	+ .09	0	13.4	13.4	—	+ 1.32

NOTES:
1. Parent material allowable stress = 31.0 KN/cm^2
2. Max stress outside weld heat affected zone
3. Basic bulkhead thickness = .064 cm (except for config. 1)

3.4.2 MANUFACTURING DISCONTINUITIES. The major joint manufacturing discontinuity effects are weld mismatch and weld sinkage. Both of these effects were evaluated for a constant thickness (0.127 cm) cylinder-to-bulkhead joint.

Based on experience with fabrication of tanks similar to the proposed lightweight tank design, weld mismatch can be held to less than 10% of the weld thickness. This is accomplished by using tooling to accurately align and hold the weld joint in position during the welding operations.

Convair's discontinuity analysis program P5007 was used to determine discontinuity stresses due to a weld mismatch equal to 10% of the weld thickness. The full geometric discontinuity (0.10t) was conservatively used. Meridional pressure-coupling effects were included in the analysis.

Analysis results are shown in Figure 3-33. The major impact of the mismatch is a significant increase in peak meridional discontinuity stress in the weld heat affected zone, as summarized in Table 3-11. Weld mismatch does not significantly impact peak hoop stresses in the weld heat-affected zone.

Table 3-11. Effect of weld mismatch on maximum weld stresses.

	Maximum Meridional Stress (KN/cm^2)				
	σ_ϕ Membrane	σ_ϕ Disc	σ_ϕ Total	$\frac{\sigma_\phi \text{ Total}}{\sigma_\phi \text{ Membrane}}$	M.S. σ_ϕ
Constant t (0.127 cm) (No Mismatch)	12.8	0.6	13.4	1.05	+0.15 (T)
Constant t (0.127 cm) (Mismatch = 0.10 t)	12.8	3.9	16.7	1.30	-0.07 (T)

Weld sinkages occur due to differential thermal expansion/contraction in the weld joint during the welding operation. The effects of weld sinkage on peak stresses in the weld joint were evaluated, using the analysis methods in Lockheed Report LMSC/4-05-69-7, "Elastic and Plastic Stresses at Weld Sinkages and Other Discontinuities in Pressure Vessels". This analysis indicated that the primary weld sinkage geometric parameters which affected discontinuity stresses are the depth of sinkage (Δ) and the sinkage angle ($\Delta\phi$), as shown in the inset sketch of Figure 3-34.

The referenced report only considers cylindrical and spherical shells; therefore, the baseline $\sqrt{2}$ elliptical bulkhead was approximated as a spherical shell for the weld sinkage analysis. Results for an elastic analysis of the peak meridional discontinuity stresses due to weld sinkage as a function of Δ and $\Delta\phi$ are shown in Figure 3-34.

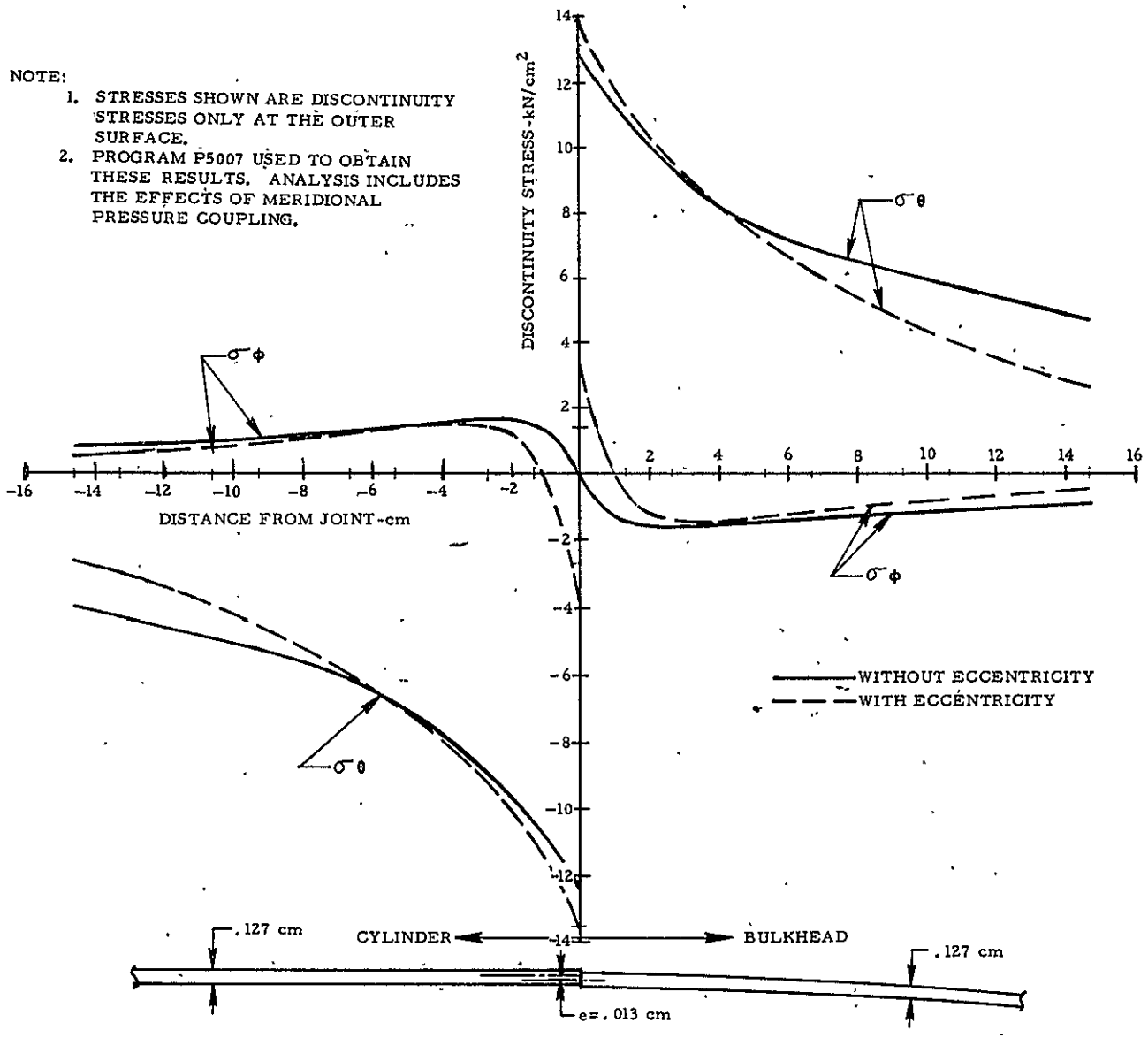

Figure 3-33. Cylinder/bulkhead discontinuity stresses - constant thickness.

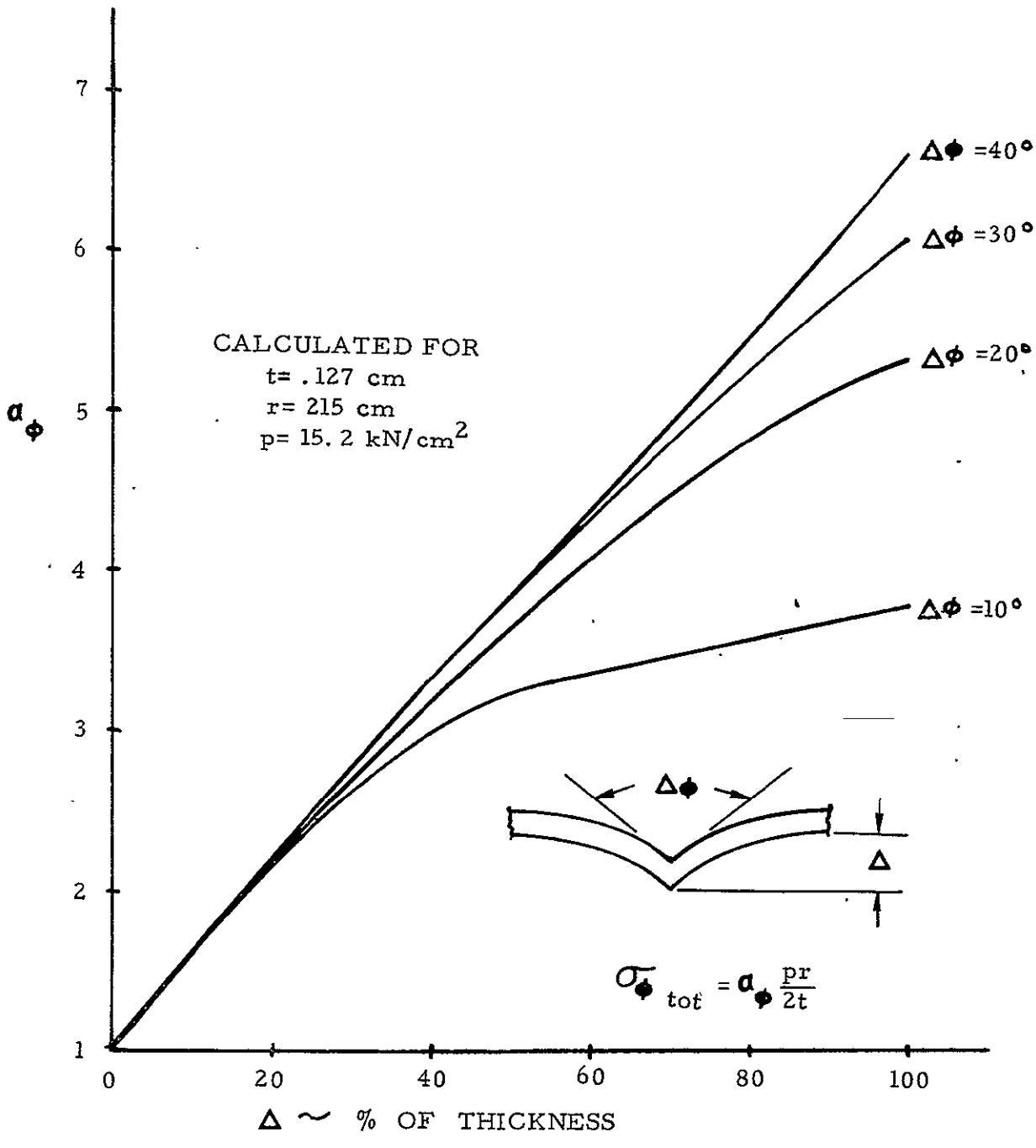

Figure 3-34. Meridional discontinuity stress for weld sinkage.

Peak discontinuity stresses increase significantly due to weld sinkage. (See Figure 3-35.) A weld sinkage only 0.023 cm (0.18 t) deep will double the total meridional stress in the weld. To evaluate the effects of weld sinkage on tank joint designs, the maximum expected weld sinkage depth and the weld sinkage angle must be established. This can only be accomplished by welding complete specimens representative of the joint and measuring the weld sinkage geometry. An alternate approach is to use design, tooling, and weld procedures to eliminate weld sinkage effects. This has been done on tanks of similar geometry fabricated by Convair in the past. The use of carefully designed backup tooling, multiple weld passes, and weld shaving will minimize any weld sinkage effects as shown in Figure 3-35.

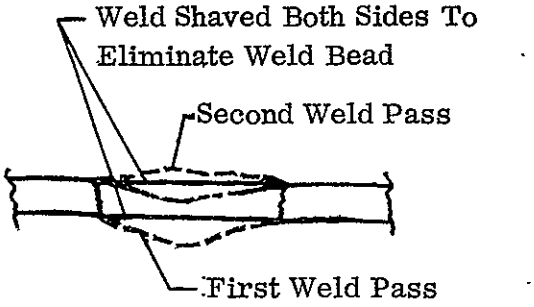

Figure 3-35. Elimination of weld sinkage effects.

3.4.3 SUMMARY OF DISCONTINUITY EFFECTS.

a. Design and manufacturing discontinuities can significatnly influence the tank joint designs. Careful design and manufacturing procedures must be employed to minimize these discontinuity effects for a truly lightweight tank.

b. Local eccentricities due to thickness changes in the weld lands produce the highest design discontinuity stresses. Eccentricity is also the most difficult variable to account for in analyzing discontinuity stresses. Use of the full geometric eccentricity produces a very conservative estimate of the discontinuity stresses. Careful design of the weld lands will minimize the effects of these local eccentricities.

c. The best thickness transition design from the point of minimizing discontinuity stresses is a symmetrical continuous taper. However, a symmetrical double step design produces maximum stresses only slightly higher than the continuous taper.

d. Weld mismatch and weld sinkage are the major manufacturing discontinuities. Both can have a significant effect on the tank joint designs. However, the effects of both weld mismatch and weld sinkage can be controlled by careful design, tooling, and welding procedures.

e. Discontinuity factors stated in Table 3-12 can be used for the lightweight tank preliminary design.

Table 3-12. Preliminary design discontinuity stress factors.

Area	Type Joint	Geom Factor	Mfg Factor	Total Factor
Weld Joint	Symm. Double Step	1.04	1.15*	1.20
	Ecc. Cont. Taper	1.08	1.15*	1.23
	Ecc. Double Step	1.09	1.15*	1.25
Bulkhead Membrane	Symm. Double Step	1.05	1.00	1.05
	Ecc. Cont. Taper	1.11	1.00	1.11
	Ecc. Double Step	1.23*	1.00	1.23
Cylinder Membrane	Symm. Double Step	1.00	1.00	1.00
	Ecc. Cont. Taper	1.00	1.00	1.00
	Ecc. Double Step	1.00	1.00	1.00

* One-half of calculated discontinuity stress due to eccentricity used

3.5 CANDIDATE TANK AND SUPPORT CONCEPTS

The initial contour screening identified the general bulkhead candidate contours as ellipsoidal, Cassinian, and controlled N_θ/N_ϕ for the LH_2 tank and ellipsoidal and controlled N_θ/N_ϕ for the LO_2 tank. A review of the interrelationship of contour, inertia loads, and ullage pressure effects indicates the most promising contours within the various candidate contour families are the ones which exhibit no hoop compression, with the baseline support system as a limit. Therefore, the defined candidate contours are:

Ellipse	$a/b = \sqrt{2}$	(LO_2 and LH_2 Tanks)
Cassinian	$n = 1.879$	(LH_2 Tank only)
Controlled N_θ/N_ϕ	$n_o = .2$, $m = .5$	(LO_2 and LH_2 Tanks)

A review of the strut loads and effects data suggests three candidate support systems for the LO_2 tank: 24 struts with slopes of 0.762, 0.611, and 0.436 radians in a laced pattern.

The boiloff weights based on these configurations and the dual deployment single retrieval mission of 140 hours are as follows:

a. $\beta = 0.762$ B/E 2.33 Kg
G/E 1.51 Kg

b. $\beta = 0.611$ B/E 2.50 Kg
G/E 1.73 Kg

c. $\beta = 0.436$ B/E 2.22 Kg
G/E 1.95 Kg

The weights of tank weld lands and tank brackets are 14.07, 14.09, and 14.01 kilograms for Configurations a, b, and c, respectively.

The strut weights are as follows:

a.	B/E	0.38×24 =	9.12 Kg
	G/E	0.55×24 =	13.16 Kg
b.	B/E	0.38×24 =	9.22 Kg
	G/E	0.64×24 =	15.39 Kg
c.	B/E	0.49×24 =	11.84 Kg
	G/E	0.95×24 =	22.71 Kg

Due to the propellant inertial head pressure acting on the LO_2 tank aft bulkhead, a zone of hoop compression loading will occur near the tank support plane for support plane slopes of less than 0.76 radian. In the configuration where the main engine is supported directly from a 0.8-meter-diameter ring welded into the aft LO_2 bulkhead, a shell compression zone occurs near this ring due to ground-handling bending loads. Therefore, an analysis was performed to determine the requirements for integral isogrid stiffening to stabilize the LO_2 aft bulkhead for these compression loads. To facilitate forming of bulkhead gores, a relatively shallow, unflanged isogrid design was selected. Although less efficient than a deeper flanged isogrid design, this concept offers manufacturing and material savings with only a small weight penalty for the low compression loading experienced by the LO_2 tank. Three basic compression failure modes, i.e., general instability, skin buckling, and stiffener crippling, were used to size the isogrid. The equations from NASA CR-124075, Isogrid Design Handbook for a spherical shell loaded by a uniform external pressure, modified to account for the elliptical bulkhead geometry and loading, were used. These relationships are summarized below.

$$Ncr_1 = \frac{C_0 E t^2}{R} \beta \quad \text{(General Instability)}$$

$$Ncr_2 = C_1 E t (1 + \alpha) \frac{t^2}{h^2} \quad \text{(Skin Buckling)}$$

$$Ncr_3 = C_2 E t (1 + \alpha) \frac{b^2}{d^2} \quad \text{(Stiffener Crippling)}$$

Where:

C_0 = general instability coefficient (0.26)

C_1 = skin buckling coefficient (10.2 for simply supported triangular panel loaded in uniaxial compression)

C_2 = Stiffener crippling coefficient (0.634 for stiffener with 3 edges simply supported and 1 edge free)

E = Young's modulus

t = skin thickness

R = local radius of curvature

h = height of isogrid triangle (0.866 times isogrid node-to-node spacing)

b = width of stiffener

d = depth of stiffener

$$\alpha = \frac{bd}{th}$$

$$\beta = \sqrt{3\alpha\left(1+\frac{d}{t}\right)^2 + (1+\alpha)\left[1+\alpha\left(\frac{d}{t}\right)^2\right]}$$

The baseline LO_2 tank geometry a/b = 2, a = 1.83 meters was used in this study. The hoop compression loads and locations were determined for various strut locations as shown in Figure 3-36. Using the local radius, equivalent external pressure, and the physical properties of 2219 T87, the basic equations for Ncr_1, Ncr_2, and Ncr_3 were solved parametrically as shown in Figures 3-37 and 3-38. The basic isogrid weights for these same cross sections were also plotted parametrically, see Figures 3-39 and 3-40. The minimum weight for a compatible pattern was then selected, and the $\bar{t}$ used for shell-stiffening weights (Figure 3-41).

Similar data for the LH_2 tank system was developed as discussed earlier. The selected LH_2 support system is the 12 strut with a slope of .698 radian.

3.6 MEMBRANE THICKNESS REQUIREMENTS

Tank membrane thickness requirements were developed for all candidate contours using the program discussed in Subsection 3.2. This program defines areas, arc lengths, and weights for each contour, based on the defined loading conditions and termination points. Basic theoretical shell weights were developed from this program and local weld or discontinuity buildup gauges, and weights were hand calculated. The areas and arc lengths are exact as calculated by the program. Tables 3-13 and 3-14 were constructed to itemize these quantities for comparison purposes. The coordinates of all circumferential welds are given along with the arc lengths between these welds, to define gore weld lengths. The membrane gages were incrementally calculated by computer to idealize the membranes, assuming a minimum gage of 0.064 cm (0.025 in.).

The last column presents the tank weight and surface area, including tank closures such as, door or thrust cone.

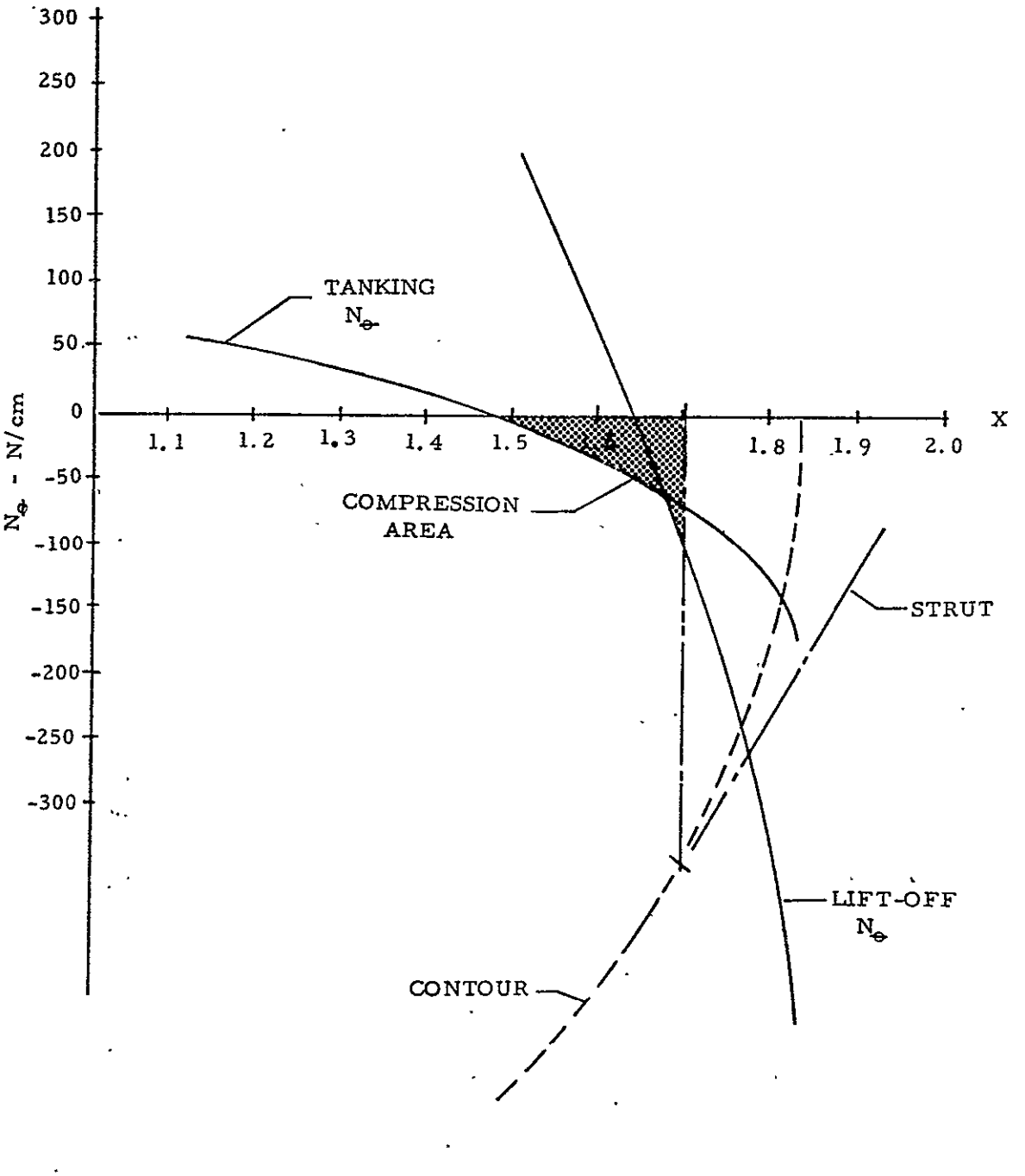

Figure 3-36. Maximum hoop compression loading LO_2 tank.

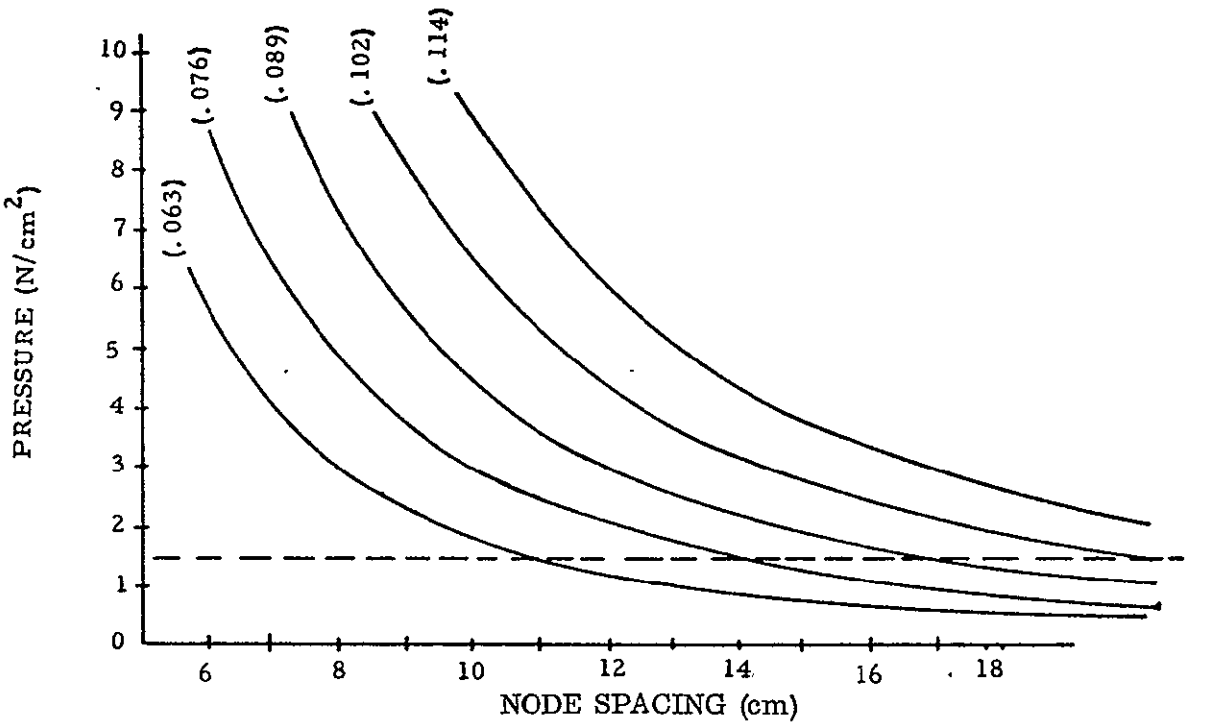

Figure 3-37. Allowable crushing pressure, isogrid shell, R = 1.96 m, flange = 0.317 cm, depth = 0.635 cm.

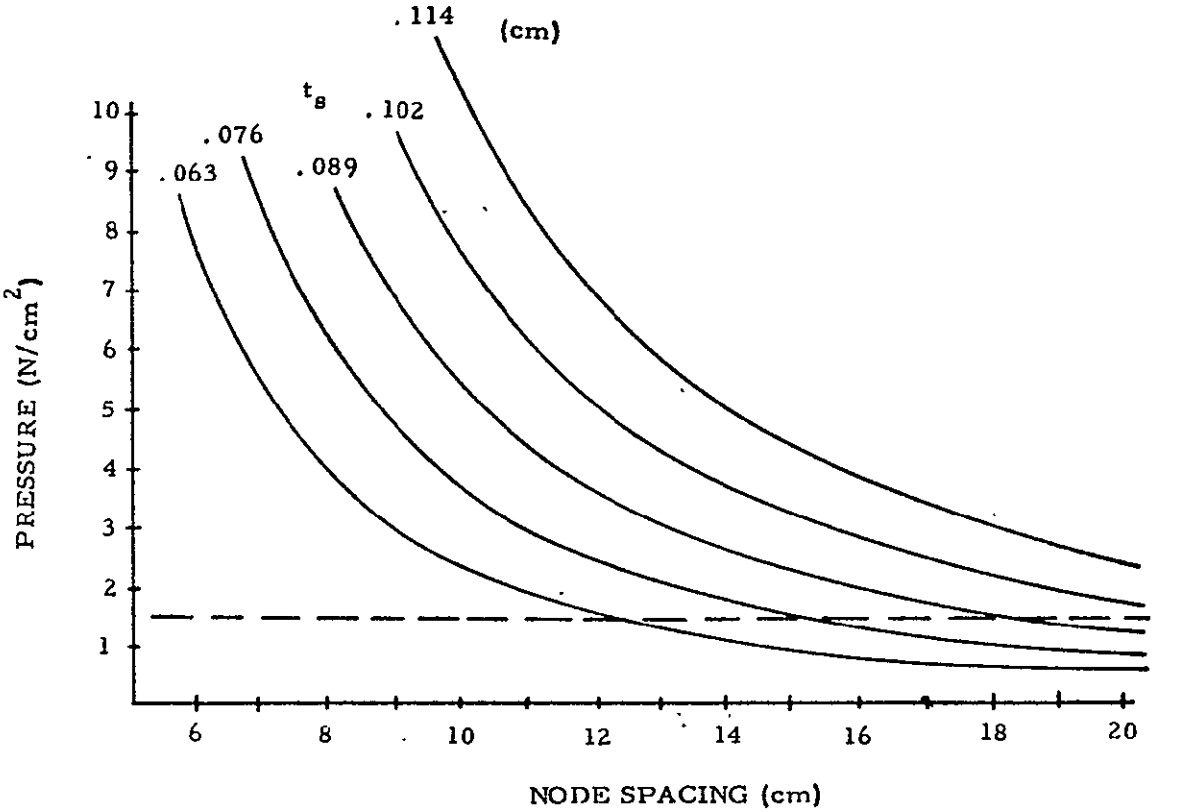

Figure 3-38. Allowable crushing pressure, isogrid shell, R = 1.96m, flange = 0.635 cm, depth = 0.635 cm.

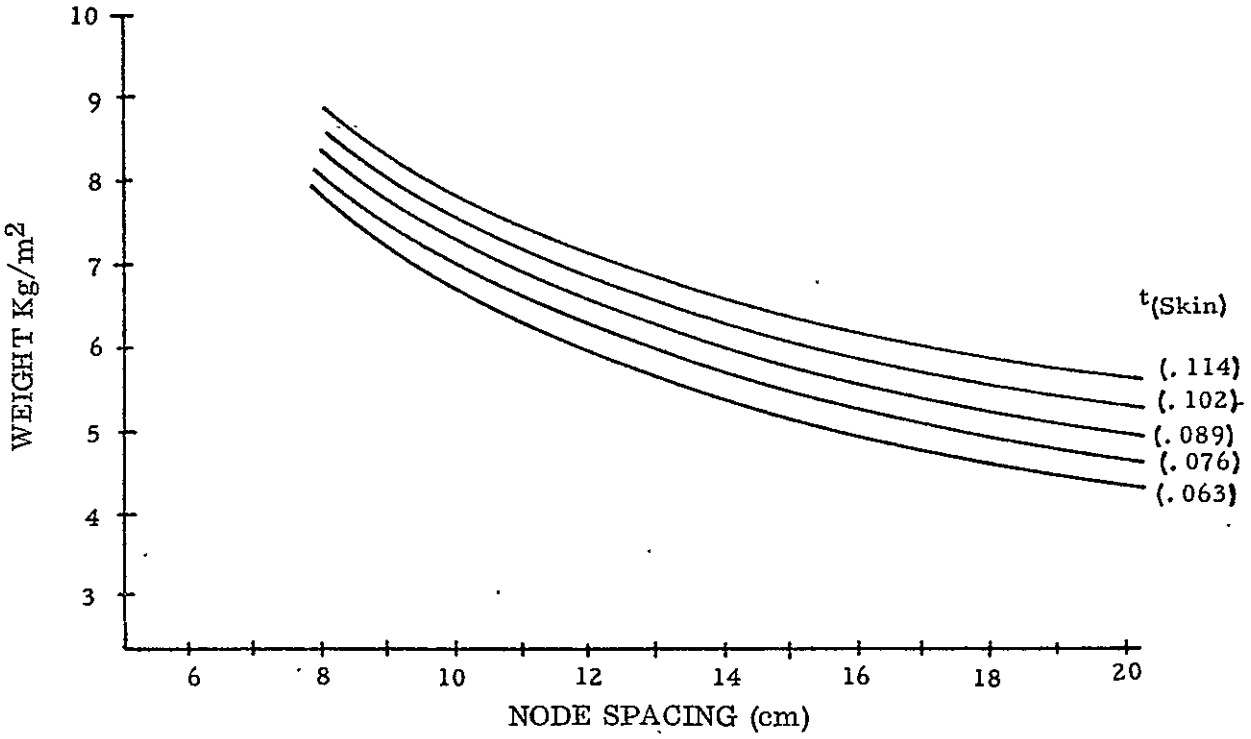

Figure 3-39. Isogrid weight, depth = 0.6535 cm, flange = 0.635 cm.

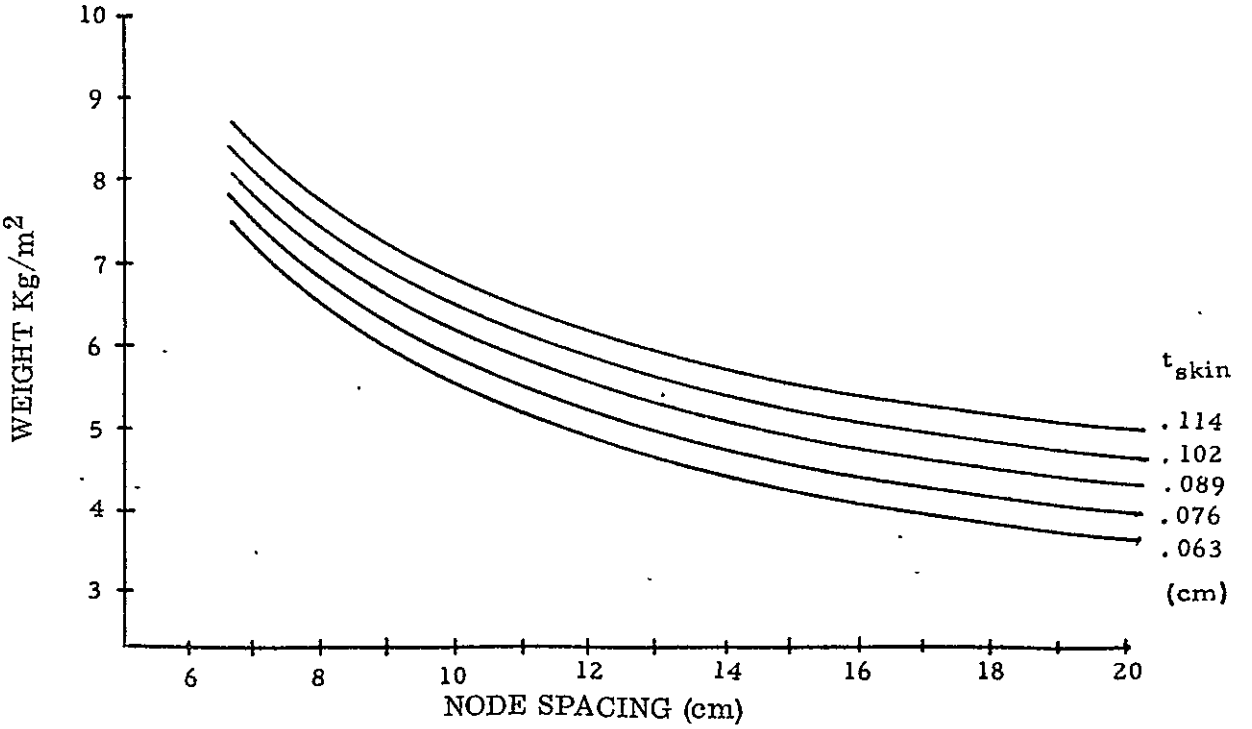

Figure 3-40. Isogrid weight, depth = 0.635 cm, flange = 0.312 cm.

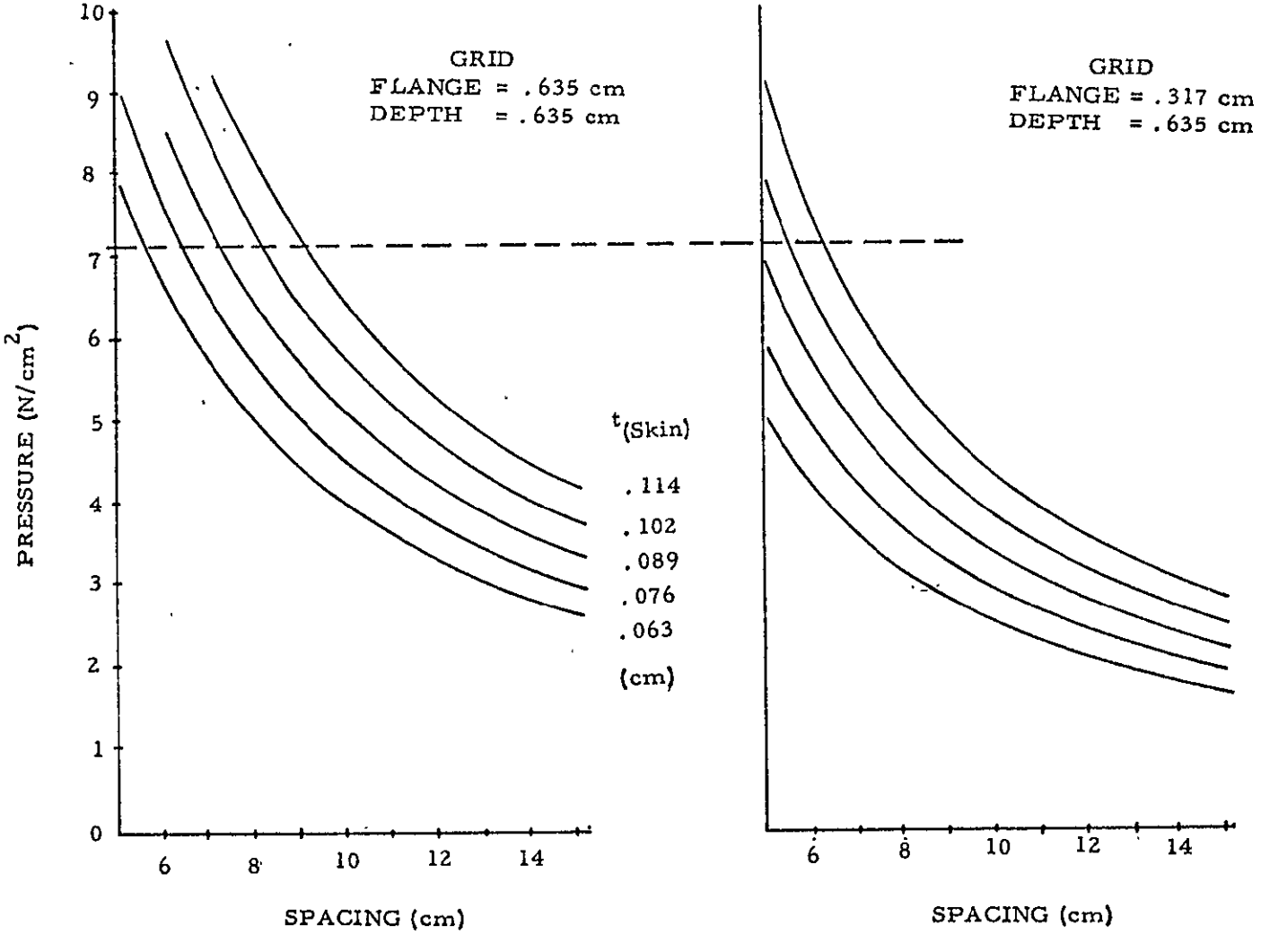

Figure 3-41. Allowable crushing pressure, isogrid shell, R = 2.56 m.

4

MATERIAL SAMPLE TESTING

The objective of the material sample testing task was to verify the fracture toughness of tank membrane material by testing material specially processed to simulate actual tank fabrication and processing.

The material sample test plan is outlined in Figure 4-1. The material tested was thin sheet 2219T87 aluminum alloy processed in a manner to represent the actual processing which will be accomplished in the fabrication of the tank shell. As indicated in Figure 4-1, the basic material, 0.3175 cm sheet was sheared into two 0.6 m by 1.2 m panels, and thirty 7.62 cm by 1.2 m panels. These panels were then separated into two groups. Group 1 panels were stretched and chem-milled. Group 2 panels were stretched, chem-milled and welded. Specimens then were fabricated from these panels and distributed for testing as shown in Figure 4-1 (K_c testing, K_{th} testing and K_{IE} testing).

The 7.6-cm-wide strips were sheared in both the longitudinal and transverse grain directions. The strips were then installed in a tensile test machine and loaded in tension until the desired elongations were obtained. The fracture test data on the stretched and chem-milled material are shown in Tables 4-1 and 4-2. Tests were performed on both part-through-cracked (surface crack) and center-cracked (through crack) specimens, for two grain directions at room temperature and 20°K. The fracture test data on stretched, chem-milled, and welded material are shown in Table 4-3.

As anticipated, the part-through-cracked specimens were difficult to control in the somewhat thin chem-milled condition (approximately 0.127 cm). In fact, in two cases at room temperature (L-14-2 and T-13-1), the cracks propagated through the thickness. (See Table 4-1.) At 20°K, two specimens, L-12-1 and T-13-2, fractured through the grip ends of the specimens. (See Table 4-2.) These two test specimens were subsequently retested and fractured at room temperature to determine the size and shape of the surface flaw.

All center-cracked specimens behaved as expected at both room temperature and 20°K. As expected, the plane stress fracture toughness (K_C) was greater for the longitudinal grain direction than for the transverse direction, at both temperatures. K_C was calculated using Irwins tangent formula without plastic zone correction.

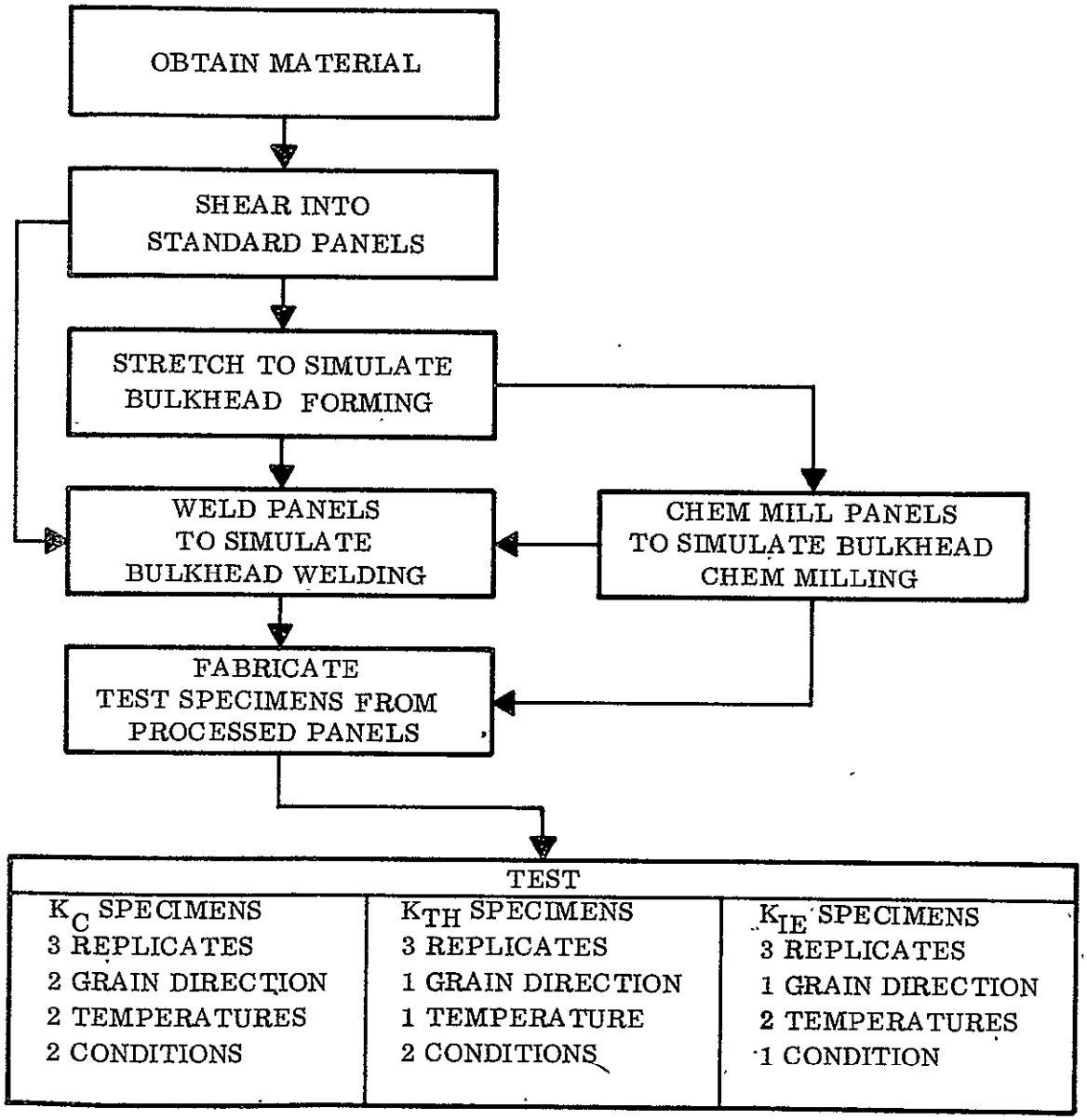

Figure 4-1. Test plan flow chart.

Table 4-1. Static fracture toughness for stretched and chem-milled 2219-T87 aluminum at room temperature.

Ident.	Thick cm	Width cm	Crack Len. 2a-2c, cm	Crack dep a, cm	Max Load N	σG KN/cm^2	σN KN/cm^2	K_C $(KN/cm^2)\sqrt{cm}$	K_{IE} $(KN/cm^2)\sqrt{cm}$	Stretch %
Center-Cracked Specimens										
L-13-1	0.1262	7.3716	2.7305	—	20.3	21.8	34.6	48.0	—	3.0
L-14-3	0.1201	7.3670	2.819	—	18.2	20.6	33.4	46.3	—	4.0
T-12-2	0.1237	7.3673	2.819	—	17.8	19.5	30.9	43.9	—	3.5
T-14-4	0.1242	7.3663	2.718	—	17.4	19.1	30.2	41.9	—	3.5
Part-Through-Cracked Specimens										
L-12-4	0.1229	7.3619	0.254	0.1016	36.5	40.3	—	—	21.5	7.0
T-14-2	0.1237	7.3673	0.635	0.1237	33.6	36.8	40.3	36.9	—	3.5
T-13-1	0.1212	7.3673	0.330	0.1212	37.8	42.4	44.3	30.5	—	4.0

Table 4-2. Static fracture toughness for stretched and chem-milled 2219-T87 aluminum at 20°K.

Ident.	Thick cm	Width cm	Crack Len. cm	Crack dep cm	Max Load N	σG KN/cm^2	σN KN/cm^2	K_C $(KN/cm^2)\sqrt{cm}$	K_{IE} $(KN/cm^2)\sqrt{cm}$	Stretch %
L-9-2	0.1239	7.341	2.95	—	23.3	25.7	42.9	51.4	—	5.5
L-12-2	0.1247	7.366	2.79	—	24.8	27.0	43.5	60.3	—	4.0
L-13-3	0.1224	7.315	2.82	—	25.1	28.1	45.7	63.1	—	5.5
L-14-1	0.1265	7.404	2.74	—	25.7	27.4	43.6	60.5	—	3.0
T-12-1	0.1285	7.368	2.74	—	24.7	26.1	41.5	57.6	—	3.5
T-14-2	0.1262	7.341	2.79	—	22.4	24.1	39.0	54.0	—	4.0
L-12-1*	0.1339	7.417	0.20	0.08	49.4	49.7	—	—	>22.4	3.0
T-13-2*	0.1229	7.341	0.28	0.10	43.1	47.8	—	—	>24.9	4.0
T-14-3	0.1255	7.353	0.33	0.12	48.0	52.1	—	—	32.0	3.5

*Ultimate Fracture at Grip. All values based on this ultimate load.

Table 4-3. Static fracture toughness of stretched, chem-milled and welded 2219-T87 aluminum alloy.

Ident.	Thick (CM)	Width (CM)	Crack (CM)	Max Ld. (KN)	G (KN/CM^2)	N (KN/CM^2)	Kc [$(KN/CM^2)(\sqrt{cm})$]	Temp (^oK)
L8-16-6	.1143	4.966	2.16	6.338	11.2	19.1	22.4	297
L8-16-2	.1189	5.006	2.13	6.694	11.3	19.6	22.4	297
L8-16-1	.1196	5.019	2.13	7.028	11.7	20.5	23.3	297
L8-16-3	.1173	4.961	2.11	6.627	11.4	19.8	22.5	297
L8-16-14	.1260	4.943	2.03	7.339	11.8	20.0	22.7	297
L8-16-4	.1173	4.968	2.13	6.539	11.2	19.7	22.4	297
L8-16-5	.1252	4.978	2.08	9.210	14.8	25.5	29.0	20
L8-16-15	.1151	4.991	2.08	9.697	16.9	29.0	33.1	20
L8-16-13	.1285	4.968	2.08	10.675	16.7	28.8	32.8	20
L8-16-11	.1186	4.951	2.08	10.097	17.1	29.7	33.7	20
L8-16-9	.1151	4.976	2.13	8.340	14.6	25.5	29.0	20
L8-16-7	.1118	4.966	2.08	8.295	14.9	25.7	29.3	20

Plane strain fracture toughness (K_{IE}) was calculated as follows:

$$K_{IE} = 1.1\sigma \sqrt{\frac{\pi a}{Q}} M_K$$

where

σ = gross stress	Q = flaw shape parameter
a = crack depth	M_K = magnification factor

Values shown in Tables 4-1 and 4-2 are apparent values and are not meant to be confused with the same designations as described ASTM E399.

At room temperature, the surface flaws propagated through the thickness for specimens L-14-2 and T-13-1. Consequently, the toughness values for these two specimens were calculated in the same manner as center-notched specimens, using Irwin's tangent formula.

As mentioned, specimens L-12-1 and T-13-2 failed through the grip ends at 20°K and were retested at room temperature to examine the surface flaw shape and dimensions. The fracture toughness of these specimens was calculated using the maximum load at 20°K and the flaw size observed on the fractured surfaces. The true toughness of those two specimens, therefore, exceeds the calculated values shown in Table 4-2.

5

FRACTURE MECHANICS ANALYSIS

The objectives of the fracture mechanics analysis task were: (a) to select the proofing criteria with respect to mission requirements, (b) to establish a set of preliminary acceptable initial defect sizes, and (c) to define a fracture mechanics plan.

5.1 PROOFING CRITERIA

From the fracture mechanics point of view, the purpose of a proof test is to screen out flaws larger than the size that would cause unstable crack growth at the proof pressure stress. A properly designed proof test can be very effective for thick-walled tanks; i.e., very small flaws can be screened out and the crack growth life of remaining flaws can be predicted. However, this procedure may not be appropriate for tanks made of thin, tough, materials.

If the smallest flaw that can be critical is through the thickness, and leakage in operation is not permissible, then the proof test cannot be used to screen flaws and a simple leak test at lower pressure will suffice. Initial flaw sizes must be established by some other NDI techniques.

The following analysis shows the LO_2 and LH_2 tanks to be in the thin, ductile category and, therefore, proof tests cannot be used to support the fracture mechanics analysis of residual strength and cyclic life.

5.1.1 LH_2 TANK ANALYSIS.

	Parent Material	Weld Material
$\sigma_p \leq .95\,\sigma_{ty}$	$< .95\ (51) \leq 333.7\ MN/m^2$ (48.4 KSI)	$.95\ (25) = 163.7\ MN/m^2$ (23.7 KSI)
$\sigma_{op} \leq \frac{\sigma_p}{1.05}$	$\leq \frac{48.4}{1.05} \leq 317.8\ MN/m^2$ (46.1 KSI)	$\frac{23.75}{1.05} = 156.0\ MN/m^2$ (22.6 KSI)
$t = \frac{pr}{\sigma} \geq$	$\frac{21.9\,(14 \times \frac{12}{2})}{46100} \geq .101$ CM (.040 in.)	$\frac{21.9\,(84)}{22600} = .206$ CM (.081 in.)

5.1.2 LO_2 TANK ANALYSIS.

	Parent Material	Weld Material
$\sigma_p \leq .95\ (51) \leq 333.7\,MN/m^2$ (48.4KSI)		$163.7\,MN/m^2$ (23.7 KSI)
$\sigma_{op} \leq \frac{28.4}{1.05} \leq 317.8\,MN/m^2$ (46.1KSI)		$156.0\,MN/m^2$ (22.6KSI)
$t \geq \frac{24.0\,(12\times\frac{12}{2})}{46100} \geq .094\,CM$ (.037 in.)		$\frac{24.0\,(84)}{22620} = .226\,CM$ (.089 in.)

5.1.3 CRITICAL FLAW SIZES. Critical flaw sizes were calculated for a range of thicknesses and stresses for parent material and weld material, using two equations.

The equation for surface flaws is:

$$a_{cr} = \left(\frac{K_{IE}}{1.1\,M_K\,\sigma}\right)^2 \frac{Q}{\pi}$$

The equation for through cracks is:

$$2a_{cr} = \frac{K_c^2\left[2-\left(\frac{\sigma}{\sigma_{ty}}\right)^2\right]}{\sigma^2\pi}$$

Results are plotted in Figures 5-1 through 5-4. Figure 5-1 shows that for P.M. thickness less than .155 cm (.06 in.) the tanks will leak before break at the maximum possible proof stress. Figure 5-2 shows that for weld material thickness less than $.1 \times 2.4 = .61$ cm (.24 in.) leak will occur before break. Figure 5-3 shows the critical length of through cracks in P.M. under the maximum possible proof stress to be about 1.90 (.75 in.). Figure 5-4 shows the critical through crack length in weld material to be in the range of 2.4 to 2.5 cm (1.0 in.).

5.1.4 DISCUSSION. For the operating stresses and material thicknesses used, the "leak before burst" failure mode is critical. A proof test alone will not ensure that the tank will not leak during the design life.

Final tank gages must be determined based on crack growth life of initial flaw sizes to be defined by NDI. A combination of analytical and empirical studies for pre-flawed specimens is needed.

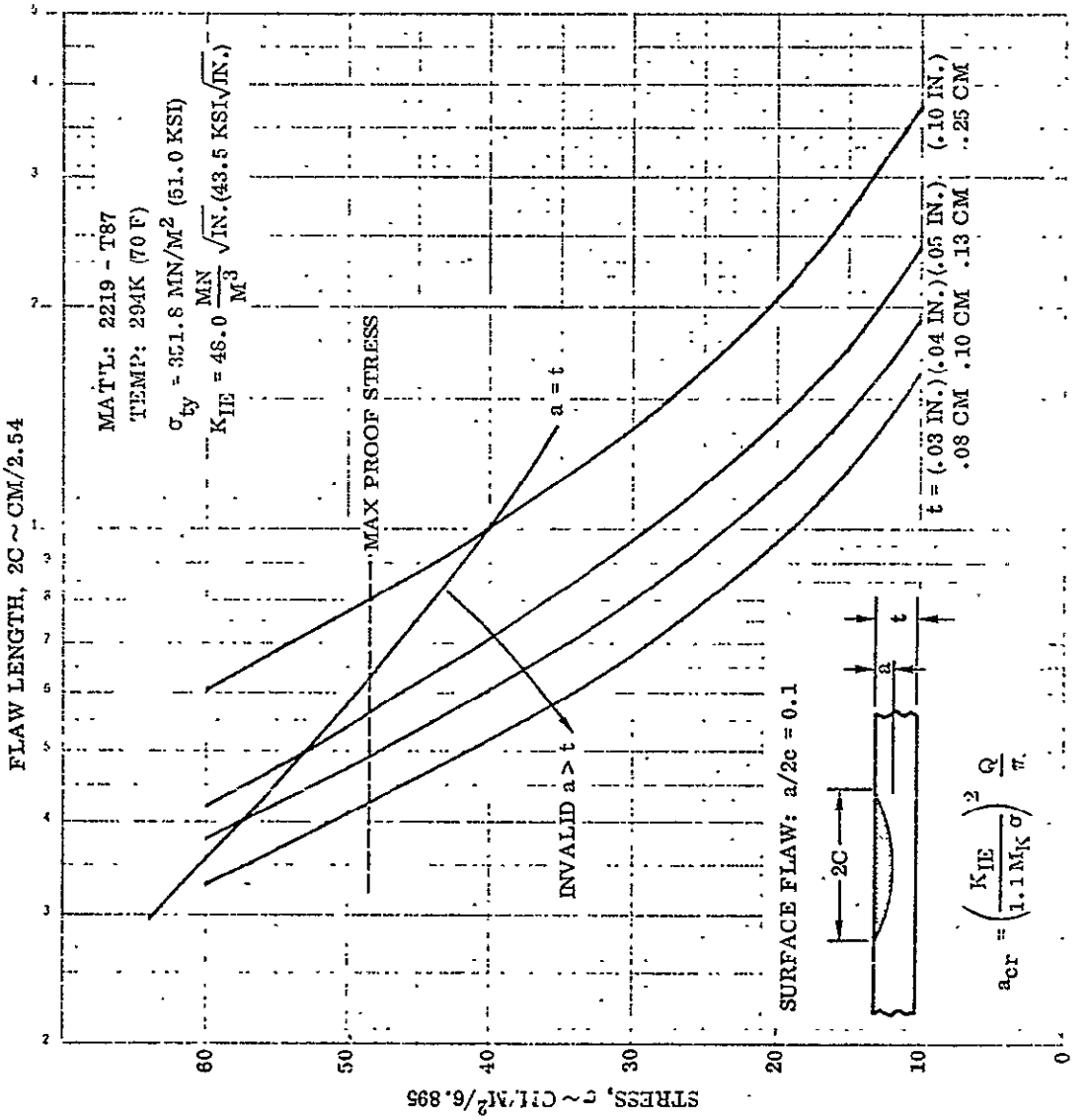

Figure 5-1. Stress vs critical flaw size.

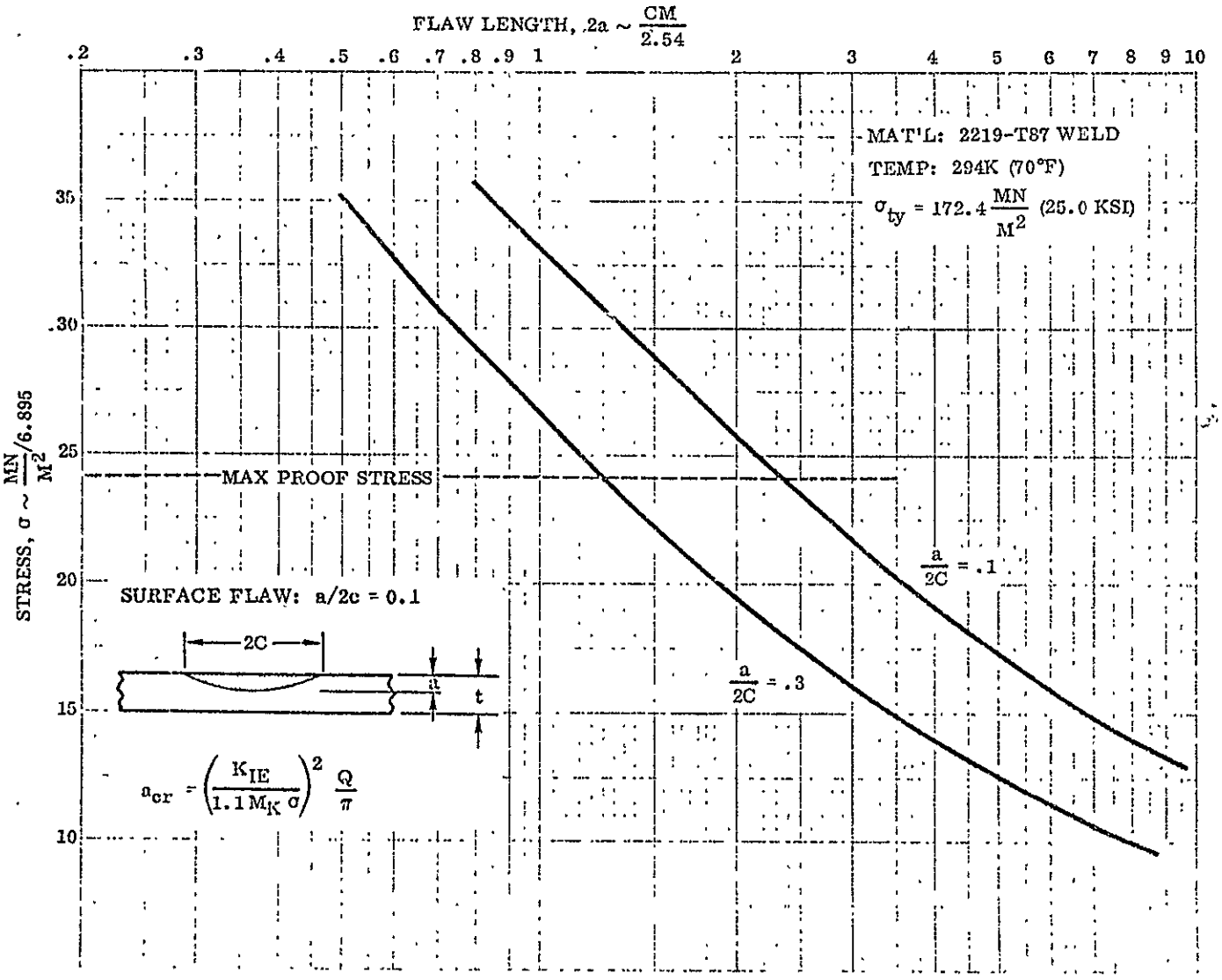

Figure 5-2. Stress vs critical flaw size.

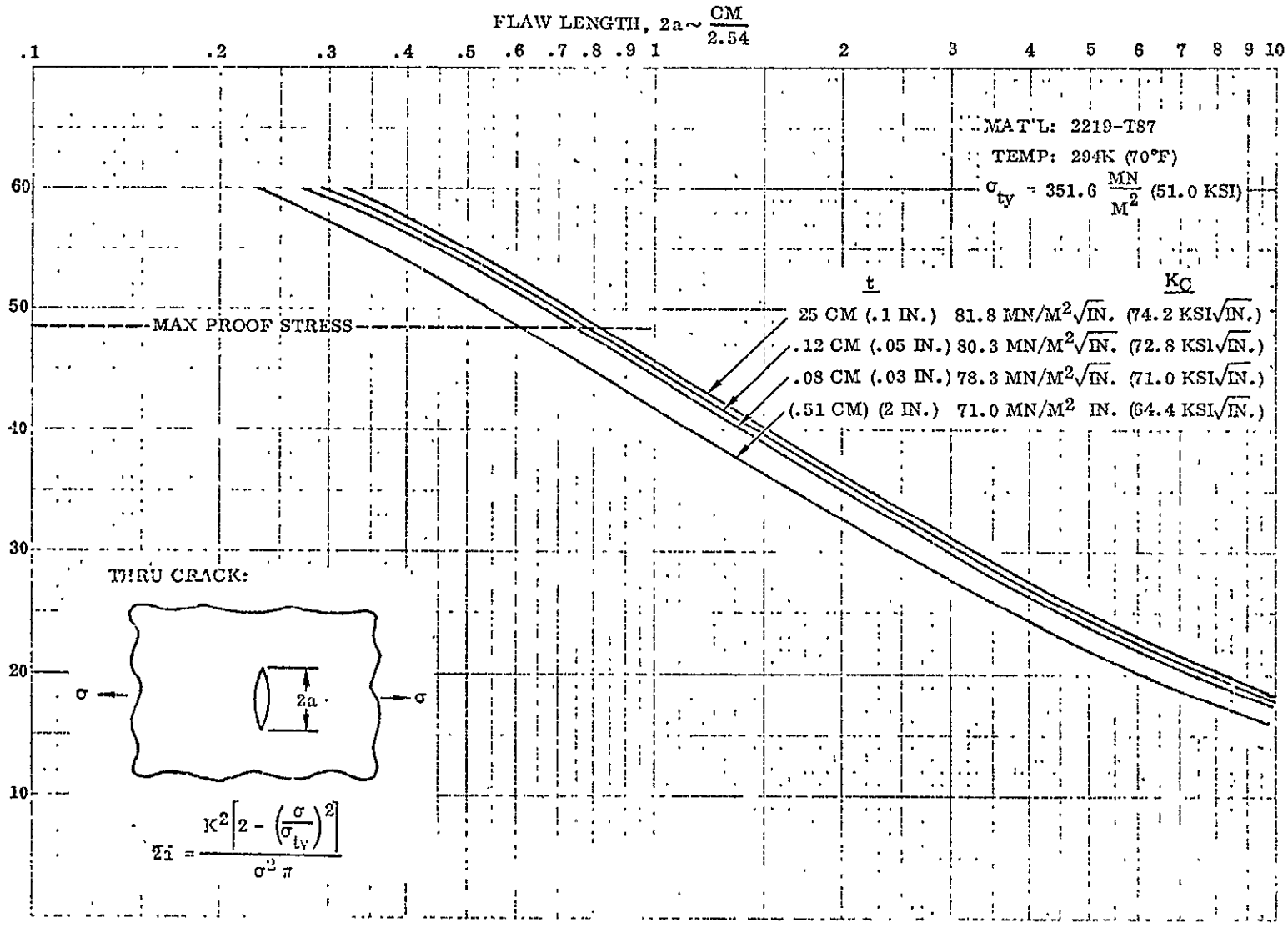

Figure 5-3. Stress vs critical flaw size.

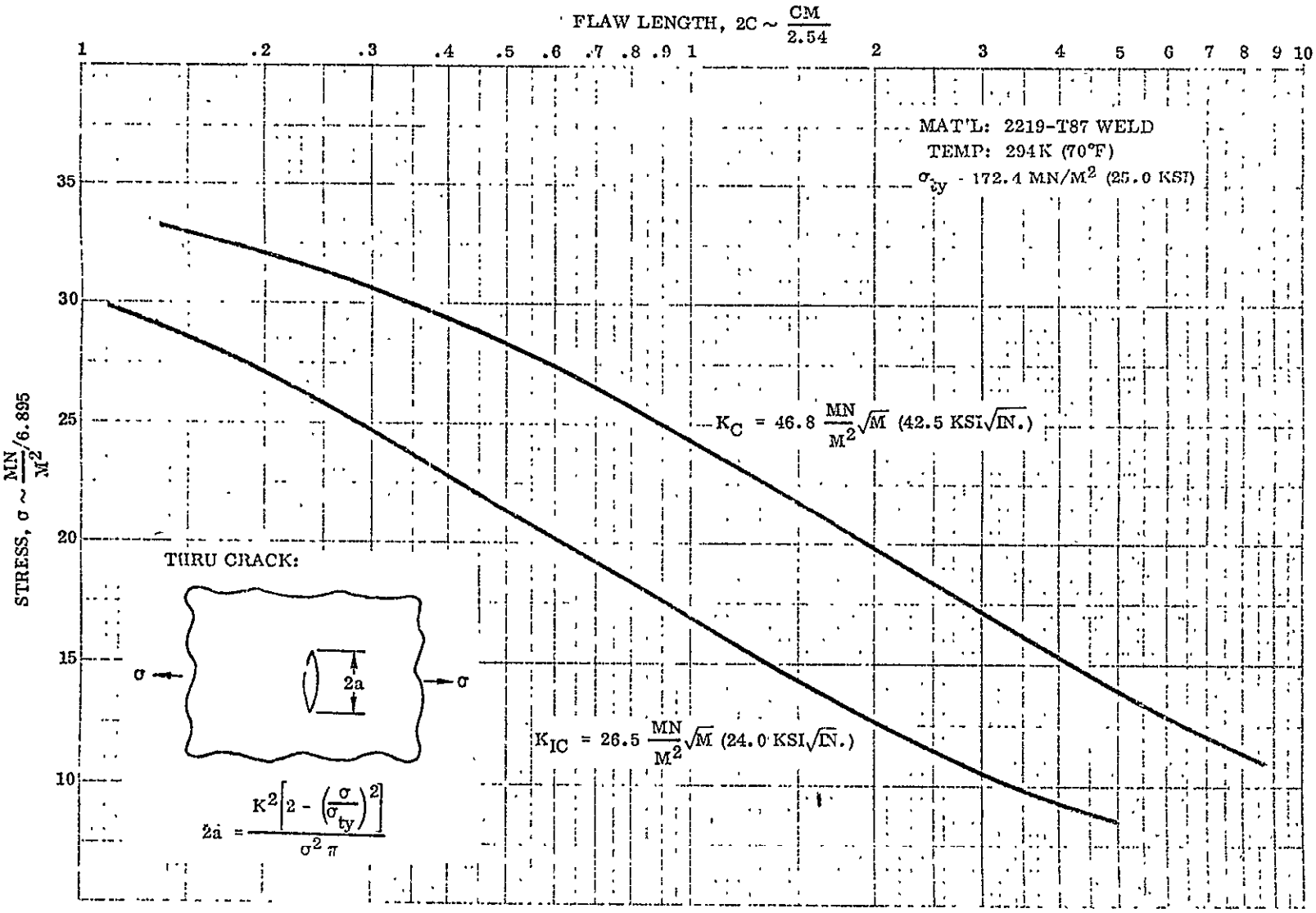

Figure 5-4. Stress vs critical flaw size.

5.2 ACCEPTABLE INITIAL DEFECT SIZES

5.2.1 GENERAL DISCUSSION. Initial cracklike flaws are assumed to exist in any area of the tank. The purpose of this analysis is to calculate the number of flights which can be made before initial cracks grow through the thickness (leak) or to the critical size (catastrophic failure). The FLAGRO-2* computer program can be used to facilitate the analysis. Input to the program consists of initial flaw geometry, load spectrum, material properties, and load-stress functions. Output includes crack size and stress intensity factor at each load step for each mission. The flight in which the crack grows through the thickness, and the flight in which the crack becomes critical, are flagged. By plotting results from several computer runs with varying initial flaw sizes, it will be possible to determine the maximum initial flaw sizes which will provide the required life of 50 missions (with a scatter factor of 4). With these results for several tank wall thicknesses for parent material and weldments, it is possible to establish NDI limits on permissible undetected flaws.

5.2.2 LOAD SPECTRA. The LH_2 tank design pressure profile has been idealized for analysis purposes as shown in Figure 5-5. Definitions required for the FLAGRO program are shown below the figure.

NOTE: Burn hold times of 2 to 3 minutes will cause sustained load crack growth as the crack nears critical length. Therefore, cutoff values of 0.8 Kc will be used in Phase I analysis to preclude sustained load growth.

5.2.3 MATERIAL PROPERTIES. A considerable amount of material property data must be screened and converted to the proper units.

5.2.4 LOAD-STRESS FUNCTIONS. Hoop stress-pressure relationships for the 4.29 meter diameter LH_2 tank are shown in Table 5-1.

Table 5-1. Hoop stress-pressure relationships.*

Thickness, t (cm)	P (KN/m^2)	σ (KN/cm^2)
0.076	69	19.37
0.102	69	14.43
0.127	69	11.59
0.152	69	9.68
0.203	69	7.25

* 4.29 m-dia LH_2 tank, based on $\sigma = \frac{Pr}{t}$

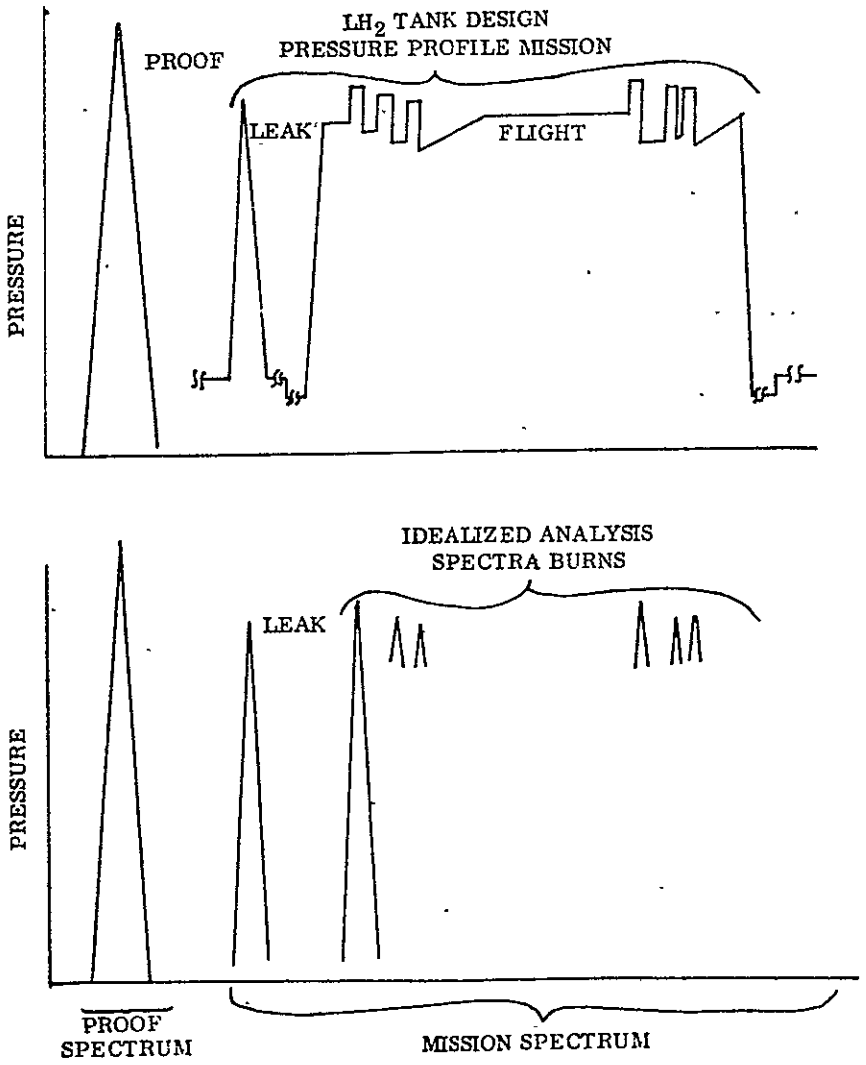

NOTE:

PROOF SPECTRUM: 1 PROOF = 1 BLOCK = 1 LIFE = 1 DESIGN LIFE

MISSION SPECTRUM:

1 MISSION = HOLD + LEAK + FLIGHT = 1 BLOCK

1 LIFE = 50 BLOCKS

1 DESIGN LIFE = 4 LIFETIMES = 200 BLOCKS

Figure 5-5. Load spectra for crack growth analysis.

5.2.5 CRACK GROWTH ANALYSIS RESULTS. Table 5-2 and Figure 5-6 show preliminary results for the LH_2 tank with T = 0.102. Room temperature material properties were used in these checkout computer runs. Several additional runs will be made and results will be similarly tabulated and plotted.

Table 5-2. Summary of crack growth analysis.

Run No.	Case No.	Material	Temperature	Thick (cm)	A_i (cm)	C_i (cm)	Number of Flights			A_f	C_f
							Leak	Sustained Growth	Break		
1	1	Parent	Room	0.102	0.051	0.508	-	-	-	0.076	
	2	Parent	Room	0.102	0.076	0.762	30	60+	69	0.102	2.03
	3	Parent	Room	0.102	0.089	0.889	3	20+	27	0.102	2.03
	4	Parent	Room	0.102	0.051	0.152	-	-	-	0.063	0.155
	5	Parent	Room	0.102	0.076	0.229	-	-	-	0.102	0.297
	6	Parent	Room	0.102	0.089	0.267	25	-	-	0.102	0.465

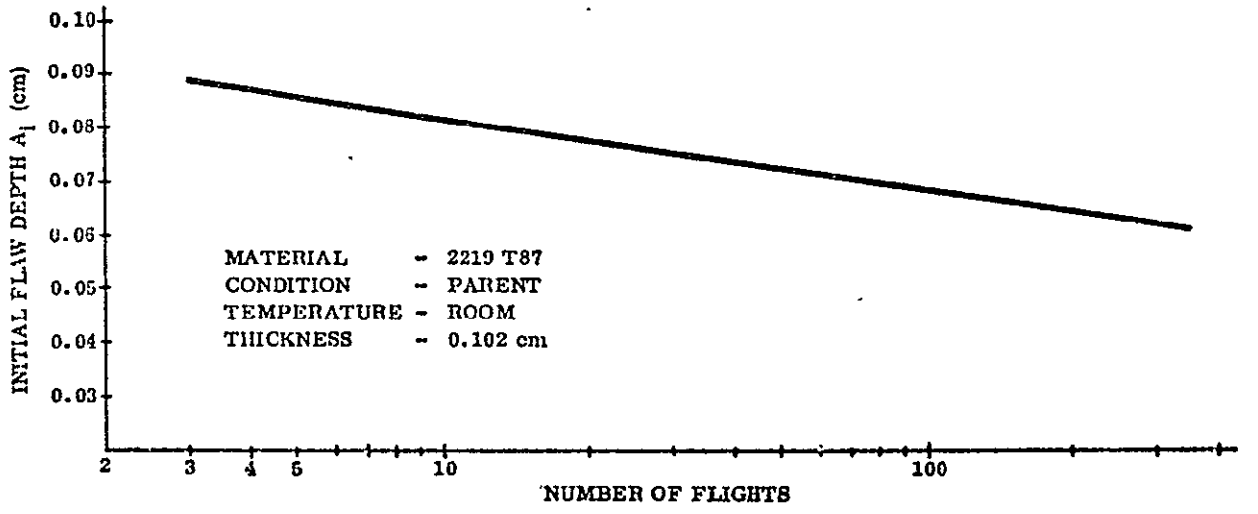

Figure 5-6. Initial flaw size versus flights to leak.

FLAGRO computer runs were made for the LH_2 tank, to investigate the effects of tank wall thickness and initial flaw depth on crack growth life. Figure 5-7 shows a plot of this data - number of flights vs. initial flaw depth. All of these cases include a proof test at room temperature, followed by the idealized analysis spectrum at -196°C (-320°F). Liquid hydrogen temperature was not used because insufficient data are available to determine the Paris coefficients needed in FLAGRO. The resultant error should be

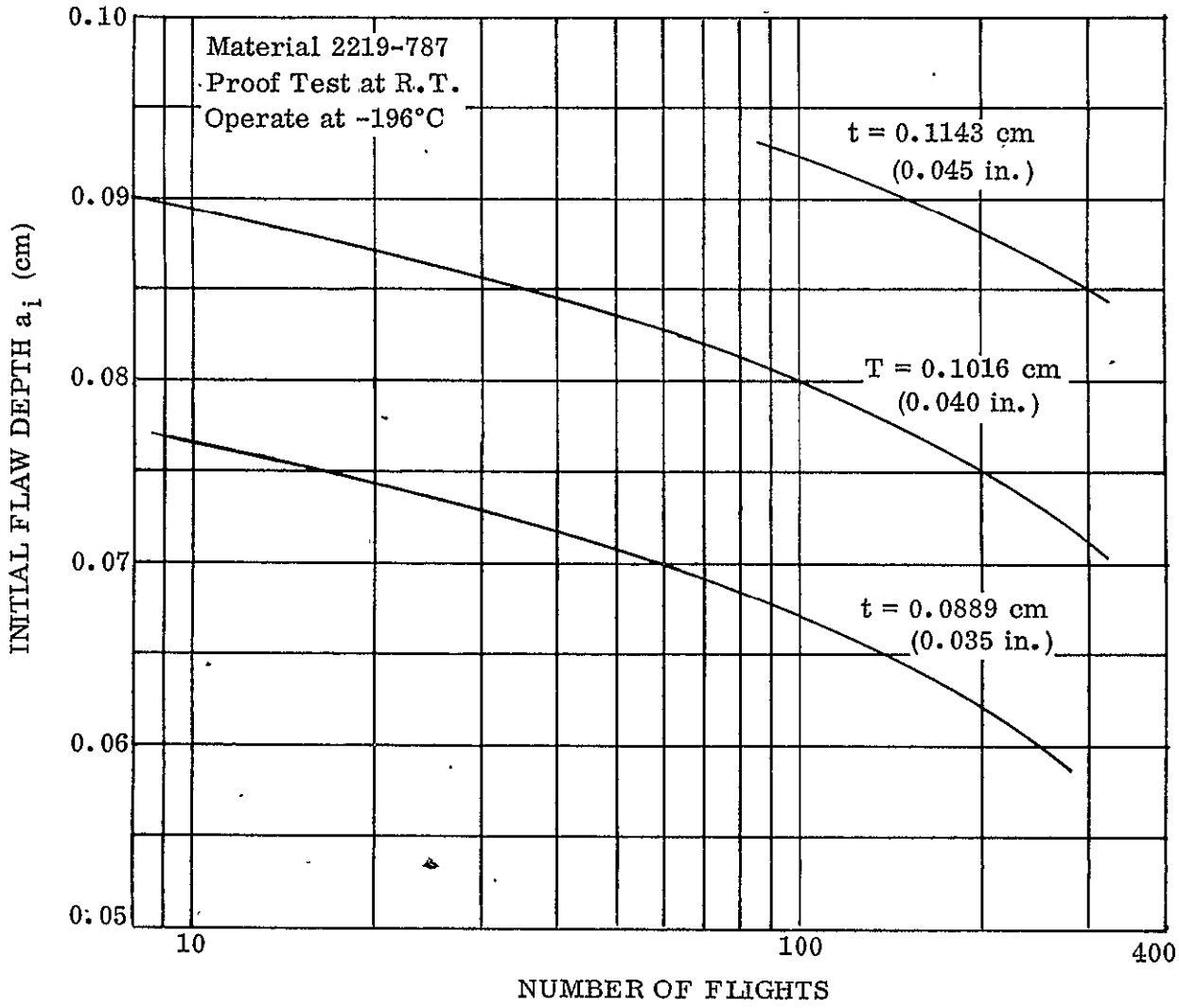

Figure 5-7. Initial flaw size vs. missions to leak for LH_2 tank.

small and conservative, since 2219-T87 is slightly tougher at LH_2 temperature. Figure 5-7 shows that a tank with an initial wall thickness of 0.100 cm would not grow through to leak in the design life of 200 missions.

5.2.6 PRESSURE-STRESS FUNCTIONS FOR THE LO_2 TANK. These functions are shown in Table 5-3. The data were input to the FLAGRO program and results are shown in Figure 5-8. Again the permissible flaw depth for no leakage in 200 missions is about 3/4 of the wall thickness.

Table 5-3. Pressure-stress functions for LO_2 tank.

t (cm)	R (cm)	P (KN/m^2)	σ (MN/m^2)
0.0762	182.9	68.9	165.5
0.1016	182.9	68.9	124.1
0.1270	182.9	68.9	99.3
0.1524	182.9	68.9	82.7
0.2032	182.9	68.9	62.1

5.3 FRACTURE MECHANICS PLAN

Fracture Control Plan, Lightweight LO_2 and LH_2 Propellant Tanks, PD75-0065 was created for this contract, using the fracture control plan for the Space Shuttle Orbiter mid-fuselage as a guide. This document includes design requirements, flow detection, and fracture analysis. The purpose of this plan was to identify, define, and assign responsibility for all tasks necessary to insure that lightweight LO_2 and LH_2 propellant tanks comply with the service life and residual-strength requirements of the tank design requirements document, PD75-0044. More specifically, these tasks are aimed at:

a. Prevention of failure that would cause loss of the space vehicle or injury to personnel due to growth of undetected flaws or cracks in the main propellant tanks.

b. Minimizing vehicle down-time and refurbishment costs due to repair or placement of a leaking tank.

These requirements are based on the design criteria for the Space Tug main propellant tankage system.

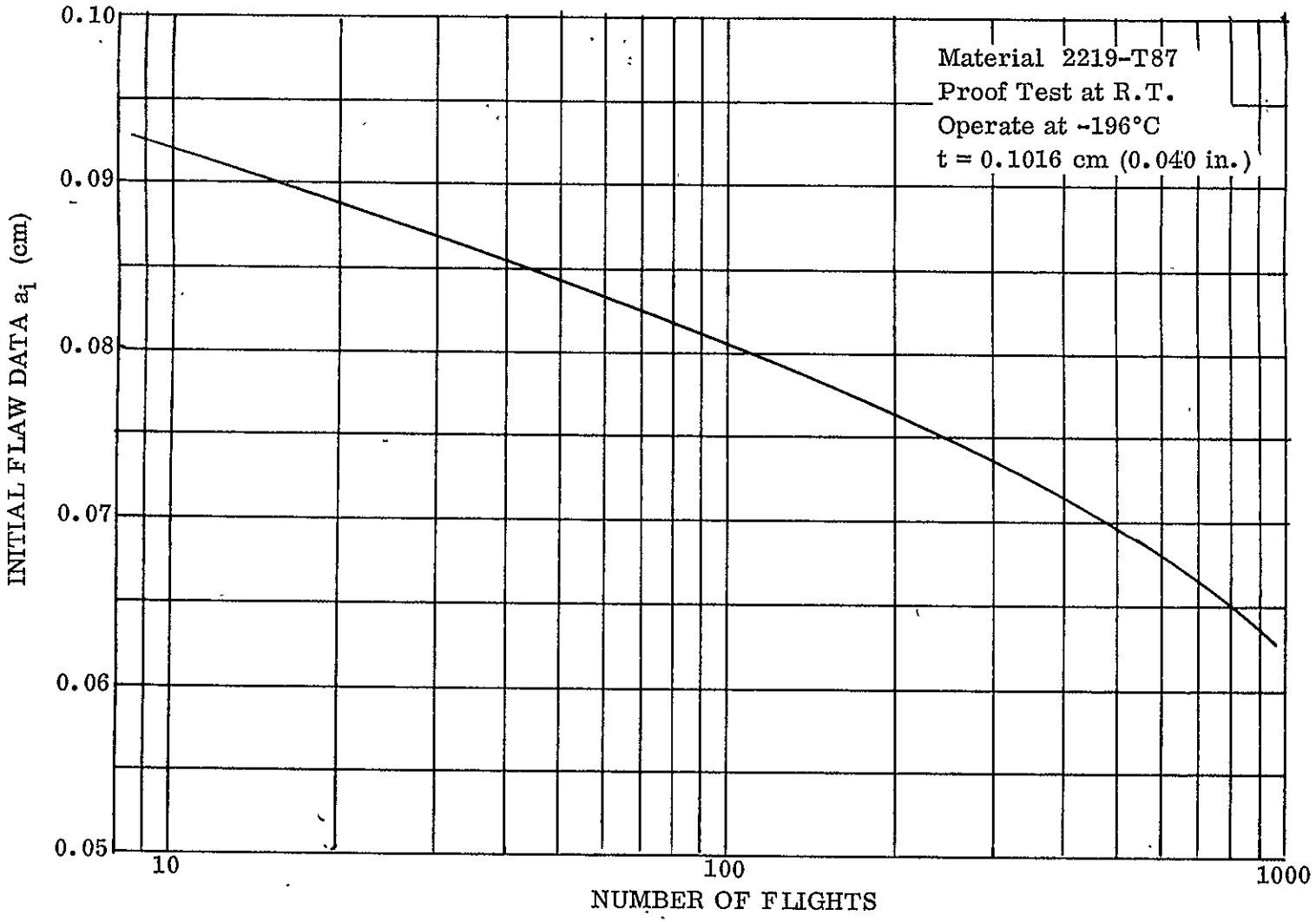

Figure 5-8. Initial flaw size vs. missions to leak for LO_2 tank.

6

TUG STRUCTURAL SYSTEM EFFECTS

The objectives of the Tug structural system effects task were to: (a) assemble tank concepts into total tug tankage systems; (b) determine the weight effects of tank, shell, and subsystems; and (c) determine payload weight effects to be used for total tank system evaluation.

6.1 GENERAL DISCUSSION

As part of this task, additional oxidizer tank sizing was performed to include an ellipticonic aft bulkhead. The cone geometry was analyzed for engine interface effects, including installation clearance requirements. Figure 6-1 describes the interference and clearance problem areas associated with an assumed baseline of 0.52-radian half-cone angle: the engine bell deployment mechanism will strike the cone before the engine can gimbal its full travel; the static clearance (2.54 cm) between the LH_2 feed duct and tank/bell is considered inadequate; and the LO_2 feed duct requires tight bends to remain within the bell envelope. Figure 6-2 illustrates one solution to these problems; i.e., to add a 7.62-cm spacer thrust block between the engine and thrust cone. This will ensure a 3.81-cm clearance with the tank cone at the extreme engine gimbal angle and will develop adequate LH_2 feed line clearances. The LO_2 line routing is also greatly simplified since it can then be routed outside the engine bell envelope. Figure 6-3 illustrates a second method to overcome the baseline problems. In this case the thrust cone angle is greater than the tank shell cone angle. The thrust cone angle is 0.70 radian while the shell cone angle remains 0.52 radian. The results are similar to the spacer addition. A third approach is depicted in Figure 6-4. In this case, the basic cone angle is revised to 0.65 radian and all the improvements are gained as in the previous case.

There were two reasonable solutions to the interference problem of the assumed baseline continuous 1.047 radian cone: the 0.916 radian (52.5 degree) cone configuration and the biconic, configuration, with a bulkhead cone angle of 1.047 radians (60 degrees) and a thrust cone of 0.916 radian (52.5 degrees). Length and weight comparison data are shown in Table 6-1 for the reference contour ($\sqrt{2}$ ellipse). Though there is only a small difference in weights, the 0.4 meter difference in length is significant, and the biconic approach was selected as the conic bulkhead concept candidate. This concept was evaluated with respect to the NASA baseline truss configuration in terms of system weight and overall tank length.

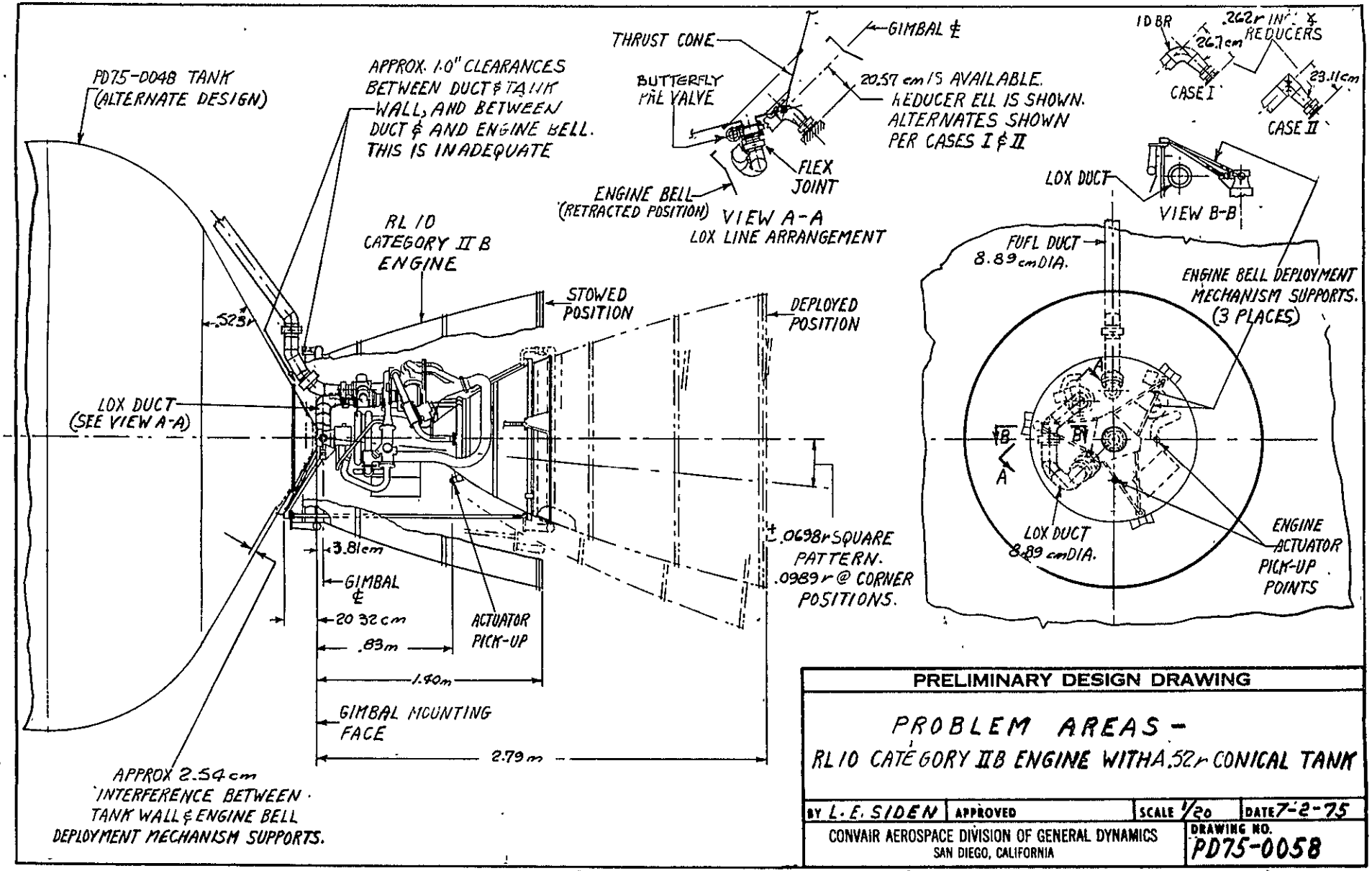

Figure 6-1.

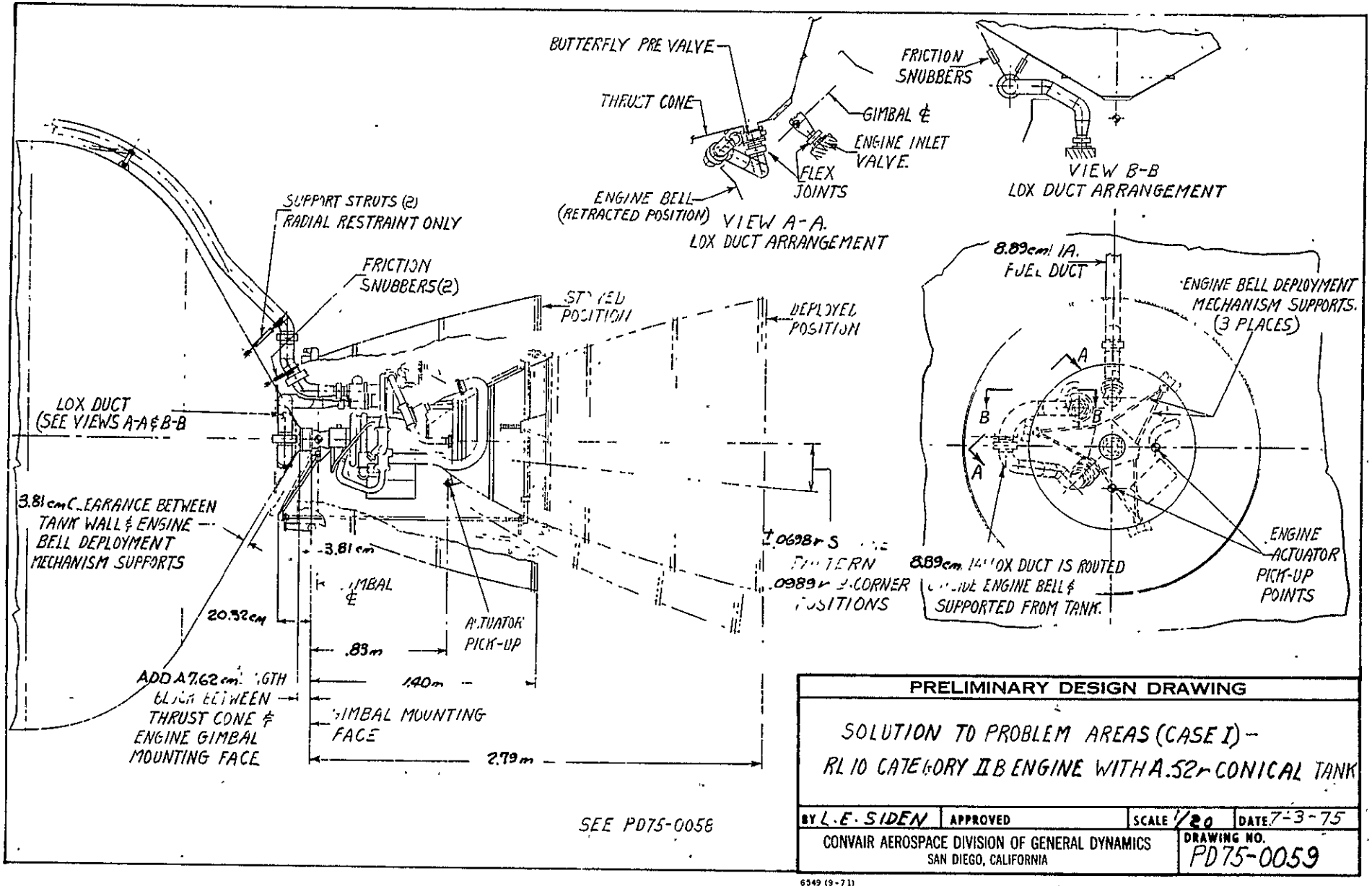

PRELIMINARY DESIGN DRAWING			
SOLUTION TO PROBLEM AREAS (CASE I) – RL 10 CATEGORY II B ENGINE WITH A 52r CONICAL TANK			
BY L. E. SIDEN	APPROVED	SCALE 1/20	DATE 7-3-75
CONVAIR AEROSPACE DIVISION OF GENERAL DYNAMICS SAN DIEGO, CALIFORNIA		DRAWING NO. PD75-0059	

6549 (9-71)

Figure 6-2.

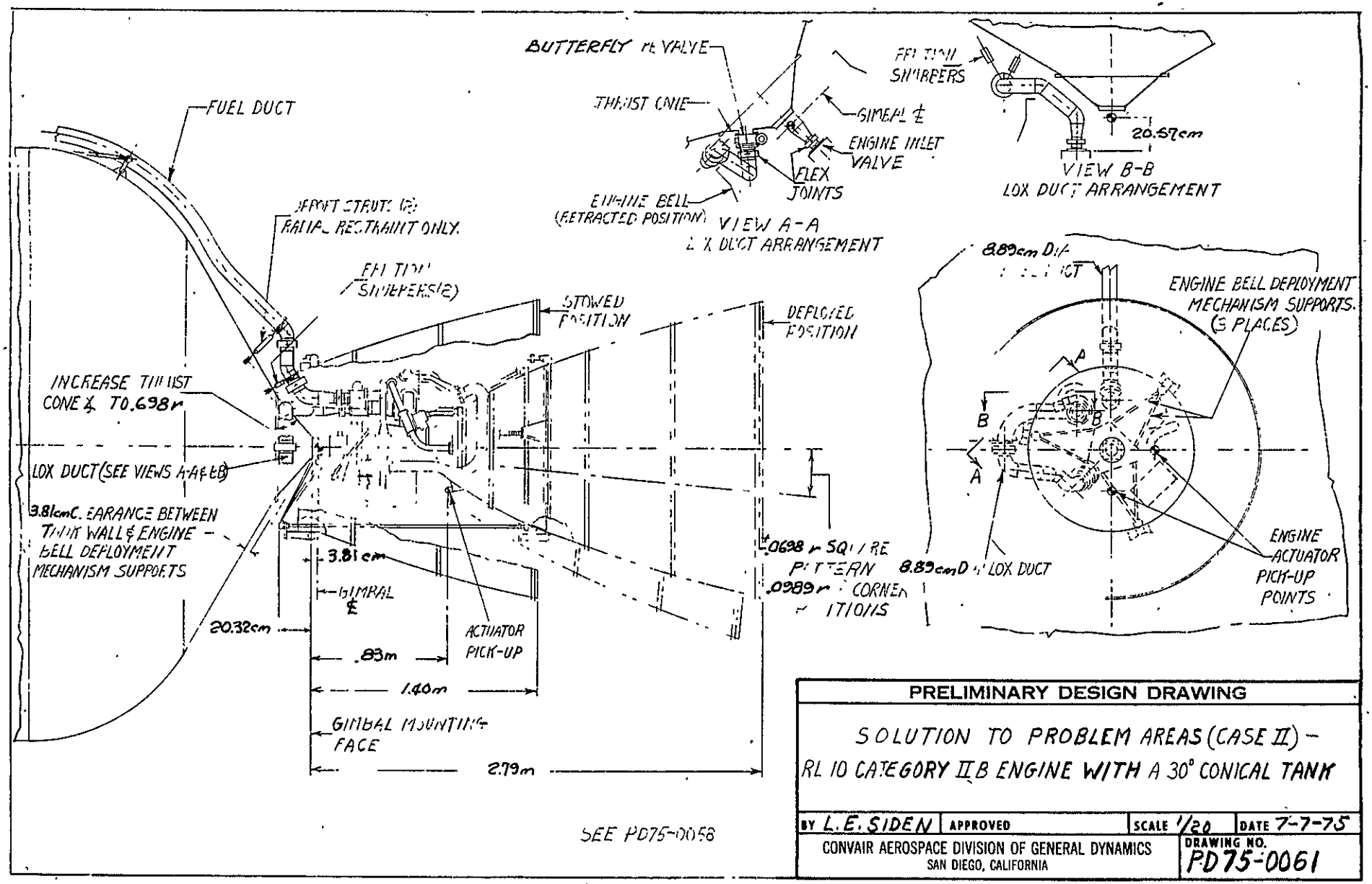

PRELIMINARY DESIGN DRAWING			
SOLUTION TO PROBLEM AREAS (CASE II) - RL 10 CATEGORY IIB ENGINE WITH A 30° CONICAL TANK			
BY L.E. SIDEN	APPROVED	SCALE 1/20	DATE 7-7-75
CONVAIR AEROSPACE DIVISION OF GENERAL DYNAMICS SAN DIEGO, CALIFORNIA			DRAWING NO. PD75-0061

6549 (9-71)

Figure 6-3.

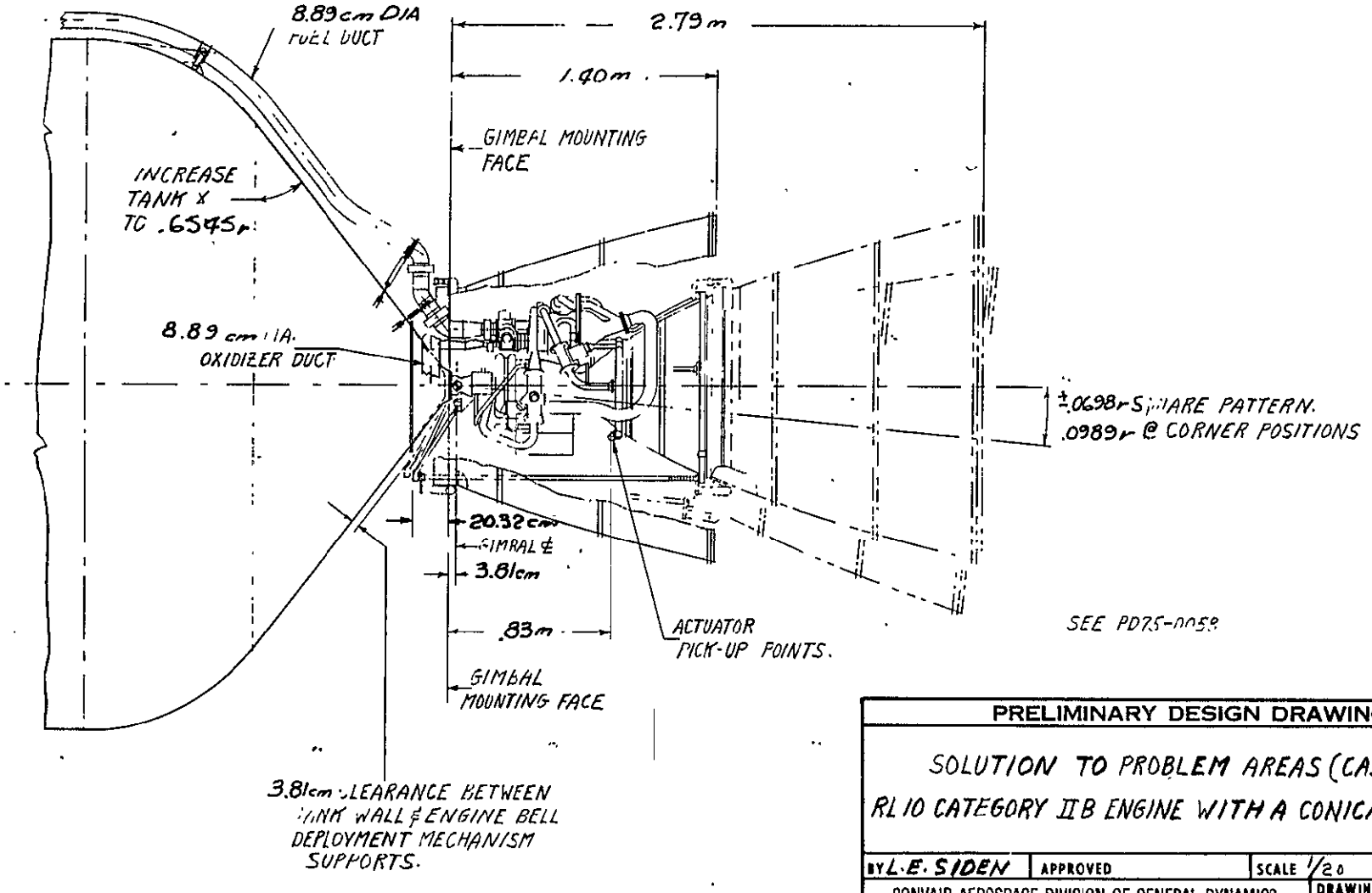

PRELIMINARY DESIGN DRAWING			
SOLUTION TO PROBLEM AREAS (CASE III) RL 10 CATEGORY IIB ENGINE WITH A CONICAL TANK			
BY L. E. SIDEN	APPROVED	SCALE 1/20	DATE 7-8-75
CONVAIR AEROSPACE DIVISION OF GENERAL DYNAMICS SAN DIEGO, CALIFORNIA			DRAWING NO PD75-0062

6549 (9-71)

Figure 6-4.

Table 6-1. Ellipticonic comparison.

Cone Angle (radians)	Length (m)	Membrane Weight (Kg)
0.916 constant	3.1	65.9
1.045/0.916 biconic	2.7	65.3

The NASA baseline thrust structure, as defined in MSFC 68M00039-2 "Baseline Space Tug Configuration Definition", is an open fiberglass truss conic frustum with a 0.179-m-dia engine gimbal block, a forward diameter of 2.31 meters, a height of 0.72 meter, and a weight of 13.2 Kg. A basic weights analysis was performed to ensure that all comparable elements were included in the thrust structure weight; i.e., the tank weld pads, tank brackets, stable strut assemblies, and actuator interface supports.

The fundamental truss loading was developed using the baseline engine thrust at an angle of 0.1 radian (corner of square pattern) on the truss geometry as described above. The ultimate strut compressive load was 30 KN. The basic strut was sized based on Figure 3-39 in NASA CR 120937 "Fiberglass Supports for Cryogenic Tanks". The resulting strut weight was 1.12 Kg, including end fittings. The clevis type weldment brackets with weld lands were 0.14 Kg each. The present Centaur uses tripod trusses to support the engine actuators, similar to those which would be needed on the Tug; therefore, the actual weights of these trusses were used (1.34 Kg, with an additional 0.27 Kg for tank weldments). The thrust block weight is 9.9 Kg. Considering a stable nine-strut system, the total weight for the truss thrust system is 14.9 Kg. The weight of a thrust cone with comparable interface is 8.06 Kg, as follows:

Ring	4.3 Kg
Actuator Fillings	0.45
Blades	0.45
Penetrations	0.23
Risers	0.59
Skin	0.86
Block	1.18
Total	8.06 Kg

The ellipsoidal and N_θ/N_ϕ oxidizer tanks were resized with conic transitions in the aft bulkheads, while maintaining the same volume. New tank weights were developed using the same design loads as the spheroid tanks. These weights and tank lengths are shown in Table 6-2. The primary cone weights were determined based on flight loads only.

Table 6-2. Thrust structure comparison.

Configuration	Tank Length (M)			Shell Weight (Kg)	Thrust Structure Weight (Kg)	Summation Weight (Kg)
	Forward Bulkhead	Girth to Gimbal	Total			
Baseline	1.293	1.730	3.023	79.57	14.88*	94.57
$\sqrt{2}$ Ellipse with Cone	1.284	1.678	2.962	78.59	8.06	86.65
N_θ/N_ϕ with Cone	1.239	1.685	2.924	80.19	8.06	88.25

*Includes tank brackets, weld lands, and activator supports.

If the engine is not independently supported during transportation and erection, the oxidizer tank's aft bulkhead must support the engine as a cantilevered load. The resulting moment on the conic bulkhead would be 9062 Newton-Meters (80,214 in.-lbf), based on engine weight of 200 Kg (442 lbm) with a load factor of two for handling and an ultimate factor of two. The skin gage necessary to resist this bending moment varies with internal pressure, as shown in Figure 6-5. This curve was developed using the methods defined in the "Shell Analysis Manual" NASA MSC, Section 3.24.1B, Axial Compression, Unstiffened Cone, Pressurized. An equivalent thrust load was used:

$$T_{eq} = \frac{2M}{R} \quad \frac{2(9062)}{0.425} = 42644 \text{ N}$$

The fundamental critical buckling stress was defined by:

$$\sigma_{cr} = (C_c + \Delta C_c) \frac{Et}{R_e}$$

where the factor C_c is taken from a curve in the Shell Manual for unpressurized cones, ΔC_c is the incremental increase for internal pressure, and

E = Youngs modulus,

t = skin gage,

R_e = small end radius divided by the cosine of the cone half angle.

Therefore, if the standby pressure (2.75N/Cm^2, 4 psi) is maintained, the tank weight must be increased by 1.73 Kg (3.8 lbm). If the tank must support the engine without the benefit of internal pressure, the tank weight must be increased by 4.9Kg (10.8 lbm). For the end result with the worst condition (no pressure), the ellipticonic tank membrane weight is 78.12 lbm, equal to the baseline weight but 0.06 meter shorter.

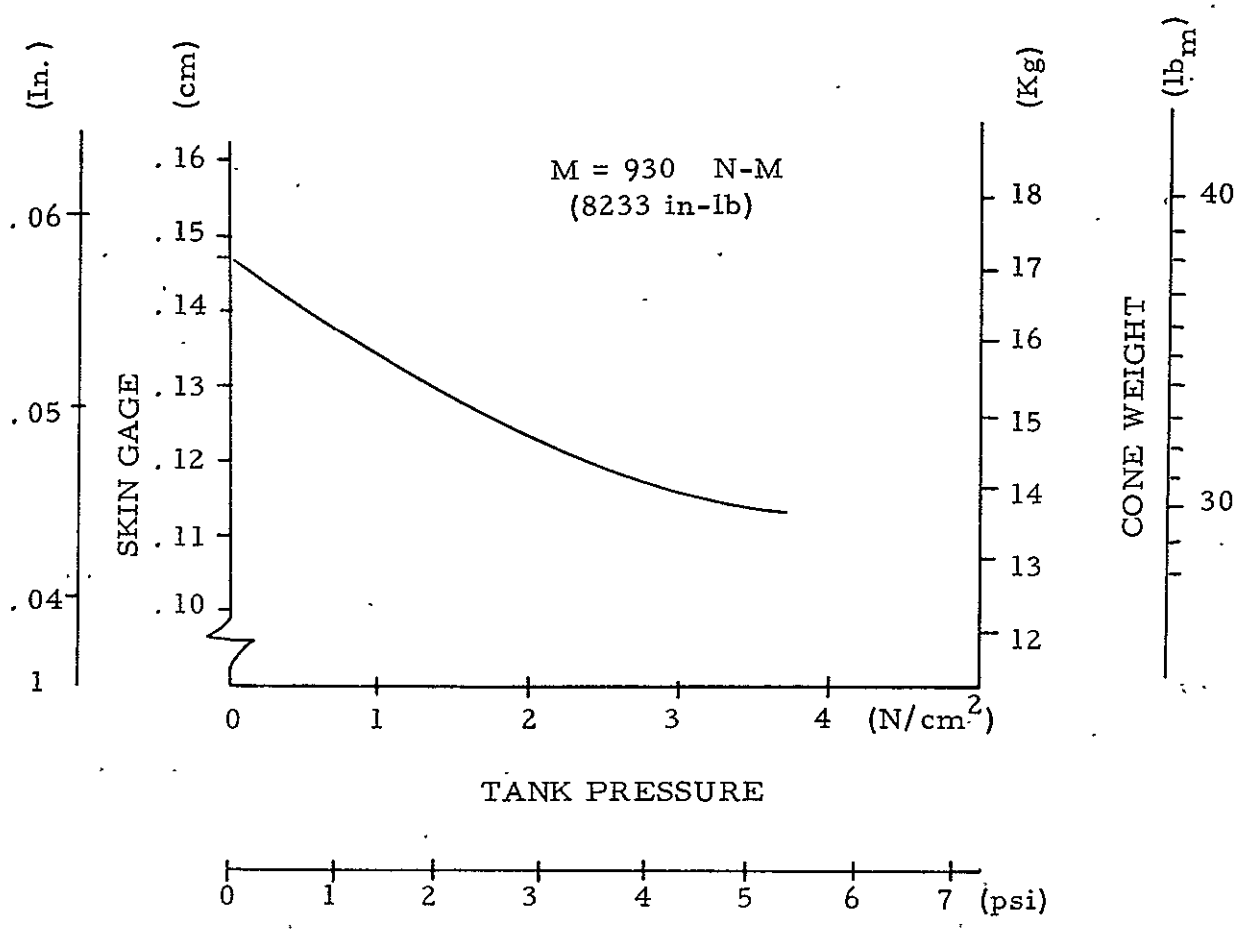

Figure 6-5. Conic bulkhead sizing for compressive loads.

Those tank weight penalties required to support the engine during transportation are noted, but the basic tank system comparison and predesign will not include these weights, since the present requirement is that ground loads shall not design flight hardware.

A propellant residuals analysis was performed to determine the optimum size of tank sump and plate, and to compare the residuals in the ellipticonic cone with the sump in a spheriod tank. The basic tradeoff and selection of an outlet configuration is based on its contribution to overall vehicle drag weight and the effects on nonusable (residual) propellants. The residual propellants were determined for the baseline ($a/b = \sqrt{2}$ ellipsoidal) bulkhead, the shallow N_θ/N_ϕ bulkhead, and the conic thrust cone configurations. In the case of the bulkheads, the residuals were determined with and without a sump; for the cone, residuals were determined with and without an inverted flow line, as shown in Figure 6-6.

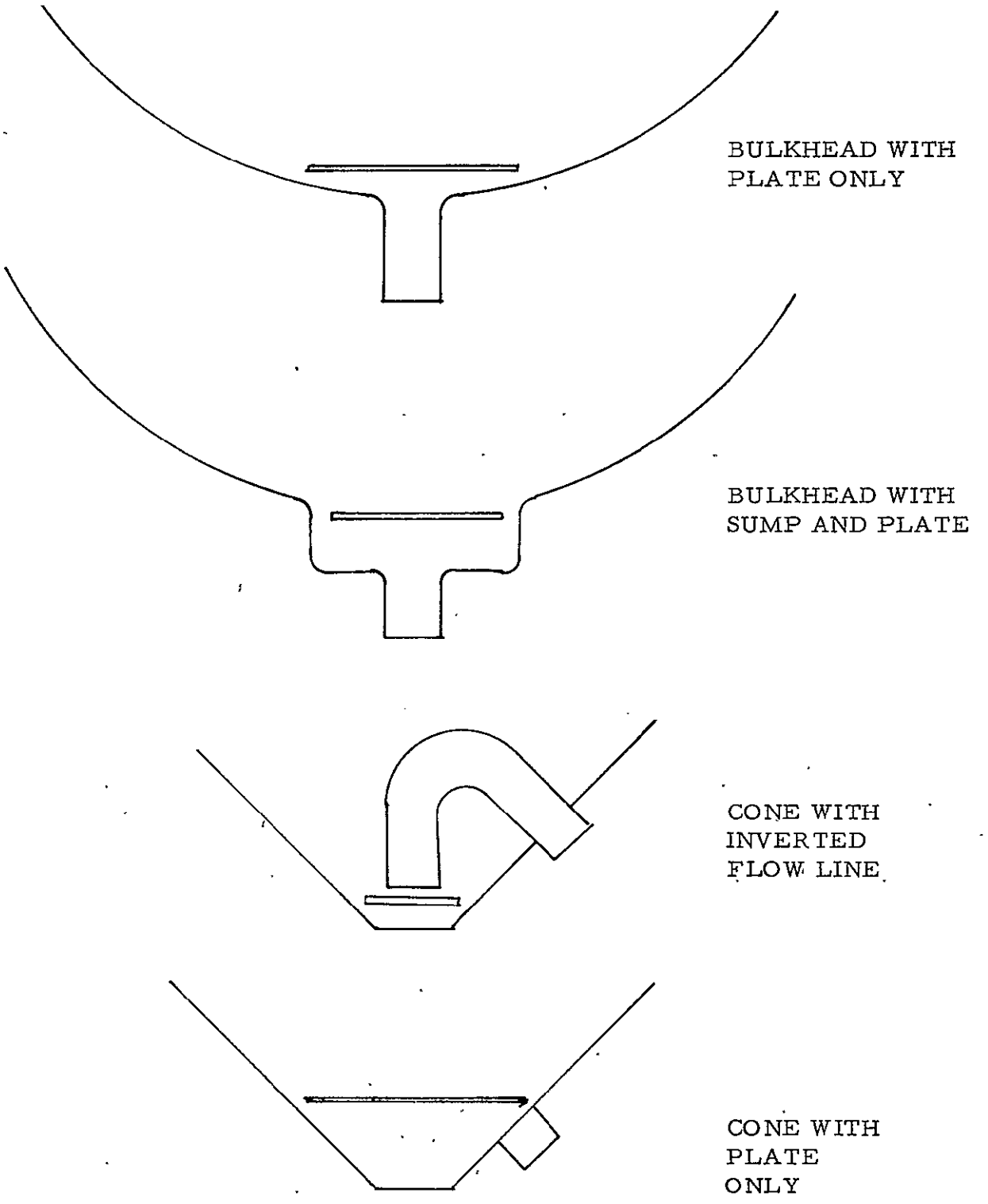

Figure 6-6. Outlet configurations.

The flow requirements were developed from the NASA Baseline Document, which presented the following data:

Thrust	= 66.72 Kn	V_o	= 0.0113M^3/sec
I_{sp}	= 4566.14 N.S/Kg	V_f	= 0.0303M^2/sec
M.R.	= 6.0	Burnout thrust/weight	= 2.06

Half the propellant volume contained below the plate was considered usable at the time of pull-through around this plate. The curves in Figure 6-7 represent the effects of plate or sump diameter on residuals for the two bulkhead contours. The optimum sizes were selected from these curves, as shown in Table 6-3.

Table 6-3. Optimum outlet configuration, bulkhead contours.

Radius (m)	2.48		3.65	
Type	Sump	Plate	Sump	Plate
Diameter (m)	0.305	0.381	0.381	0.457
Residual Weight (Kg)	4.8	7.0	6.1	8.0

The conical sump residuals versus pull-through plate diameter are shown in Figure 6-8 and from these curves the optimum sizes were selected as shown in Table 6-4.

Table 6-4. Optimum outlet configuration, cone.

Cone Angle (rad)	1.83		2.09	
Type	Inverted	Asymmetric	Inverted	Asymmetric
Diameter (m)	0.15	0.37	0.15	0.38
Residual Wt (Kg)	3.5	7.2	3.8	6.7

The curves in Figure 6-9 represent the effects of plate or sump diameter on residuals in the LH_2 tank.

6.2 ASSEMBLE TANK CONCEPTS INTO TOTAL TUG TANKAGE SYSTEMS

The individual tank data was assembled into tank combinations which could be reviewed in terms of total Tug vehicle effects. Figure 6-10 shows the overall dimensions, areas, and weights for combinations using the spheroid oxidizer tank. Figure 6-11 shows similar information for the combinations using the ellpticonic oxidizer tank. From these figures, the shortest configuration would be the N_θ/N_ϕ LH_2 tank with the ellipticonic LO_2 tank, and the lightest combination would be the Cassinian LH_2 and elliptical LO_2.

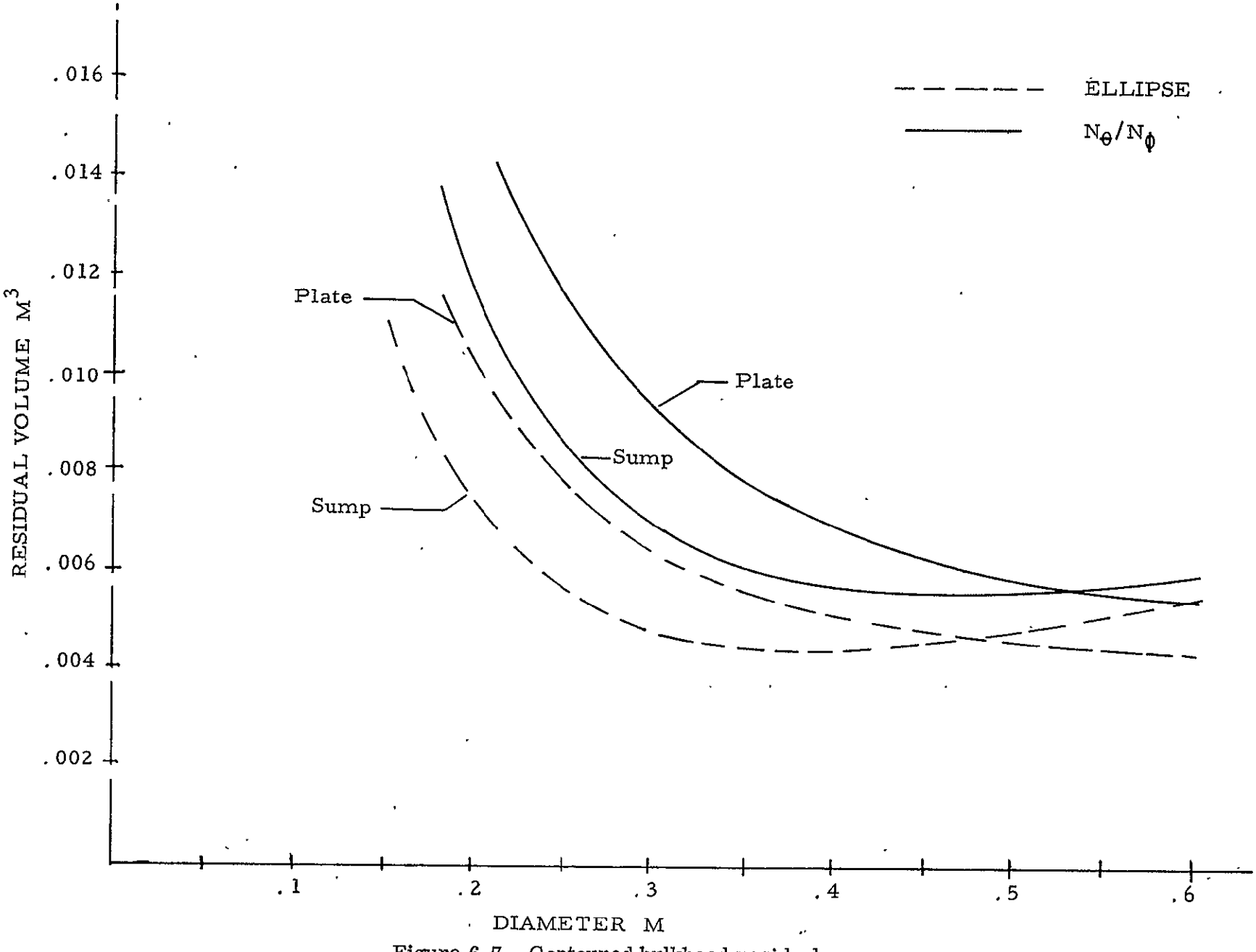

Figure 6-7. Contoured bulkhead residuals.

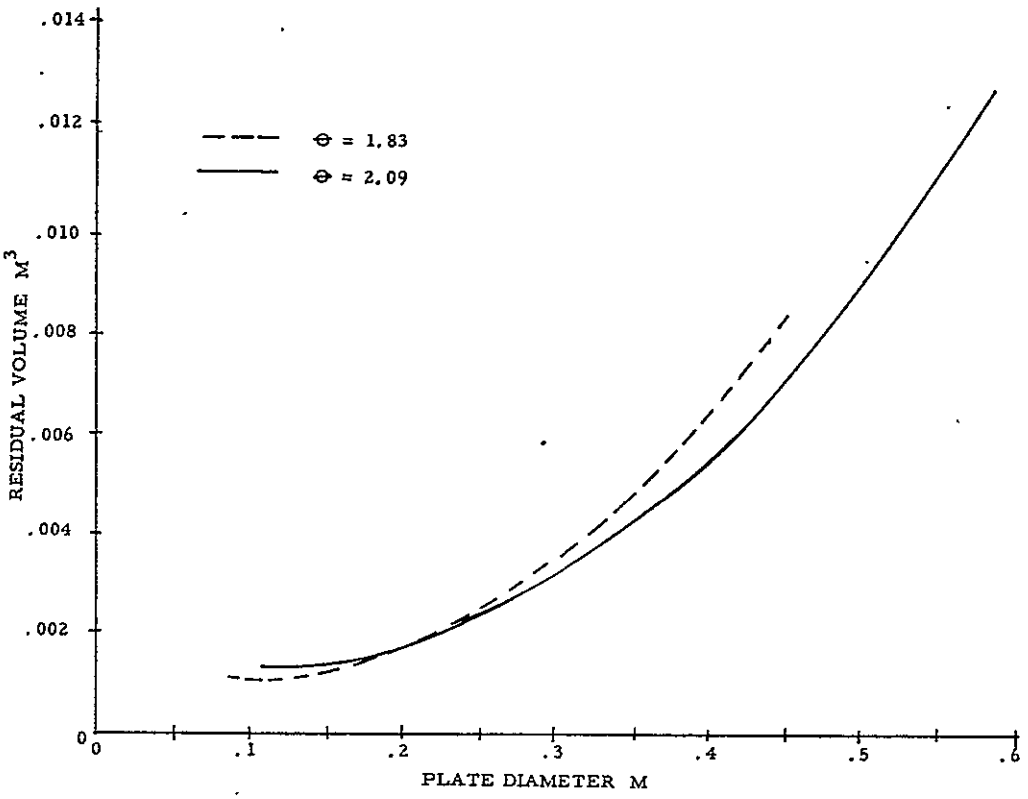

Figure 6-8. Conic sump residuals.

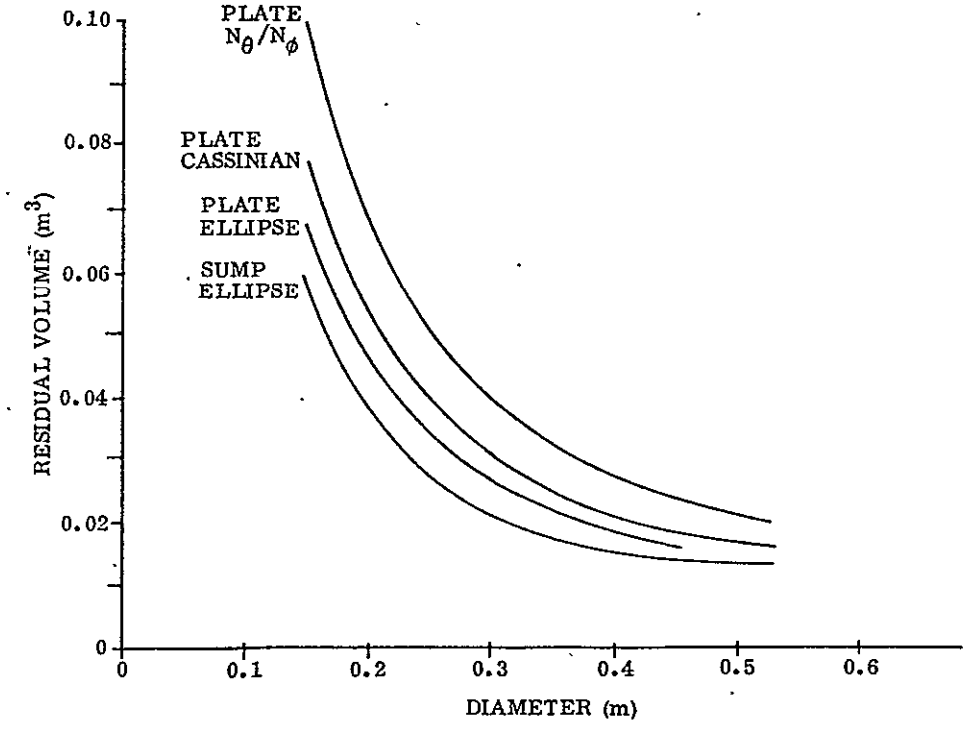

Figure 6-9. LH_2 tank residuals.

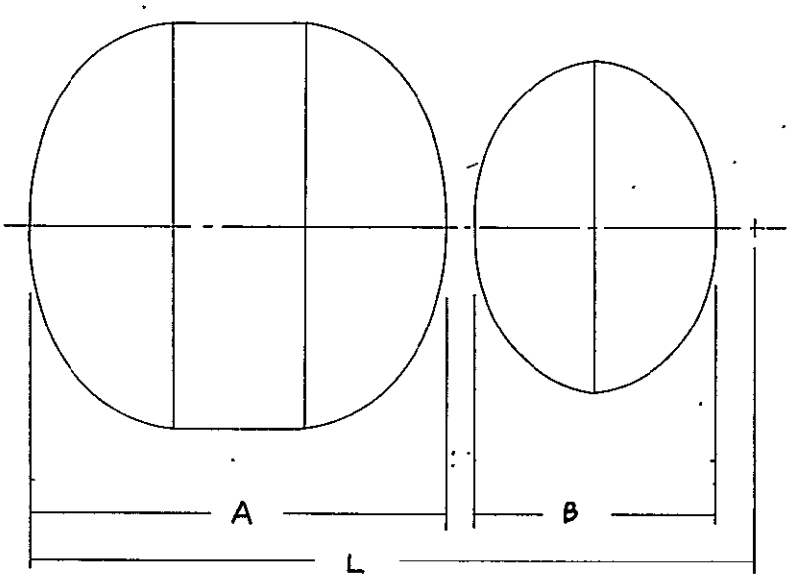

Configuration		A (m)	B (m)	L (m)	Total Area (m^2)	Total Weight (Kg)
LH_2 Tank	LO_2 Tank					
Elliptical	Elliptical	4.43	2.59	7.71	99.94	241.98
Elliptical	N_θ/N_ϕ	4.43	2.50	7.62	99.98	246.85
N_θ/N_ϕ	Elliptical	4.26	2.59	7.54	100.19	248.00
N_θ/N_ϕ	N_θ/N_ϕ	4.26	2.50	7.45	100.23	252.88
Cassinian	Elliptical	4.37	2.59	7.65	99.99	238.87
Cassinian	N_θ/N_ϕ	4.37	2.50	7.56	100.03	243.74

Figure 6-10. Total vehicle effects with spheroid LO_2 tank.

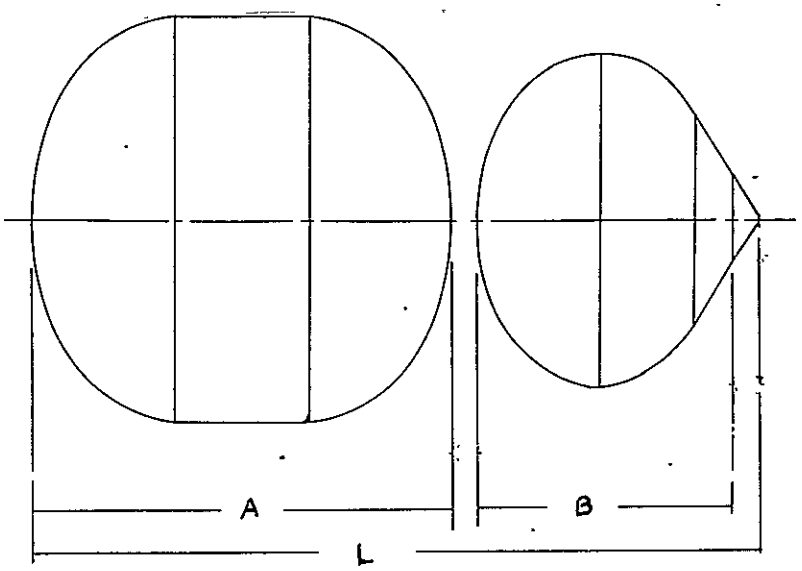

Configuration		A (m)	B (m)	L (m)	Total Area (m^2)	Total Weight (Kg)
LH_2 Tank	LO_2 Tank					
Elliptical	Ellipticonic	4.43	2.70	7.65	99.98	249.06
N_θ/N_ϕ	Ellipticonic	4.26	2.70	7.48	100.13	255.09
Cassinian	Ellipticonic	4.36	2.70	7.58	99.94	245.95

Figure 6-11. Total vehicle effects with ellipticonic LO_2 tank.

6.3 DETERMINE THE WEIGHT EFFECTS OF TANK, SHELL AND SUBSYSTEMS

The Tug system weights defined during the Space Tug/Shuttle Interface Compatibility Study were used to develop weight deltas versus change in length for the various areas of the Tug affected by tank length changes. These factors are presented in Table 6-5.

6.4 DETERMINE PAYLOAD WEIGHT EFFECTS TO BE USED FOR TOTAL TANK SYSTEM EVALUATION

Tug performance partials for a synchronous payload deployment mission were retested for use in computing delta payload weights. These partials are:

$$\frac{\partial PL}{\partial W_{Tug}} = -2.62 \qquad \frac{\partial PL}{\partial W_{Non\text{-}Tug}} = -0.38$$

where Tug weights represent all items that are physically part of the Tug and non-Tug represents those items which are part of the Orbiter deployment adapter.

Table 6-5. Tug vehicle weight deltas.

Item	Delta (Kg/cm)	Total Delta (Kg/cm)
Subsystem Weight Effects Due to Overall Length Change		
Fuel Tank Vent Subsystem	0.012	
Fuel Tank Pressure Subsystem	0.027	
Fuel Loading Measuring Subsystem	0.021	
Avionics Harnesses	0.027	
Miscellaneous	0.050	
		0.137
Shell Weight Effects		
Forward Section at P/L Interface		
Sandwich Sidewall	0.311	
P/L Longerons	0.045	
Pans under Longerons	0.038	
		0.394
Mid-Section		
Sandwich Sidewall	0.321	
		0.321
Adapter Section		
Sidewall (including reinforcement)	0.369	
Latch Longerons	0.055	
Pans for Latch Longerons	0.033	
		0.457

Table 6-5. Tug vehicle weight deltas. (Concluded)

Item	Delta (Kg/cm)	Total Delta (Kg/cm)
Subsystem Weight Effects Due to Individual Tank Length Change		
Fuel Tank		
Fuel Vent Subsystem	0.012	
Fuel Pressure Subsystem	0.027	
Fuel Loading Measuring Subsystem	0.021	
		0.060
Oxidizer Tank		
Oxidizer Vent Subsystem	0.011	
Oxidizer Pressure Subsystem	0.030	
Oxidizer Loading Measuring Subsystem	0.034	
Fuel Tank Feedline	0.012	
Insulation Purge Lines	0.055	
Miscellaneous Items	0.036	
		0.178
	Values	
Surface Area Effects		
Fuel Tank		
Insulation/Purge Bag	1.343 Kg/m^2	
Oxidizer Tank		
Insulation/Purge Bag	1.265 Kg/m^2	

7

TANK CONCEPT SELECTION

The objectives of this task were to: (a) compare concepts based on total Tug effects, and then (b) select concepts to be used in the preliminary design development in Phase II.

7.1 CONCEPT COMPARISON

The total vehicle geometry effects which were defined in Figures 6-10 and 6-11, were evaluated using the Tug vehicle weight deltas of Table 6-5 and the payload partials. An elliptical/cone configuration was added to this list, wherein the engine thrust cone was attached directly to the LO_2 aft bulkhead. Table 7-1 lists all the candidate configurations and their delta weights and delta payload weights with respect to the baseline configurations.

7.2 CONCEPT SELECTION FOR PHASE II

As discussed in Subsection 3.5, three LO_2 strut systems were selected for further consideration from the originally developed families of strut systems. Those selected were the laced 24-strut systems at slopes of 0.762, 0.611, and 0.436 radian. The weight comparisons of support system, shell effects, and boiloff are tabulated for each support configuration in Table 7-2.

The configuration producing the greatest payload capability (the system with the 0.762-radian slope) was selected for the Phase II predesign LO_2 tank. The LH_2 tank support system was analyzed as discussed in Section 3. Since no additional tank effects exist (such as the stiffening required in the LO_2 tank), the 12-strut system with a slope of 0.698 radian was selected for the Phase II predesign LH_2 tank.

The total system configuration resulting in the greatest payload capability was selected for Phase II predesign. This system was the Cassinian LH_2 tank and the elliptical LO_2 tank with engine thrust cone.

The selected tank systems are:

LH_2 Tank	-	Cassinian Contour, N = 1.88
		12 Support Struts
LO_2 Tank	-	Elliptic Contour, $a/b = \sqrt{2}$
		24 Support Struts
		Thrust Cone Engine Mount

Table 7-1. Total system weight effects

Configuration*		Delta Weights (Kg)					
LH_2 Tank	LO_2 Tank	Tank With Engine Support	Vehicle System	Tank Int.	Tank Ext.	Σ	P.L. Wt.
Baseline †		0	0	0	0	0	0
Ell.	N_θ/N_ϕ	+4.9	-4.8	-1.6	+.1	-1.4	+3.7
N_θ/N_ϕ	Ell.	+6.0	-9.0	-1.0	+.3	-3.7	+9.7
N_θ/N_ϕ	N_θ/N_ϕ	+10.9	-13.8	-2.6	+.4	-5.1	+13.4
Cass.	Ell.	-3.1	-3.2	-0.4	+.1	-6.6	+17.3
Cass.	N_θ/N_ϕ	+1.7	-8.0	-2.0	+.1	-8.2	+21.7
Ell.	Ell. Conic	-7.7	-3.2	+2.0	+.1	-8.8	+23.1
N_θ/N_ϕ	Ell. Conic	-1.7	-12.2	+1.0	+.3	-12.6	+33.0
Cass.	Ell. Conic	-10.8	-6.9	+1.6	0	-16.1	+42.2
Ell.	Ell./Cone	-12.1	-1.4	0	0	-13.5	+35.4
N_θ/N_ϕ	Ell./Cone	-6.1	-10.4	-1.0	+.3	-17.2	+45.1
Cass.	Ell./Cone	-15.2	-4.6	-0.4	+.1	-20.1	+52.7

*Configurations:

Ell. = Elliptical bulkhead configuration
N_θ/N_ϕ = Controlled hoop/meridan stress ratio bulkhead configuration
Cass. = Cassinian bulkhead configuration
Ell. Conic = Ellipticonic bulkhead configuration
Ell./Cone = Elliptical bulkhead with engine thrust cone

† Baseline = Elliptical bulkhead on both LH_2 and LO_2 tanks

Table 7-2. Support configuration comparison.

Strut Configuration			Shell Weight Delta (Kg)	Adapter Weight Delta (Kg)	Support System Weight Delta (Kg)	Boiloff Weight Delta (Kg)	Tank Comp. Stfng. (Kg)	Payload Effects. (Kg)
Quantity	Pattern	Slope (Radian)						
24	Laced	0.762	0*	0*	0*	0*	0*	0*
24	Laced	0.611	-3.3	+10.9	+2.2	-.22	+6	-16.4
24	Laced	0.436	-8.3	+27.5	+9.6	-.45	+12	-44.2

(*) Comparison basis (-) = Reduced weight (+) = Added weight

8

CONCLUSIONS AND RECOMMENDATIONS

8.1 CONCLUSIONS

Due primarily to the great difference in propellant density, the optimum tank geometry and support systems are very different for the LH_2 and LO_2 tank.

The systematic approach to loads analysis and contour effects developed in this program was applied to each propellant tank design independently, and the tank characteristics (such as length surface area and weights) were compared with respect to total vehicle effects.

The low density of LH_2 results in requirement of a large tank with low propellant inertia effects. With the large volume requirement and the diameter limitations of the Shuttle cargo bay, a cylindrical section is required for the LH_2 tank. The Cassinian contour assumes the characteristics of a cylinder within its own geometry, so there are no discontinuities due to geometry change at the bulkhead-to-cylinder joint. This feature also results in a minimum cylindrical length. The LH_2 tank with the Cassinian bulkheads weighs less than elliptical or controlled N_θ/N_ϕ contoured bulkheads with cylindrical mid-sections.

The controlled N_θ/N_ϕ contour is a unique use of the membrane stress equations to define the physical contour such that the ratio of the hoop stress and meridional stress over the contour of the bulkhead is defined by a constant or an equation.

Because of the higher density of LO_2, the tank volume required is small and the diameter of the cargo bay is not a limiting factor, so a tank cylindrical section is not necessary. The Cassinian contour with its transition to a cylinder is not advantageous in the LO_2 tank. A tank formed by two Cassinian-contoured bulkheads is much longer than either elliptical or N_θ/N_ϕ contoured tanks containing the same volume and using membrane compression as a limiting consideration to the contour flatness selection. Though the N_θ/N_ϕ contour can lead to development of a very short tank while maintaining hoop tension in the membrane, the elliptical contour results in the lightest LO_2 tank.

The material selected for the tank membranes was 2219-T87 aluminum alloy. This selection was based on its excellent fracture toughness, good weldability, and repair weldability plus high stress/corrosion cracking resistance.

The tank support systems were optimized considering strut weights, bracket weights, boiloff weights, and tank membrane effects as well as system stiffness. The

selected support systems which met these requirements were the laced 24-strut system for the LO_2 tank and a separate 12-strut system for the LH_2 tank. For the LO_2 tank, the strut-to-bulkhead tangent point location was critical because size of the hoop compression zones is a function of the support tangent point relative to the tank girth. For the Tug loading conditions and the elliptical LO_2 tank contour, the critical location is 0.76 radian with respect to the tank centerline. Any smaller angle would allow compressive forces to exist below the support plane, and membrane stiffening would be required.

The baseline main engine support system was reviewed in connection with its effect on the LO_2 tank configuration. An ellipticonic bulkhead was originally to be considered as an alternate for the truss mounted baseline support. The selected system was a thrust cone mounted directly to the LO_2 elliptical aft bulkhead door, which resulted in the shortest and lightest overall LO_2 tank. This thrust cone is dry: the cone itself does not contain any propellant. The door of which the cone is a part has a membrane and outlet inside the cone envelope. In this way, the feed line prevalve can also be located inside the cone envelope, while the three flex joints which allow full engine gimbal can be located with a minimum of additional line routing prior to interfacing with the engine.

A trade-off was performed on the method used for the membrane transition to increased weld land thicknesses. In general, this was a comparison between chem-milling transition steps on one surface only and steps on both surfaces. For the LO_2 tank geometry the bulkhead membrane joint showed an eighteen percent improvement going from the one-surfaced step to the balanced or two-surfaced step. Therefore, the predesign tank configurations will have transition steps on both sides (external and internal) of the membrane.

The fracture mechanics analysis showed that the proof test alone will not ensure that the tank will never leak during the design life since, based on the operating stresses and material thicknesses used in this study, the "leak before burst failure mode" is critical. A series of curves showing depth versus number of missions were developed to define the requirements for nondestructive inspection flaw size detection capability.

8.2 RECOMMENDATIONS

8.2.1 PHASE II

a. Use the Cassinian contour for the LH_2 tank bulkheads with the 12-support-strut arrangement.

b. Use the $\sqrt{2}$ elliptical contour for the LO_2 tank bulkheads with the laced 24-support-strut arrangement.

c. Use the bulkhead mounted dry cone main engine support system.

d. Use double step (inside and outside surface) weld transitions.

8.2.2 OTHER

a. The NASA baseline tug configuration presented in MSFC 68M00039-2 "Baseline Space Tug Configuration Definition" should be revised to reflect the tankage and support system geometries developed in Phase I of this study.

b. Additional detailed preliminary design should be performed on strut members and representative struts should be fabricated for further testing with the test tank when it is installed in the test shell structure.

9

REFERENCES

1. Hertz, J., Investigation of Potential Low Temperature Insulations, General Dynamics Astronautics Report GD/A-ERR-AN-688, December 1964.

2. Hertz, J., et al, Advanced Composite Applications for Spacecraft and Missiles Phase I - Final Report Volume II: Material Department AFML-TR71-186 Vol. 2, March 1972.

3. Betts, W.S. and Howell, G.A., An Analytical Solution for Determining the Heat Leakage to the 86.7-Inch Tank, General Dynamics Convair Report 584-4-416, 23 October 1969.

4. Fowler, Joseph M., Thermal Analysis and Design of Liquid Hydrogen Tank Fluid Line Fittings, Paper presented to the Conference on Propellant Tank Pressurization and Stratification at NASA/MSFC, 20-21 January 1965.

5. Keller, C.W., Fiberglass Supports for Cryogenic Tanks, Final Report NASA CR-120937, prepared under Contract NAS3-12037 by Lockheed MSC, 10 October 1972.